UNIVERSITY OF CALIFORNIA SAN DIEGO

The geochemistry and Sr-Pb isotopes of Toro Ankole and Virunga lavas provide constraints for a unified tectono-magmatic evolution of the East African Rift System

A thesis submitted in partial satisfaction of the
requirements for the degree Master of Science

in

Earth Sciences

by

Hugo Abe

Committee in Charge:

Professor Paterno R. Castillo, Chair
Professor Sarah Aarons
Professor Emily Van Allen

2022

The thesis of Hugo Abe is approved, and it is acceptable in quality and form for publication on microfilm and electronically.

University of California San Diego

2022

DEDICATION

I would like to dedicate this thesis to my father, my brother, and my mother. Thank you all for your support throughout the years. I hope to make you all proud.

TABLE OF CONTENTS

LIST OF SUPPLEMENTAL FILES

abe_EthiopiaTrace_MgOPlots_PartitionCoefficients.doc

LIST OF FIGURES

LIST OF TABLES

ACKNOWLEDGEMENTS

I would like to acknowledge Professor Paterno Castillo for his support during the 2 years I was working on this project. Without his invaluable guidance and patience, I would have not been able to produce such a meaningful thesis.

I would like to acknowledge my committee members, Professor Emily Van Allen and Professor Sarah Aarons who provided valuable feedback on my work. Professor Emily Van Allen was also kind enough to let me use her lab's desktop SEM for the petrographic analysis.

I would also like to acknowledge Professor James Day and the Scripps Isotope Geochemistry Laboratory for analyzing my samples for the trace element data.

In addition, I would like to acknowledge the assistance provided by James F. Natukunda of the Uganda Ministry of Energy and Mineral Development and Godfrey Bahati of the Uganda Geothermal Resources Department in collecting the samples used in this study and the financial assistance provided by UCSD through the Academic Senate Grant RG096597 to Professor P. Castillo and by the NSF through Grant EAR-1019489 to Professor D. Hilton.

Finally, I would like to acknowledge UCSD and the department of SIO for providing me the educational resources and the opportunity to work with all the people I have met over the course of 6 years.

This thesis, in full, contains material currently being prepared for publication. Abe, Hugo; Castillo, Paterno R.; Day, James M.D.; Halldórsson, Sæmundur A.; Scarsi, Paolo; Natukunda, James F.; Bahati Godfrey. "The geochemistry and Sr-Pb isotopes of Toro Ankole and Virunga lavas provide constraints for a unified tectono-magmatic evolution of the East African Rift System". The thesis author was the primary investigator and author of this paper.

ABSTRACT OF THE THESIS

The geochemistry and Sr-Pb isotopes of Toro Ankole and Virunga lavas provide constraints for a unified tectono-magmatic evolution of the East African Rift System

by

Hugo Abe

Master of Science in Earth Sciences

University of California San Diego, 2022

Professor Paterno R. Castillo, Chair

Volcanism in the Toro Ankole and Virunga provinces at the northernmost tip of the Western Branch of the East African Rift system (EARS) is associated with the earliest stages of rifting. Although the provinces are spatially close, Toro Ankole lavas are relatively more silica-undersaturated, potassic, carbonatitic, and geochemically enriched than Virunga lavas. New petrographic, major-trace element and Sr-Pb isotopic data indicate such compositional differences are due to the different stages of tectonic rifting and concomitant magmatism in the region. Its underlying continental lithospheric mantle (CLM) is being metasomatized by volatile-rich small degree partial melts from the African Superplume. With decreasing pressure,

carbonatite-rich volatiles exsolve ahead of the upwelling partial melts and accumulate in the uppermost CLM layers beneath the cold, strong crust prior to rifting. Initial rifting in Toro Ankole generates explosive volcanism drawn from the uppermost carbonatite-metasomatized CLM layers. As rifting progresses in Virunga, less explosive volcanism emanates from the deeper silicate-metasomatized CLM. More advanced rifting in the nearby South Kivu province additionally involves the asthenospheric mantle. The Ethiopian rifts in the Eastern Branch of the EARS are most likely advanced stages of the same dynamic tectono-magmatic evolutionary process. Additionally, however, the Western Branch is underlain by the relatively more stable Paleoproterozoic to Archean basement whereas the Eastern Branch in Ethiopia is underlain by the Neoproterozoic Mozambique Mobile Belt. Thus, rifting and magmatism in the entire EARS is due to the dynamic interaction between the African Superplume and the local CLM.

1. Introduction

The plate tectonics theory that governs how the Earth evolves is based on a number of geologic processes that are still poorly understood. These include continental rifting, a critical precursory stage of continental lithosphere breakup through magmatism and tectonism that eventually leads to plate divergence and concomitant ocean basin formation. The most prominent and currently active example of continental rifting is the East African Rift System (EARS). Here, the compositional range of magmatic products is very broad and includes very unique continental lavas that are highly silica-undersaturated and alkaline relative to the voluminous, typical mid-ocean ridge basalts (MORBs) generated directly from the upper mantle beneath the ocean basin. Moreover, EARS lavas can be generally grouped into different suites or volcanic provinces that, to a first order, can be associated with the different stages of rifting, from that with the least to that with the most pronounced structural rifts. Thus, the EARS is a collection of rift segments of varying rift tectonic maturity and volcanic lava diversity that provides a convenient overview of a near-continuous sequence of rift development with associated magma evolution.

The extensive research conducted on the EARS through the years converges to a general consensus that the bulk of magmatism in this region is produced from the interactions of upwelling mantle plumes with the local underlying continental lithospheric mantle (CLM – e.g., Ebinger et al., 1989a; Latin et al., 1993; Marty et al. 1996; Scarsi et al., 1996; Rogers, 2006; Furman, 2007; Castillo et al., 2014). Defining the details of such interactions, including the number of plumes and how each or all interact with the CLM and with each other to produce the diverse EARS lavas, however, is still yet to be accomplished and is undoubtably one of the most debated topics in Earth Science.

The primary focus of this research is to constrain the source and evolution of lavas associated with the earliest stage of rifting in the EARS. To accomplish this goal, lava samples from the Toro Ankole volcanic province, located in the youngest rift segment of the EARS, and the adjacent Virunga volcanic province to the south, were analyzed for their petrographic features and chemical and Sr-Pb isotopic compositions. Notably, studies on the younger rift segments of the EARS have not been as prolific as those on the more mature rifts. Thus, to better comprehend the continental rifting process in the EARS, it is crucial to compare and contrast the petrogeneses of lavas from mature and young EARS rifts. A better elucidation of the rifting process in the EARS, in turn, will provide broader understanding of plate tectonics as a whole.

2. Geological Background

2.1. Regional Setting

The EARS is comprised of a series of rift and fault structures with varying degrees of lithospheric extension with associated magmatism of varying petrologic and geochemical signatures. It can be broadly separated into two main branches: the Eastern and Western Branch (inset in Fig. 1). The Eastern Branch, covering a distance of ~2200 km, extends from the Afar triple junction near the Red Sea in the north, through the Ethiopian highlands, the Main Ethiopian Rift (MER) and the Kenya (Gregory) Rifts down to northern Tanzania in the south (Harðarson, 2015). The bulk of lavas erupted in the Eastern Branch particularly along the MER generally define a tholeiitic to transitional-alkalic rock compositional affinity (Furman, 2007). Clear exceptions are the trachytic to pantelleritic lavas from volcanic complexes in central and southern Kenya and the markedly silica-undersaturated lavas in Chyulu Hills. Chyulu Hills form a separate, off-axis volcanic province (Furman, 2007; Spath et al., 2000), but their alkalic lavas are generally more sodic compared to the more potassic magmas of the Western Branch (Rosenthal et al., 2009). Most of the regions in Ethiopia are underlain by the Mozambique Mobile Belt, which is a region that was tectonically reworked by the Neoproterozoic Pan African Orogeny (Stern, 1994). On the other hand, the basement is more complex under the Kenya Rift which consists of Archean Tanzania craton crust, reactivated craton margins from the Pan African orogeny, and the Mozambique Belt (Smith and Mosely, 1993; Rogers et al., 2000). Due to the complex nature of the basement of the Kenya Rift and how some of it overlaps with the basement of the Western Branch, we chose to focus herein on the tholeiitic to transitional-alkalic lavas from mainly off-rift volcanism in southern Ethiopia, the NW highlands or plateaus and the MER over Kenyan rift lavas. Furthermore, as one of the main objectives of this study is to

Figure 1. Map of the study areas in the Toro Ankole and Virunga provinces of the Western Branch of the East African Rift System. Inset shows the relative location of the study area within the EARS (fault lines taken from Castillo et al., 2014). Physical map taken from Google Maps.

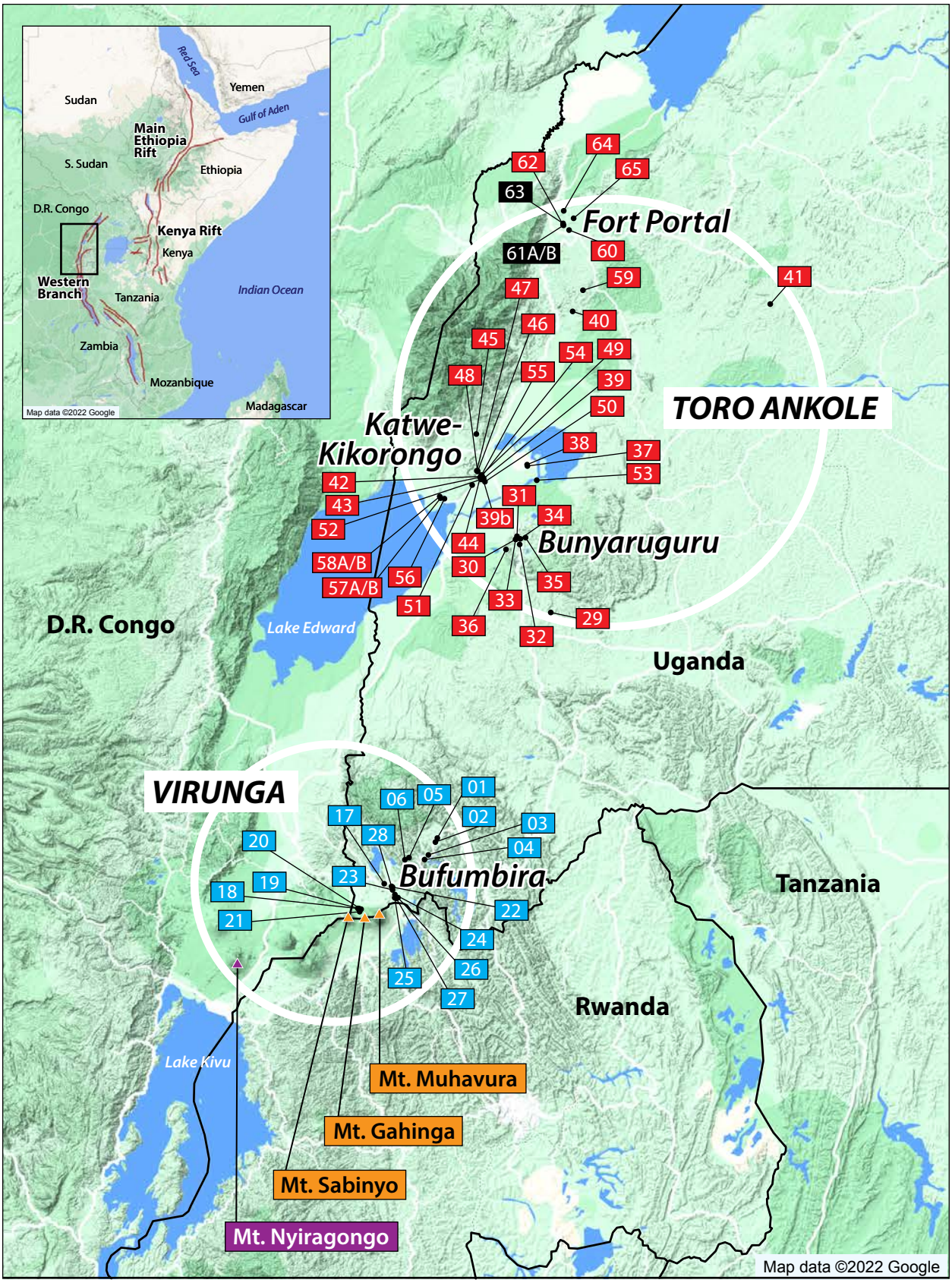
Red Sea
Yemen
Sudan
Gulf of Aden
Main Ethiopia Rift
S. Sudan
Ethiopia
D.R. Congo
Kenya Rift
Kenya
Western Branch
Tanzania
Indian Ocean
Zambia
Mozanbique
Madagascar
Map data ©2022 Google
Fort Portal
TORO ANKOLE
Katwe-Kikorongo
Bunyaruguru
D.R. Congo
Lake Edward
Uganda
VIRUNGA
Bufumbira
Tanzania
Rwanda
Lake Kivu
Mt. Muhavura
Mt. Gahinga
Mt. Sabinyo
Mt. Nyiragongo
Map data ©2022 Google

compare the different developmental stages of structural or tectonic rifting between the Western and Eastern Branch, we focus on the relatively more mature rifts of the MER. Therefore, any mention of the Eastern Branch in subsequent discussions mainly refer to southern Ethiopia, the MER and the NW plateaus unless otherwise specified.

The Western Branch extends for ~2100km from Lake Albert in the north to Lake Malawi in the south (Harðarson, 2015). Unlike the magmatism that runs along more or less continuously with the rifts in the Eastern Branch, magmatism in the Western Branch is volumetrically smaller and spatially limited to four volcanic provinces from south to north: Rungwe, South Kivu, Virunga, and Toro Ankole. The Western Branch lies along the margins of Paleoproterozoic to Archean crust, specifically the Tanzania craton, with Toro Ankole possibly underlain by ancient cratonic lithosphere that connected the Tanzania and Congo cratons (Link et al., 2010). A general trend of decreasing silica and increasing carbonate contents, as well as increasing geochemical enrichment particularly in K can be seen in the same direction (Pouclet et al., 1981; Rosenthal et al., 2009). This is evidenced by the presence of carbonatites and ultra-potassic/silica-undersaturated lavas in the north (Barker and Nixon, 1989; Rosenthal et al., 2009; Stoppa et al., 2000; Tappe et al., 2003), and alkalic and tholeiitic lavas in the south (Bell and Powell, 1969; Furman and Graham, 1999). The compositional spectrum of Western Branch lavas is thought to be due to varying degrees of partial melting of the underlying CLM metasomatized by carbonatitic fluids, and further complicated by its content of accessory phases such as phlogopite, amphibole, sphene, and apatite (Furman, 1995; Rosenthal et al., 2009; Castillo et al., 2014).

Overall, Western Branch lavas are more silica-undersaturated and highly potassic compared to Eastern Branch lavas, particularly to the voluminous MER lavas. However, some

Eastern Branch lavas, including those in Chyulu Hills and particularly the Amaro and Gamo lava suites that predate major extension (45–35 Ma), are also lithologically diverse and geochemically enriched compared to lavas produced after rifting was more tectonically developed (George and Rogers, 2002). Thus, data seem to indicate that the structural/tectonic development of the rift could be an important factor in determining lava composition; that is, the diverse compositional spectrum of lavas throughout the EARS is indeed tied to the varying degrees of its rift tectonic development.

2.2. Geologic History

The earliest volcanism in the EARS is thought to have started in the Turkana Depression near southern Ethiopia around 45 to 37 Ma (Furman, 2006). Rift initiation followed shortly after or penecontemporaneously with the opening of the northern Kenya Rift thought to be around 45 to 40 Ma, and by 30 to 20 Ma rifts and volcanic activities in the Eastern Branch were widespread, generally propagating southward (McDougall et al., 2009; Ebinger et al., 1989b; Morley et al., 1992; Ebinger et al., 2000).

Volcanism in the Western Branch is younger than that in the Eastern Branch. Many set the date for the Western Branch's earliest volcanic activity to be around 11 to 12 Ma in the Virunga province (Ebinger, 1989a; Kampunzu et al., 1998), although recently there has been a suggestion that initiation was more contemporaneous with the Eastern Branch, setting the date around 25 Ma (Roberts et al., 2012). Volcanism and rifting (typically associated with trachybasaltic volcanism) in the South Kivu province began as early as 10 Ma (Ebinger, 1989b), which was followed by the Rungwe province around 8 Ma with less potassic but overall similar subordinate alkalic volcanism (Furman, 1995). The Toro Ankole province is the youngest in the

Western Branch, erupting its distinct silica-undersaturated, potassic and carbonate rich lavas as recently as 46 Ka (Boven et al., 1998).

2.3. Mantle Plumes and Metasomatized CLM

From early gravitational anomaly studies and geochemical studies, it has been generally accepted that mantle plume activities are involved in EARS magmatism (e.g., Ebinger and Sleep, 1998; Latin et al., 1993; Marty et al., 1996; Scarsi et al., 1996), but characterizing the plume nature (e.g., separate or distinct plume heads or stems versus a unified or common mega plume) has been the topic of debate in the literature surrounding East African geology.

Two geochemically distinct plumes, defined as the Afar and Kenyan plumes, have been suggested to lie underneath the Ethiopian and Kenyan rifts, respectively, based on the trace element and Sr, Nd, Pb isotopic signatures of their respective lavas (e.g., Rogers et al., 2000). As studies expanded towards the Western Branch, additional plumes were found in the Virunga and Rungwe provinces with high $^{3}He/^{4}He$ ratios and distinct isotopic signatures (Chakrabarti et al., 2009a; Hilton et al., 2011; Foley et al., 2012; Castillo et al., 2014). Interestingly, the reported occurrences of such compositionally distinct mantle plumes in discreet locations also fueled parallel investigations on the role of a mega mantle plume in EARS magmatism.

For instance, Furman (2007) proposed some modifications of the two-plume model by arguing for a single African Superplume, where individual plume upwellings in different EARS segments branch from a common, but heterogenous sub-lithospheric plume. Lavas from the Kenya Rift in the Eastern Branch and South Kivu province in the Western Branch resemble ocean island basalts (OIBs) with isotopic compositions nearing the so-called HIMU (high μ or high U/Pb) mantle plume source component whereas lavas from the plume in the Ethiopian rifts are mostly non-radiogenic in isotopic composition. Each plume also has metasomatized the

underlying CLM at varying degrees, further diversifying the plume signature in each location. Moreover, Furman et al. (2016) later revised their model by suggesting that the compositional heterogeneity of EARS lavas is also due to whether or not drip melting of the metasomatized CLM was induced and incorporated by the upwelling plume.

A unified plume model was also proposed by Castillo and co-workers (Castillo et al., 2014, 2020; Halldórsson et al., 2014, 2022), in which the bulk of EARS magmatism is produced by mixing the African Superplume with the CLM, generating a common lava composition "V". As a general framework, binary mixing between the African Superplume and the Neoproterozoic Pan-African CLM produces Ethiopian and northern Kenya Rift lavas whereas mixing with the Paleoproterozoic to Archean Tanzanian Craton produces southern Kenya Rift and Western Branch lavas. Composition "V" represents the convergence or average composition of the mixtures above individual plume heads and/or stems that originate from the African Superplume. The superplume has ponded beneath the thick African continent, perhaps, since ca. 500 Ma and has been continuously metasomatizing the asthenosphere and the CLM (Castillo et al., 2014, 2020; Halldórsson et al., 2014, 2022).

Accordingly, the investigations also focus on how mantle plumes metasomatize the EARS CLM. Studies have shown signs of past metasomatized CLM sources in the Eastern Branch, such as beneath the northern Kenya Rift, in the form of lavas produced from amphibole-lherzolite melting, at least, during the Tertiary until the Pleistocene (Furman et al., 2006a; Class et al., 1994). From the Quaternary onwards, lavas from anhydrous spinel lherzolite melting became common in the region, suggesting an overall decrease in the metasomatic signature of the CLM source as rifts developed or as the lithosphere thins in the Eastern Branch (Furman, 2007; Furman et al., 2016).

Studies have also indicated that the CLM beneath the Western Branch is more metasomatized than that beneath the Eastern Branch. As mentioned before, the volcanics in the Western Branch, especially towards the north, are very unique in geochemical signatures characterized by extreme enrichment in incompatible trace elements and have a highly alkaline/potassic composition. Such highly potassic signatures have been attributed to phlogopite and amphibole in the source (Furman, 2007), most likely stabilized by a hydrous metasomatic agent or metasome. Adding further complexity, lavas from Virunga's Nyiragongo volcano have high CaO and modal calcite (Sahama, 1978; Chakrabarti et al., 2009a, 2009b) and in Toro Ankole, carbonatite lavas occur (Barker and Nixon, 1989; Stoppa et al., 2000). Thus, the complicated history of metasomatism experienced by the CLM particularly beneath the northern Western Branch provides insights on the metasomatic processes and/or events that lead to the variable compositional signatures of EARS lavas.

For instance, results of later studies in the Toro Ankole province have indicated that the metasomatic history of Western Branch volcanics is not a single, but a multi-stage event. Rosenthal et al. (2009) proposed a two-stage metasomatism, initially through silicate metasomatism, as evidenced by MARID-like (mica-amphibole-rutile-ilmenite-diopside) assemblages, followed by a later carbonatitic metasomatism. This was shown through the Sr-Nd-Hf-Os isotopic signatures of Toro Ankole lavas which indicated mixing between the two end-member metasomes. Significantly, more recent studies have reached similar conclusions of episodic metasomatic events that involve both low-degree silicate melts and carbonatitic melts in the CLM source beneath the Toro Ankole and possibly Virunga province (e.g., Muravyeva et al., 2014; Pitcavage et al., 2021).

In this study, we aim to elucidate the metasomatic history of the CLM source of the northern Western Branch magmas by investigating lava samples from the Toro Ankole and Virunga provinces. Samples from these volcanic provinces, ranging from very enriched carbonatites and highly-alkaline or highly-potassic foidites to trachy-basalts, were analyzed for major and trace elements and Sr-Pb isotopes. Incompatible trace element data and rare earth element (REE) in particular indeed suggest dual episodes of silicate and carbonatitic metasomatism of the CLM beneath the northern Western Branch. The isotope data further suggest that these two metasomatic episodes are products of mixing between the local CLM and the bulk of plume component, which is generally similar to that beneath the Eastern Branch. The proposed interaction between this common plume component and the respective local CLM beneath the Western and Eastern Branch provides a framework for a new and unified tectono-magmatic model to explain the general rifting and bulk magmatism along the EARS.

3. Samples and Methods

3.1. Samples

The Toro Ankole volcanic province is located along the northernmost segment of the Western Branch in southwestern Uganda (Fig. 1). The volcanic field consists of three volcanic centers from north to south: Fort Portal, Katwe-Kikorongo and Bunyaruguru. Eruptive activity of Toro Ankole is significantly young compared to magmatism of the EARS as a whole, as the oldest rocks from this field only date back to 46 Ka (Boven et al., 1998), though recent studies have suggested an earlier phase from around 87 Ka and/or 188 Ka from Katwe-Kikorongo and Bunyaruguru, respectively (Pitcavage et al., 2021). The youngest rocks in Toro Ankole are dated to be around 6 Ka to 4 Ka (Barker and Nixon, 1989) in Fort Portal, which is coincidentally where carbonatites occur. Toro Ankole volcanism is characterized by mostly explosive eruptions from maars and low-lying craters, erupting mostly pyroclastic tuffs and rare lava flows (Holmes and Harwood, 1932). In sum, most volcanic products are a result of volatile-rich eruptions where magma transport is very rapid.

The Virunga volcanic province is also located along the Western Branch, immediately south of Toro Ankole, and extends across the border between Uganda, Rwanda and the Democratic Republic of Congo (Fig. 1). There are 8 volcanoes in Virunga, of which two—Nyiragongo and Nyamuragira, both in the westernmost region —are currently active. Gahinga, Muhavura, and Sabinyo are older volcanoes located in the eastern part of Virunga that, henceforth, are called the “eastern volcanoes” (of Virunga). The cinder cone field, Bufumbira, is the easternmost volcanic feature of Virunga that lies north of the eastern volcanoes, but is not considered here as part of the eastern volcanoes. The earliest volcanic activity predates rifting and is recorded to be 12.6–8.6 Ma near Bishusha-Tongo in the northwestern part of the province,

just above Nyamuragira (Bellon and Pouclet, 1980; Kampunzu et al., 1998). Volcanism in central Virunga associated with rifting began from around 2.6 Ma with the Mikeno volcano (Guibert et al., 1975) and continues till present day in Nyiragongo and Nyamuragira. As mentioned earlier, Nyiragongo is very unique because its silica-undersaturated and highly alkalic lavas are quite similar to Toro Ankole lavas (Chakrabarti et al., 2009a).

The samples investigated in this study were selected from a collection of lava, pyroclastic, and xenolith samples collected during a 2016 field expedition in southwestern Uganda. The Virunga samples were collected from the eastern volcanoes (Muhavura, Sabinyo, Gahinga) and the Bufumbira cinder cones. On the other hand, the Toro Ankole samples were collected from or near Fort Portal, Katwe-Kikorongo and Bunyaruguru volcanoes. As noted earlier, the Toro Ankole volcanics are generally younger compared to those from Virunga. Bunyaruguru samples are estimated to be as old as 46 Ka (Boven et al., 1998) whereas the Fort Portal carbonatites are estimated to be around 6 Ka to 4 Ka (Barker and Nixon, 1989).

As the focus of this study is on the petrogeneses of the lavas through major and trace element plus Sr-Pb isotope geochemistry, only lava samples with visibly minimal to no alteration were selected for analysis. Pyroclastic rocks and samples with significant crustal or mantle xenoliths were excluded. Pyroclastics are more prevalent than lavas in Toro Ankole, so the number of Toro Ankole samples analyzed (18) is less than that from Virunga (28) out of the total (46) lavas analyzed. Lava samples were chipped into cm-sized fragments and, then, rock chips from sample interiors without signs of weathering, alteration, veins, and xenoliths were pulverized using a tungsten-carbide shatterbox to generate sample powders for major and trace element analysis. Powders for Sr and Pb isotope analyses were pulverized from similarly chosen

rock chips using an alumina-ceramic shatterbox. The types of analysis conducted on each sample is listed in Supplemental Table 1.

Thin sections were made from samples representing major lava types. Petrographic analysis was done through standard petrographic microscopy. Additional petrographic data were acquired through qualitative chemical analysis on uncommon, highly unusual minerals, especially those that occurred as crystallites, using a Phenom Pro XL, a desktop compatible Scanning Electron Microscope (SEM) with energy-dispersive X-ray spectroscopy (EDS) capabilities, at the Shared Optical Microscopy Lab, Scripps Institution of Oceanography.

3.2. Chemical and Isotope Analysis

Sample powders were sent to Activation Laboratories Ltd., Canada for major element analysis. Samples were made into fusion disks following the heavy absorber technique of Norrish and Hutton (1969) and were analyzed via wavelength dispersive X-ray fluorescence (XRF) spectroscopy. Trace element analysis was performed at the Scripps Isotope Geochemistry Laboratory (SIGL) at Scripps Institution of Oceanography (SIO). The digested samples were prepared using standard procedures described in Day et al. (2014) and Durkin et al. (2020), along with USGS standards: BHVO-2, BCR-1, BIR-1, and W-2. 100 mg of powdered samples were dissolved in Teflon beakers with doubly-distilled HF:HNO_3 (2:1) mixture, ultrasonicated for ~15 minutes and left over a hot plate overnight (some samples required several days) until completely dissolved. These were then dried also over a hot plate and then re-dissolved and evaporated twice in doubly-distilled concentrated HNO_3. The dissolved samples were diluted in a 1:5000 proportion in a 2% HNO_3 and doped with a 1 ppb In solution to correct for instrumental drift. These solutions were analyzed using a ThermoScientific iCAPq quadrupole inductively coupled plasma mass spectrometer (ICP-MS) also at the SIGL.

Based on chemical analyses, Toro Ankole and Virunga samples best representing incompatible trace element enriched and depleted were selected for Sr and Pb isotopic analysis (Toro Ankole: UG-45, UG-55; Virunga: UG-25, UG-06). Additionally, samples with the highest K_2O/Na_2O (UG-34) and most crustally contaminated (UG-15), plus two carbonatite samples (UG-61A, UG-63) were chosen. As the carbonatites contain a significant amount of what appears to be secondary calcite amygdales (fuzzy and/or sparry texture) under the microscope, ~90 mg of UG-61A and UG-63 sample powders were leached using a 2M doubly-distilled acetic acid. Then the mixtures were ultrasonicated for one hour and the leachates (presumed to be containing secondary calcite) were separated from solid residues. After drying, both leachates and residues were treated as sample powders.

To dissolve the sample powders for isotopic analysis, the same digestion procedures for trace element analysis described above were followed except that after the HNO_3 step, the samples were further dissolved using doubly-distilled 4.5N HCl. Thirty to 35 mg of powders were originally dissolved; about 7 mg of each was aliquoted for Sr and REE separation and the remaining amount was used for Pb separation. Strontium was separated through cation-exchange chromatographic columns following the procedures described in Durkin et al. (2020). Strontium was purified further by passing the Sr cuts through Sr-specific extraction chromatographic columns; the procedures and performances are described in detail by Pin et al. (1992). Lead was separated through small anion-exchange HBr columns also following the procedure described by Durkin et al. (2020). Strontium and Pb isotopic data were collected using a VG-Micromass Sector multi-collector thermal ionization mass spectrometer (TIMS) also at SIO. Details of the TIMS analysis including accuracy and precision of the results are listed under the analytical results table.

4. Results

4.1. Petrography

Toro Ankole samples consist of basaltic lavas that exhibit trachytic texture with little to no vesicles. Phlogopite and feldspathoids are present primarily as phenocrysts but also as groundmass phases in many samples. Most are sparse to moderately phyric with pyroxene as the most dominant phenocryst, followed by phlogopite, olivine, and occasional feldspathoids.

UG-29 is an olivine melilitite from the Katunga volcano, south of Bunyaruguru. It is very highly phyric (≤ 40% phenocrysts) due to large amounts of melilite interspersed with glomerophyric clusters of olivine and some perovskite in a cryptocrystalline groundmass. Some leucite and clinopyroxene crystallites were identified through SEM analysis. UG-61B is a carbonatite from Fort Portal. It is highly phyric (≤ 20% phenocrysts) and contains a high amount of secondary, sparry calcite filling the amygdules (up to ~25%). Phlogopite phenocrysts are sparse (< 2%) along with clinopyroxene, spinel (magnetite), and apatite (hydroxylapatite).

UG-34 and UG-36 are both kamafugites (katungite, mafurite and ugandite), more specifically, ugandites from Bunyaruguru. They are fine to medium grained (0.1–3 mm) and highly phyric (20–25% phenocrysts) with phenocrysts of olivine, clinopyroxene, perovskite, spinel (chromite and magnetite), and phlogopite in order of decreasing abundance. Veins filled with secondary sparry calcite and iddingsite are fairly common. Although kalsilite was not visually identified, it is reasonable to assume that this mineral along with phlogopite make up the cryptocrystalline groundmass considering the fact that UG-34 is the most potassic samples we analyzed ($K_2O/Na_2O = 9.67$) followed by UG-36 ($K_2O/Na_2O = 6.6$). UG-43 is a fine to medium grained (0.1–3.4 mm), feldspathoid–rich alkali basalt from Katwe-Kikorongo. It is highly phyric (≤ 20% phenocrysts), with phenocrysts of mostly clinopyroxene. There are also small amounts of

spinel (magnetite) and perovskite microphenocrysts in a generally devitrified groundmass of nepheline and leucite.

Virunga lava samples range from sparsely phyric (< 3% phenocrysts) to high phyric (≤ 30% phenocrysts). Pyroxenes are the most dominant phenocrysts, followed by olivine, then some plagioclase in a mostly fine-grained matrix. UG-18 is an alkali basalt from Bufumbira. It is fine- to medium-grained (0.3–3 mm) and moderately phyric (< 10%) with mainly olivine and clinopyroxene glomerocrysts plus individual plagioclase phenocrysts dispersed in a cryptocrystalline groundmass.

4.2. Major Elements

Toro Ankole samples are silica-undersaturated (SiO_2: 36–45 wt% for silicates; 12–13 wt% for carbonatites) with moderate to high MgO (6–20 wt%) content (Table 1). They are also very volatile-rich as evidenced by their variable but generally high LOI values (up to 6% for silicates; 23% for carbonatites), and have high CaO content (average ~13.7 wt% for silicates; ~33 wt% for carbonatites). Virunga samples are also generally silica-undersaturated although to a lesser extent (SiO_2: 42–50 wt%) and have lower MgO content (4–16 wt%) compared to Toro Ankole lavas. They also contain lesser amounts of volatile (LOI ≤ 2 wt%).

Most of the Toro Ankole lavas are foidites with sub-ordinate basanites, very similar to previously reported Toro Ankole lavas (Fig. 2). On the other hand, most of the Virunga lavas are basanites with sub-ordinate trachy-basalts, again similar to previously reported data. Most of the evolved basaltic-trachytes are from the eastern volcanoes while samples from Bufumbira are basanites. The younger Nyiragongo lavas differ from the rest of Virunga samples as they are mostly foidites, similar to Toro Ankole lavas, and have their own separate evolution trend that, perhaps, indicates a different source or origin from

Table 1. Major element composition (in wt%) for Toro Ankole and Virunga lavas. Fe_2O_3* calculated as total iron.

Virunga												
Bufumbira												
Sample	SiO_2	Al_2O_3	Fe_2O_3*(T)	MnO	MgO	CaO	Na_2O	K_2O	TiO_2	P_2O_5	LOI	Total
UG- 1	45.0	12.44	12.31	0.183	9.07	10.98	2.15	3.04	3.24	0.53	-0.03	98.9
UG- 2	44.7	12.1	12.45	0.186	10.97	10.35	2.31	2.78	3.18	0.56	0.43	100.0
UG- 3	41.8	9.41	12.18	0.181	16.31	11.8	1.55	2.71	3.03	0.5	0.25	99.7
UG- 4	42.7	9.12	12.12	0.177	16.17	11.6	1.57	2.78	3.01	0.5	0.63	100.4
UG- 5	45.3	14.09	13.25	0.191	7.23	9.34	2.31	3.18	3.88	0.61	1.01	100.4
UG- 6	45.0	10.64	12.22	0.175	14.56	10.26	1.9	2.08	2.77	0.45	0.35	100.4
UG- 17	43.9	13.36	12.29	0.186	9.05	10.53	1.93	2.48	3.34	0.61	2.19	99.9
UG- 18	47.5	15.32	12.23	0.167	5.87	8.34	2.52	3.69	3.67	0.59	0.68	100.6
UG- 19	46.3	14.61	11.92	0.175	6.18	9.17	2.43	3.63	3.38	0.59	0.42	98.8
UG- 20	46.8	15.4	11.98	0.169	5.71	8.11	2.8	3.78	3.44	0.61	0.74	99.6
UG- 21	46.4	15.85	12.33	0.179	5.46	7.9	2.93	3.54	3.45	0.66	0.99	99.7
UG- 22	44.5	13.22	11.83	0.199	8.7	10.5	2.98	3.63	3.03	0.69	0.53	99.8
UG- 23	43.9	12.41	11.88	0.197	10.07	10.15	3.13	3.6	3.14	0.72	1.07	100.3
UG- 24	43.8	11.81	11.88	0.19	11.52	10.41	2.93	3.27	3.02	0.63	0.43	99.9
UG- 25	44.6	14.37	11.63	0.21	6.14	10.14	3.8	4.31	3.21	0.86	0.92	100.2
UG- 26	43.8	11.15	11.94	0.184	11.91	11.19	2.17	2.29	2.92	0.51	1.84	99.9
UG- 27	44.8	11.35	12.29	0.185	9.83	11.76	2.04	2.86	3.17	0.53	1.35	100.1
UG- 28	45.3	14.29	12.14	0.193	6.78	9.18	2.71	3.28	3.05	0.63	1.68	99.2
Eastern Volcanoes:												
Muhavura												
UG- 7	50.4	15.96	10.61	0.164	4.34	7.13	3.21	4.55	2.76	0.72	0.4	100.3
UG- 8	48.7	16.25	11.86	0.167	4.56	7.53	2.74	4.04	3.34	0.6	-0.12	99.7
UG- 9	47.3	14.31	12.14	0.179	6.58	9.17	2.76	3.77	3.42	0.58	0.23	100.5
UG- 10	45.2	13.52	12.06	0.179	7.54	10.47	2.28	2.94	3.31	0.61	1.76	99.9
UG- 11	49.5	15.14	10.96	0.172	5.37	8.09	2.92	3.88	2.89	0.67	0.67	100.2

Table 1 (continued)

Sample	SiO_2	Al_2O_3	Fe_2O_3*(T)	MnO	MgO	CaO	Na_2O	K_2O	TiO_2	P_2O_5	LOI	Total
Eastern Volcanoes:												
Sabinyo												
UG- 12	48.0	15.6	12.06	0.168	5.21	7.96	2.37	3.95	3.6	0.58	0.69	100.2
UG- 13	46.7	15.15	11.68	0.167	5.6	8.3	2.69	3.4	3.43	0.58	0.91	98.6
Gahinga												
UG- 14	49.4	16.94	9.85	0.175	3.6	6.45	3.37	4.7	2.68	0.76	1.61	99.5
UG- 15	49.7	16.16	11.74	0.168	3.85	6.72	2.93	4.3	3.61	0.59	0.61	100.4
UG- 16	46.5	15.16	12.38	0.176	6.22	8.57	2.48	3.73	3.48	0.72	0.98	100.4
Toro Ankole												
UG- 29	36.2	6.62	12.28	0.209	12.97	14.54	1.07	4.77	4.41	1.13	5.27	99.5
Bunyaruguru												
UG- 34	37.1	7.41	10.93	0.165	14.05	10.21	0.6	5.8	5.2	0.68	6.06	98.2
UG- 36	38.4	6.42	11.11	0.143	19.37	7.81	0.62	4.09	5.14	0.32	5.12	98.5
Katwe-Kikorongo												
UG- 39B	39.3	7.02	14.46	0.176	10.74	15.59	1.33	2.12	5.17	0.46	3.12	99.5
UG- 42	41.3	8.92	13.53	0.196	8.92	13.2	1.88	3.79	5.01	0.64	2.75	100.1
UG- 43	38.2	8.89	14.09	0.218	7.46	14.57	2.85	2.77	5.86	1.05	3.77	99.7
UG- 44	39.8	6.46	14.86	0.181	11.26	16.64	1.49	1.79	5.22	0.41	2.37	100.5
UG- 45	39.0	10.07	13.57	0.23	6.65	13.47	2.74	4.06	5.2	0.98	3.92	99.9
UG- 46	38.2	10.04	13.38	0.228	6.16	13.04	2.62	4.62	6.04	1.08	3.05	98.5
UG- 47	41.8	9.03	13.53	0.186	9.26	13.33	1.9	3.97	4.95	0.57	1.35	99.9
UG- 48	38.7	7.96	15.06	0.215	8.21	15.6	2.02	2.7	5.96	0.86	2.71	100.0
UG- 49	38.1	8.63	14.33	0.214	7.53	15.08	1.36	3.15	5.89	0.87	4.17	99.3
UG- 52	41.8	9.1	13.79	0.19	9.33	13.69	1.94	3.66	5.06	0.53	1.2	100.3
UG- 53	38.5	10.02	13.43	0.22	6.33	12.98	2.82	5.02	5.97	0.99	2.41	98.7
UG- 55	39.7	6.45	14.78	0.176	10.33	16.27	2.15	1.2	5.17	0.47	3.27	100.0

Table 1 (continued)

Toro Ankole												
Sample	SiO_2	Al_2O_3	Fe_2O_3*(T)	MnO	MgO	CaO	Na_2O	K_2O	TiO_2	P_2O_5	LOI	Total
Fort Portal												
UG- 61A	12.6	3.17	12.14	0.432	7.75	32.91	0.42	0.1	1.7	3.17	23.4	97.8
UG- 61B	13.1	3.36	12.89	0.456	8.12	32.26	0.34	0.14	1.8	3.38	22.62	98.5
UG- 63	12.0	3.01	12.68	0.45	7.92	33.55	0.24	0.06	1.73	3.36	22.77	97.8
Standards:												
BHVO-2 #1	49.4	13.77	12.54	0.173	7.49	11.57	2.2	0.55	2.86	0.28	-0.22	100.6
BHVO-2 #2	48.7	13.45	12.31	0.17	7.26	11.25	2.19	0.49	2.77	0.26	-0.18	98.7

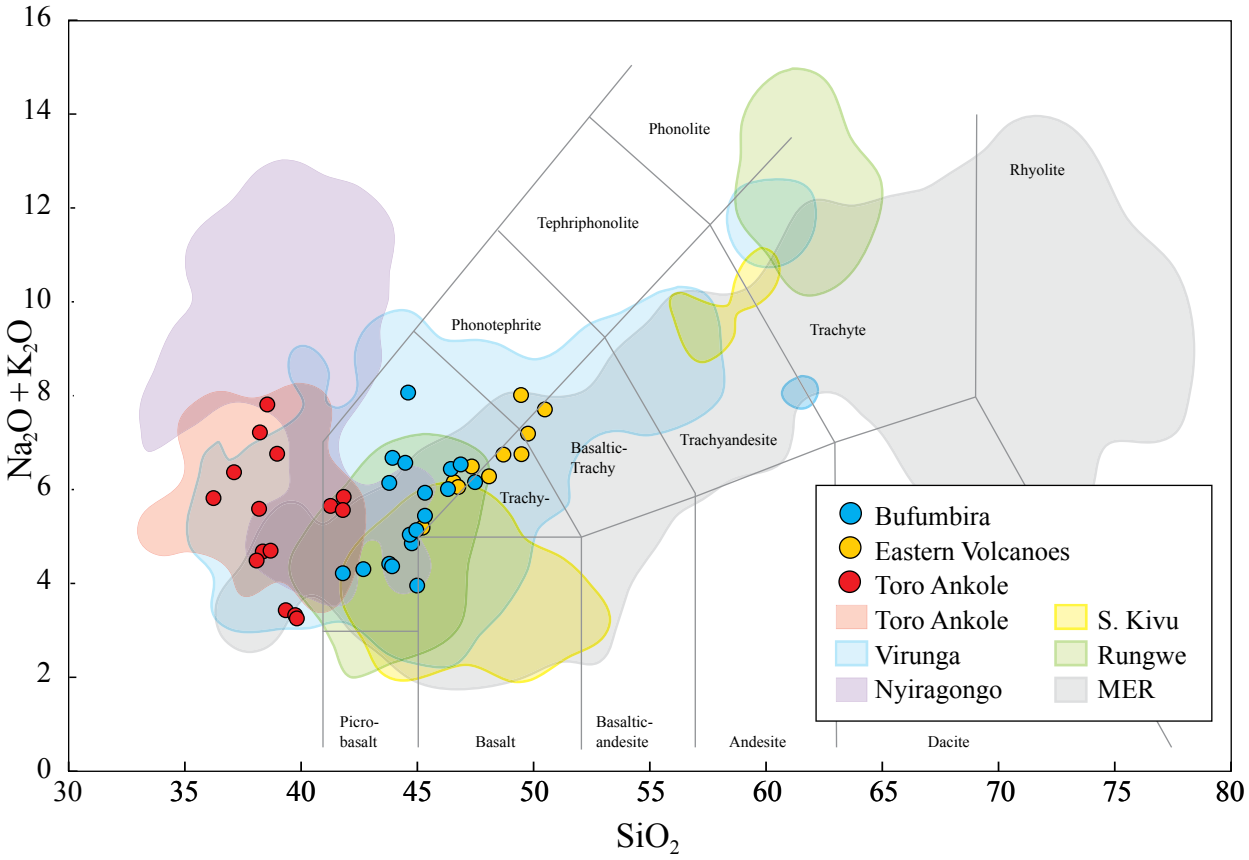

Figure 2. Total alkalis ($Na_2O + K_2O$) versus silica (TAS – after le Maitre et al., 2005) diagram for Toro Ankole and Virunga lavas. Toro Ankole samples consist of volcanics from Bunyaruguru and Katunga (carbonatites from Fort Portal -UG-61A&B, UG-63; SiO_2 << 30 wt% are not plotted). Virunga samples are divided by regions; Bufumbira and the eastern volcanoes of Muhavura, Gahinga, Sabinyo. Literature data for lavas from Toro Ankole, Virunga, South Kivu, and Rungwe provinces (https://georoc.mpch-mainz.gwdg.de//) are also plotted as fields for reference. For clarity, only MER data is plotted from the Eastern Branch.

the rest of Virunga samples (Chakrabarti et al., 2009a; Barette et al., 2017).

Both Toro Ankole and Virunga lavas are potassic, with high K_2O/Na_2O ratios (Fig. 3). Toro Ankole lavas have a large K_2O/Na_2O range that extends to very high values (up to 9.7), most likely owing to highly potassic rocks like olivine melilitite and kamafugite (i.e., ugandite). Previously reported Toro Ankole lavas that are highly potassic (> 4% K_2O/Na_2O) mostly consist of similar variants of kamafugites (Rosenthal et al., 2009; Muravyeva et al., 2014). Virunga lavas also have high K_2O/Na_2O ratios, but are generally restricted to values around 1–2; reported Virunga samples that exceed the range are mostly xenoliths (GEOROC). Nyiragongo lavas are potassic similar to the rest of the Virunga lavas, but their K_2O/Na_2O ratios are generally in the lower range of values (Chakrabarti et al., 2009a).

Within the Western Branch, Virunga and especially Toro Ankole are very silica-undersaturated and potassic. Lavas from the South Kivu province just south of Virunga mainly consist of tholeiitic lavas and sodic alkali basalts, with very few trachytes and phonolites (Fig. 2; Pouclet et al., 2016 and references therein). The Rungwe province lavas are mostly alkaline, including basanites, nephelinites and trachy-phonolites, but lack the highly potassic or sodic compositions seen in other Western Branch provinces (Furman, 1995; Castillo et al., 2014).

Both Toro Ankole and Virunga lavas are compositionally different from MER lavas (Fig. 2). Primitive MER lavas include mostly tholeiitic and transitional-alkalic basalts, trachy-basalts and very few basanites (Furman et al., 2006b; Castillo et al., 2020), while rhyolite and trachyte make up the more evolved lavas. Overall, Toro Ankole and Virunga lavas are more silica-undersaturated and more alkalic and/or potassic than MER lavas.

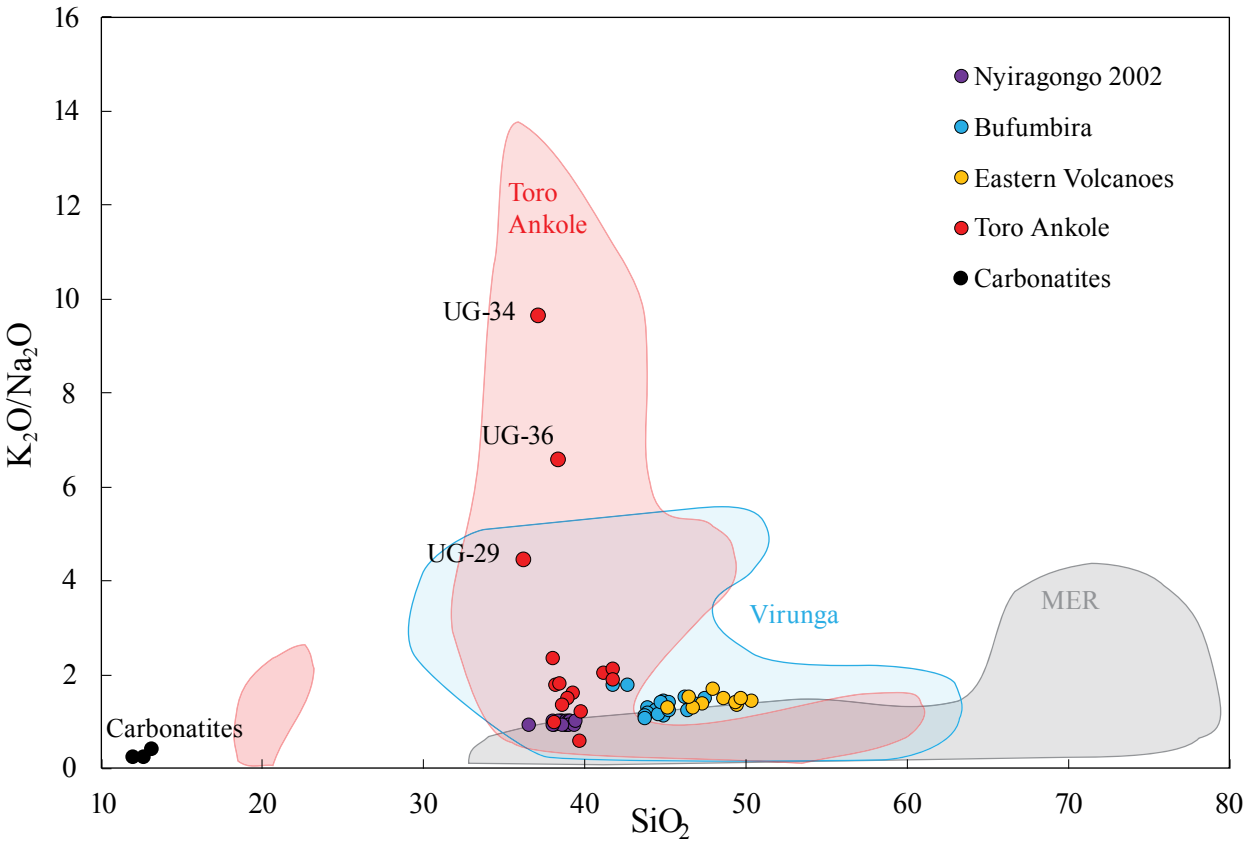

Figure 3. K_2O/Na_2O—SiO_2 plot for Toro Ankole and Virunga lavas. Symbols for Toro Ankole and Virunga (Bufumbira and eastern volcano) lavas are the same as in Fig. 2. Also included are the carbonatite samples from Toro Ankole. The labeled Toro Ankole samples: UG-29, UG-34, UG-36 are olivine melilitite, kamafugite, and ugandite, respectively. Lavas from the 2002 Nyiragongo eruption (Chakrabarti et al., 2009a) are plotted as purple circles for reference. Fields are based on the bulk of Toro Ankole, Virunga and MER data, respectively from GEOROC (https://georoc.mpch-mainz.gwdg.de//). The field for Virunga excludes few samples with high K_2O/Na_2O (> 6) for clarity.

4.3. Trace Elements

Toro Ankole and Virunga lavas are enriched in incompatible trace elements (Table 2; Figs. 4A and B), similar to previous results (e.g., Pitcavage et al., 2021). They have a more geochemically enriched normalized-concentration pattern than OIB. Significantly, despite generally being highly potassic, unlike OIB, they have relatively negative K anomaly and most Virunga samples exhibit a positive Pb concentration anomaly (see also Pitcavage et al., 2021). In detail, the trace element concentrations of Toro Ankole and Virunga lavas differ. Toro Ankole is more geochemically enriched than Virunga. The carbonatites are the most enriched and also have the highest absolute trace element contents, except that they also have the lowest Rb and K – almost two orders of magnitude lower than the most K-depleted Toro Ankole lavas. Toro Ankole lavas have no anomalous positive Pb concentration anomaly, unlike Virunga lavas that show a spike in Pb (cf. Pitcavage et al., 2021). The trace element differences between the two volcanic provinces can be summarized through their incompatible trace element concentration patterns (Figs. 4A and B). For instance, Toro Ankole lavas have higher light- and middle-REE than Virunga lavas, but the latter have higher heavy-REE than the former. The average La/Yb_N value of Toro Ankole lavas is ~87 (~90 with carbonatites) whereas that of Virunga lavas is ~26, (25.8 for eastern volcanoes and 26.2–27.2 for Bufumbira). The average Toro Ankole La/Yb_N value is also higher than that of Nyiragongo lavas particularly than the average of the 2002 eruption (41; Chakrabarti et al., 2009a). All these La/Yb_N values are also higher than that of MORB (12; Sun and McDonough, 1989).

In comparison with the trace element data for the rest of the Western Branch lavas, Virunga and Toro Ankole lavas either plot above or overlap with the most enriched lavas from Rungwe and South Kivu provinces (Figs. 4A and B). In detail, Virunga mostly overlap with the

Table 2. Trace element composition (in ppm) and select trace element ratios for Toro Ankole and Virunga lavas. Reference values for BHVO-2 taken from Jochum et al. (2016). * K calculated from major element analysis. ** Ratios normalized to chondritic values (Sun and McDonough, 1989).

Virunga															
Bufumbira															
Sample	Li	Be	B	Sc	V	Cr	Co	Ni	Cu	Zn	Ga	Ge	Se	Rb	Sr
UG- 1	6.78	1.38	43.1	30.6	311	368	49.5	107	36.4	89.5	19.7	2.20	0.31	91.0	866
UG- 2	6.89	1.50	45.3	27.0	293	504	51.6	165	28.2	90.5	19.2	2.13	0.28	95.7	916
UG- 3	5.27	1.24	66.9	25.1	288	721	69.0	380	43.9	77.7	15.1	2.05	0.24	96.7	766
UG- 4	5.25	1.25	70.7	23.5	279	678	67.5	372	53.6	105	15.1	2.00	0.26	95.5	769
UG- 5	6.12	1.64	48.5	26.6	313	201	40.3	43.5	16.6	104	21.9	2.41	0.31	80.4	998
UG- 6	4.56	1.36	118	27.0	271	763	65.5	346	46.3	80.3	16.8	1.99	0.21	59.2	743
UG- 17	7.72	1.89	38.0	29.9	316	465	49.6	159	55.3	99.8	21.6	2.44	0.31	115	993
UG- 18	11.4	2.08	40.6	23.3	305	159	36.2	32.7	19.2	104	23.9	2.45	0.33	101	914
UG- 19	11.4	1.99	63.9	25.0	304	235	37.9	29.3	15.8	101	23.3	2.38	0.32	135	1010
UG- 20	11.4	2.06	52.3	24.9	304	233	37.4	29.4	15.6	99.9	23.0	2.36	0.31	157	990
UG- 21	12.8	2.31	44.7		277	210		27.3	17.5	108	24.0	2.36	0.31	143	1076
UG- 22	10.7	2.43	47.6		287	441	45.1	152	41.6	104	21.5	2.51	0.35	109	1329
UG- 23	10.9	2.56	2.22	22.9	280	505	48.3	213	42.8	104	21.0	2.59	0.39	99.6	1363
UG- 24	9.78	2.27	1.07	25.8	286	591	53.8	271	64.7	101	20.1	2.49	0.33	92.5	1255
UG- 25	12.5	2.98	9.45	20.5	280	167	35.8	60.2	37.6	110	23.6	2.81	0.43	117	1587
UG- 26	6.65	1.82	1.59	32.8	311	729	56.1	196	53.9	96.3	18.1	2.24	0.26	87.2	964
UG- 27	7.66	1.76	5.66	34.1	339	536	54.9	142	53.0	92.6	19.8	2.35	0.28	96.6	964
UG- 28	9.16	2.24	2.07	25.0	275	284	41.1	60.5	27.8	108	22.7	2.42	0.32	101	1056
Eastern Volcanoes: Muhavura															
UG- 7	12.3	2.23	1.44	15.6	210	113	27.2	28.1	20.8	103	24.0	2.47	0.34	150	1088
UG- 8	17.1	1.85	44.1	18.2	259	79.8	31.0	10.8	7.56	107	24.7	2.37	0.32	118	976
UG- 9	10.5	1.90	135	23.0	299	296	39.9	35.2	18.6	96.8	22.4	2.31	0.30	120	966
UG- 10	11.4	2.04	44.8	26.7	309	357	44.0	69.1	23.2	97.7	21.9	2.40	0.33	182	1069
UG- 11	14.0	2.07	44.1	20.3	235	174	31.6	38.7	12.6	102	23.9	2.52	0.37	147	1056

Table 2 (continued)

Eastern Volcanoes:															
Sample	Li	Be	B	Sc	V	Cr	Co	Ni	Cu	Zn	Ga	Ge	Se	Rb	Sr
Sabinyo															
UG- 12	11.6	1.98	45.1	21.0	286	111	34.8	27.6	22.4	105	24.3	2.43	0.35	103	945
UG- 13	10.6	2.18	61.7	22.3	294	150	35.1	30.0	18.8	97.9	23.7	2.38	0.32	154	940
Gahinga															
UG- 14	11.9	2.95	49.5	11.4	193	26.6	21.6	12.3	9.88	100	25.1	2.55	0.37	161	1329
UG- 15	17.4	2.32	47.6	16.7	314	20.4	28.1	7.70	8.71	109	25.3	2.36	0.34	127	919
UG- 16	12.4	2.09	45.7	20.4	299	300	42.3	37.5	16.7	105	23.5	2.36	0.31	209	1097
Bufumbira															
Sample	Y	Zr	Nb	Mo	Sn	Cs	Ba	La	Ce	Pr	Nd	Sm	Eu	Gd	Tb
UG- 1	26.0	259	91.0	2.80	1.63	0.86	1078	71.3	147	16.7	62.2	10.2	2.89	9.19	1.07
UG- 2	25.2	268	99.7	3.39	1.77	0.94	962	76.2	157	17.7	63.9	10.1	2.83	9.23	1.06
UG- 3	18.7	210	88.1	2.17	1.54	0.95	1012	64.4	132	15.1	55.5	8.75	2.60	7.92	0.86
UG- 4	18.7	212	89.6	2.54	1.53	0.71	939	64.7	133	15.2	56.1	8.74	2.57	7.92	0.86
UG- 5	30.5	308	117	3.07	1.84	0.81	1064	89.9	186	20.9	74.9	11.7	3.33	11.0	1.27
UG- 6	21.7	219	81.0	2.21	1.45	0.74	819	62.0	126	14.5	53.7	8.73	2.46	7.86	0.90
UG- 17	29.1	304	121	2.97	1.83	1.06	1220	86.7	179	20.2	73.2	11.5	3.28	10.4	1.18
UG- 18	31.0	342	115	3.68	2.22	1.06	1338	94.4	192	21.3	76.1	11.8	3.22	10.9	1.24
UG- 19	29.4	324	118	2.92	2.02	1.43	1198	88.1	180	20.2	71.0	11.1	3.16	10.4	1.19
UG- 20	28.8	322	117	2.97	1.96	1.40	1191	87.5	179	20.2	72.3	11.3	3.16	10.2	1.16
UG- 21	29.5	350	131	3.49	2.19	1.62	1336	98.5	197	21.4	73.8	11.4	3.23	10.4	1.18
UG- 22	30.2	348	148	4.40	2.06	1.15	1290	108	218	24.4	87.0	13.2	3.74	11.7	1.27
UG- 23	29.3	354	163	4.99	2.02	1.18	1212	116	232	25.4	91.2	13.6	3.78	12.1	1.28
UG- 24	27.3	320	143	4.38	1.87	1.00	1178	105	212	23.5	82.5	12.6	3.48	11.2	1.21
UG- 25	33.4	418	193	4.88	2.30	1.41	1383	135	267	28.6	102	15.3	4.28	13.8	1.45
UG- 26	23.0	252	108	3.67	1.67	0.85	1016	77.7	157	17.9	64.5	9.83	2.79	8.92	0.98
UG- 27	25.5	261	101	2.87	1.71	0.95	1074	77.9	162	18.4	66.4	10.4	2.97	9.49	1.06
UG- 28	30.5	332	121	2.99	1.91	1.01	1017	91.1	186	20.6	73.1	11.6	3.26	10.7	1.20

Table 2 (continued)

Eastern Volcanoes:															
Sample	Y	Zr	Nb	Mo	Sn	Cs	Ba	La	Ce	Pr	Nd	Sm	Eu	Gd	Tb
Muhavura															
UG- 7	30.8	396	139	3.78	2.27	1.67	1300	119	239	26.0	90.9	13.6	3.52	12.2	1.32
UG- 8	32.0	335	115	3.27	2.12	1.48	1284	92.9	191	21.2	75.7	11.8	3.33	11.1	1.24
UG- 9	26.9	309	117	3.44	2.00	1.50	1189	86.9	174	19.3	68.8	10.8	3.01	9.87	1.11
UG- 10	26.7	322	123	3.92	2.06	1.86	1225	93.5	188	21.1	75.1	11.6	3.29	10.6	1.15
UG- 11	30.1	369	129	2.77	2.24	1.07	1274	107	218	23.8	84.5	12.8	3.38	11.5	1.25
Sabinyo															
UG- 12	31.1	344	117	2.67	2.25	0.90	1354	93.9	190	21.2	74.4	11.4	3.22	10.8	1.24
UG- 13	30.5	334	112	3.39	2.21	1.61	1354	94.8	190	21.1	74.3	11.5	3.20	10.6	1.21
Gahinga															
UG- 14	32.6	400	149	4.95	2.52	2.01	1150	123	241	26.2	91.8	13.6	3.65	12.3	1.32
UG- 15	30.9	336	116	2.94	2.32	1.14	1344	86.9	179	20.2	72.7	11.7	3.26	10.8	1.24
UG- 16	26.9	331	129	2.73	2.15	1.74	1345	92.6	186	20.4	72.9	11.0	3.12	10.1	1.11

Bufumbira													
Sample	Dy	Ho	Er	Tm	Yb	Lu	Hf	Ta	W	Tl	Pb	Th	U
UG- 1	5.49	1.00	2.67	0.35	2.24	0.32	6.33	5.38	1.06	0.12	8.93	11.5	2.12
UG- 2	5.32	0.96	2.61	0.33	2.13	0.30	6.43	6.02	1.39	0.10	9.45	12.4	2.40
UG- 3	4.11	0.74	1.98	0.25	1.54	0.22	5.20	5.25	0.86	0.08	5.90	9.17	1.83
UG- 4	4.22	0.74	1.98	0.25	1.51	0.22	5.23	5.37	1.05	0.31	5.57	9.53	1.94
UG- 5	6.40	1.18	3.28	0.43	2.76	0.39	7.43	7.17	1.62	0.00	9.75	15.0	2.75
UG- 6	4.61	0.83	2.27	0.29	1.88	0.27	5.40	4.96	1.06	0.00	6.67	10.1	1.95
UG- 17	6.00	1.09	3.00	0.38	2.45	0.35	7.20	7.17	1.32	0.31	9.66	14.3	2.57
UG- 18	6.34	1.17	3.25	0.43	2.73	0.39	8.04	6.81	1.61	0.11	12.5	18.1	3.04
UG- 19	6.06	1.10	3.07	0.40	2.53	0.36	7.47	6.93	1.39	0.10	10.3	15.9	2.95
UG- 20	5.92	1.09	3.00	0.39	2.48	0.37	7.44	6.89	1.37	0.10	9.88	15.6	2.94
UG- 21	5.93	1.10	3.06	0.40	2.61	0.37	7.65	7.83	1.56	0.12	11.7	18.0	3.34
UG- 22	6.25	1.11	3.06	0.39	2.48	0.35	7.47	8.24	1.79	0.16	13.7	17.7	3.53

Table 2 (continued)

Bufumbira															
Sample	Dy	Ho	Er	Tm	Yb	Lu	Hf	Ta	W	Tl	Pb	Th	U		
UG- 23	6.14	1.07	3.00	0.38	2.38	0.35	7.55	8.95	2.03	0.14	14.8	19.7	3.92		
UG- 24	5.80	1.04	2.87	0.36	2.28	0.32	7.02	8.15	1.58	0.13	13.6	17.8	3.50		
UG- 25	6.96	1.24	3.35	0.43	2.75	0.40	8.54	10.66	2.31	0.11	18.5	23.4	4.75		
UG- 26	4.75	0.86	2.37	0.31	1.91	0.27	5.72	6.11	1.44	0.01	8.89	12.9	2.49		
UG- 27	5.32	0.95	2.57	0.33	2.05	0.29	6.24	5.93	1.15	0.13	9.80	12.6	2.38		
UG- 28	5.96	1.12	3.17	0.41	2.65	0.38	7.44	7.10	1.26	0.06	11.0	14.8	2.79		
Eastern Volcanoes:															
Muhavura															
UG- 7	6.33	1.16	3.29	0.43	2.79	0.40	9.19	8.48	1.73	0.07	19.0	24.9	4.43		
UG- 8	6.36	1.20	3.34	0.44	2.78	0.41	7.79	6.92	0.85	0.10	13.0	17.2	2.99		
UG- 9	5.57	1.01	2.83	0.37	2.40	0.34	7.23	6.90	1.47	0.07	10.8	15.9	2.99		
UG- 10	5.58	1.01	2.75	0.35	2.25	0.32	7.41	7.30	1.54	0.27	12.3	17.3	3.21		
UG- 11	6.20	1.12	3.16	0.41	2.60	0.37	8.54	7.65	1.12	0.14	16.9	21.8	3.51		
Sabinyo															
UG- 12	6.35	1.16	3.27	0.43	2.75	0.39	7.92	6.90	1.14	0.10	12.4	18.6	2.78		
UG- 13	6.20	1.15	3.23	0.42	2.71	0.39	8.00	6.67	1.51	0.25	12.5	18.5	3.03		
Gahinga															
UG- 14	6.58	1.19	3.34	0.44	2.80	0.40	8.78	8.60	2.58	0.20	18.4	23.8	4.37		
UG- 15	6.30	1.16	3.17	0.42	2.66	0.39	7.95	6.82	1.55	0.20	16.5	16.4	3.29		
UG- 16	5.51	1.01	2.79	0.37	2.37	0.34	7.45	7.62	1.24	0.27	11.4	17.2	3.01		
Toro Ankole															
Sample	Li	Be	B	Sc	V	Cr	Co	Ni	Cu	Zn	Ga	Ge	Se	Rb	Sr
UG-29	11.5	2.77	2.81	28.0	232	500	54.9	228	137	107	16.3	3.94	0.60	121	2766
Bunyaruguru															
UG-34	8.47	2.34	20.7	22.8	136	565	60.9	346	116	99.6	15.6	2.71	0.46	194	2128
UG-36	7.21	1.87	23.8	13.1	184	808	74.3	691	99.6	91.6	13.5	2.24	0.29	168	1056

Table 2 (continued)

Katwe-Kikorongo															
Sample	Li	Be	B	Sc	V	Cr	Co	Ni	Cu	Zn	Ga	Ge	Se	Rb	Sr
UG-39B	6.29	1.67	3.39	45.1	375	502	61.2	128	101	98.5	17.4	2.65	0.28	76.3	1579
UG-42	8.28	2.40	6.09	32.5	374	347	51.9	95.2	133	107	20.7	2.94	0.40	99.5	1715
UG-43	10.6	2.93	60.9	30.1	454	103	48.4	49.5	173	118	22.2	3.38	0.49	94.2	2171
UG-44	5.64	1.44	7.64	49.5	369	446	60.4	115	89.2	106	17.1	2.64	0.29	56.5	1356
UG-45	12.1	3.47	9.60	17.3	442	156	46.4	65.5	184	123	23.5	3.77	0.67	111	3229
UG-46	10.9	3.49	1.39	19.3	491	24.4	42.5	27.2	192	124	24.4	3.75	0.66	142	2517
UG-47	8.53	2.25	2.34	34.8	374	418	53.1	103	122	105	20.2	2.86	0.40	106	1663
UG-48	8.72	2.57	3.71	34.4	440	208	53.6	68.5	135	119	21.4	3.53	0.51	86.2	2130
UG-49	8.38	2.89	2.34	30.7	445	133	50.2	56.2	156	120	22.0	3.53	0.58	86.0	2271
UG-52	9.34	2.31	0.82	36.1	388	398	53.8	103	128	108	20.3	2.89	0.38	103	1281
UG-53	8.73	3.42	1.61	20.4	508	33.4	43.2	30.2	179	123	24.4	3.73	0.59	140	2153
UG-55	7.07	1.70	2.75	47.1	382	408	58.0	107	88.4	97.6	16.4	2.58	0.29	32.1	1906
Fort Portal															
UG-61A	20.8	6.71	5.13	12.8	300	55.9	31.3	27.4	25.7	160	16.2	6.20	1.30	13.7	5720
UG-61B	21.1	6.94	2.31	14.0	317	65.6	32.8	30.6	27.6	166	17.1	6.43	1.36	6.30	5007
UG-63	18.7	6.70	3.33	12.6	289	48.9	31.7	24.9	25.6	166	15.8	6.36	1.37	5.81	5624
Standards															
Measured															
BHVO-2 avg.	4.80	1.08	2.80	32.0	317	280	45.0	119	127	103	22.0	1.60	0.18	9.12	396
Reference															
BHVO-2	4.50	1.08	2.95	31.8	318	287	44.9	120	129	104	21.4	1.62	0.18	9.26	394
Toro Ankole															
Sample	Y	Zr	Nb	Mo	Sn	Cs	Ba	La	Ce	Pr	Nd	Sm	Eu	Gd	Tb
UG-29	19.1	347	271	1.41	2.88	0.46	2383	223	459	47.9	163	21.6	5.8	17.9	1.44
Bunyaruguru															
UG-34	15.2	353	204	0.39	2.62	1.04	4312	146	295	30.9	111	14.7	4.6	12.2	1.03
UG-36	10.3	284	163	0.29	2.02	0.58	2057	116	231	24.5	82.0	10.4	3.0	8.85	0.73

Table 2 (continued)

Katwe-Kikorongo															
Sample	Y	Zr	Nb	Mo	Sn	Cs	Ba	La	Ce	Pr	Nd	Sm	Eu	Gd	Tb
UG-39B	12.4	243	129	0.30	2.44	0.79	1659	91.1	198	22.9	83.3	11.6	3.2	9.26	0.84
UG-42	17.4	327	178	0.76	2.71	1.04	1277	128	274	29.9	109	14.8	4.0	12.2	1.11
UG-43	20.2	425	230	4.78	3.17	1.11	2458	163	347	37.6	139	18.7	5.2	15.2	1.33
UG-44	11.8	209	118	0.76	2.47	0.88	1661	84.4	189	21.4	78.1	10.8	3.1	8.73	0.80
UG-45	25.3	539	310	1.11	3.42	1.26	1819	227	455	48.0	165	23.0	6.2	19.1	1.68
UG-46	23.4	482	283	0.59	3.42	1.60	1817	199	428	46.0	163	22.4	5.9	18.0	1.59
UG-47	17.0	299	172	1.26	2.74	1.19	1651	122	263	28.7	102	14.0	3.8	11.6	1.07
UG-48	18.4	357	218	1.86	3.22	1.16	1830	162	352	38.7	140	18.6	4.9	14.8	1.30
UG-49	20.3	403	238	0.59	3.14	1.06	2227	174	375	41.1	149	19.3	5.2	15.9	1.39
UG-52	16.4	306	170	0.62	2.60	1.08	1949	118	251	28.3	103	14.1	3.9	11.3	1.04
UG-53	23.1	469	280	0.91	3.41	1.40	1800	198	425	46.1	163	22.0	5.8	17.8	1.58
UG-55	12.4	231	125	16.6	2.54	1.03	872	86.6	189	21.8	79.2	10.9	3.0	8.86	0.81
Fort Portal															
UG-61A	43.2	587	532	1.44	3.13	1.21	2420	447	816	92.4	315	43.3	11.8	36.0	3.19
UG-61B	48.3	620	549	2.85	3.20	0.57	2580	468	871	97.3	332	45.6	12.3	37.8	3.42
UG-63	41.0	600	561	1.78	3.12	0.22	2430	452	776	91.5	315	42.9	11.8	36.4	3.22
Standards															
Measured															
BHVO-2 avg.	26.1	173	18.2	3.77	1.72	0.10	131	15.2	37.6	5.36	24.5	6.05	2.07	6.23	0.92
Reference															
BHVO-2	25.9	171	18.1	4.07	1.78	0.10	131	15.2	37.5	5.34	24.3	6.02	2.04	6.21	0.94
Toro Ankole															
Sample	Dy	Ho	Er	Tm	Yb	Lu	Hf	Ta	W	Tl	Pb	Th	U		
UG-29	4.89	0.73	2.03	0.20	1.25	0.18	8.29	13.5	0.96	0.10	10.8	29.9	7.02		
Bunyaruguru															
UG-34	3.81	0.58	1.56	0.16	0.98	0.13	8.41	11.3	0.41	0.23	10.8	18.9	4.36		
UG-36	2.67	0.41	1.13	0.12	0.72	0.10	7.04	10.2	0.35	0.07	7.30	14.9	3.38		

Table 2 (continued)

Katwe-Kikorongo													
Sample	Dy	Ho	Er	Tm	Yb	Lu	Hf	Ta	W	Tl	Pb	Th	U
UG-39B	3.19	0.48	1.25	0.13	0.79	0.11	6.42	8.25	0.39	0.04	5.35	11.4	2.19
UG-42	4.36	0.68	1.83	0.20	1.21	0.17	8.07	11.5	0.38	0.09	10.6	19.3	2.86
UG-43	5.10	0.78	2.12	0.22	1.34	0.18	9.81	14.4	3.67	0.07	9.47	23.1	4.82
UG-44	3.04	0.46	1.18	0.12	0.74	0.10	6.14	7.60	0.60	0.06	5.47	10.8	2.14
UG-45	6.37	0.97	2.56	0.27	1.63	0.23	10.9	15.9	0.97	0.12	16.3	30.8	8.04
UG-46	5.95	0.92	2.47	0.25	1.54	0.21	11.0	18.1	0.81	0.10	14.5	29.8	6.02
UG-47	4.20	0.66	1.75	0.19	1.17	0.16	7.61	10.7	0.49	0.09	10.16	17.3	2.09
UG-48	4.83	0.74	1.98	0.20	1.22	0.16	8.82	14.0	1.54	0.08	9.16	21.9	4.50
UG-49	5.16	0.79	2.12	0.21	1.33	0.18	9.64	15.4	0.53	0.10	12.0	25.6	4.84
UG-52	4.05	0.63	1.71	0.18	1.13	0.16	7.75	10.5	0.28	0.12	9.77	17.0	1.69
UG-53	5.77	0.89	2.44	0.24	1.51	0.21	11.0	17.7	1.10	0.09	14.5	28.8	6.06
UG-55	3.09	0.48	1.27	0.13	0.82	0.11	6.39	7.72	0.23	0.07	5.75	11.3	2.64
Fort Portal													
UG-61A	12.6	1.98	5.22	0.51	3.05	0.42	7.85	20.5	3.38	0.11	29.2	28.0	13.7
UG-61B	13.2	2.09	5.49	0.55	3.25	0.44	8.16	21.3	3.90	0.12	30.2	38.7	14.3
UG-63	12.3	1.92	5.04	0.50	2.88	0.39	7.74	21.9	5.65	0.11	28.6	30.0	14.5
Standards													
Measured													
BHVO-2 avg.	5.30	0.98	2.55	0.33	2.00	0.27	4.37	1.14	0.29	0.02	1.59	1.22	0.40
Reference													
BHVO-2	5.28	0.99	2.51	0.33	1.99	0.28	4.47	1.15	0.25	0.02	1.7	1.22	0.41

Table 2 (continued)

Virunga									
Bufumbira									
Sample	Zr/Hf	Ti/Eu	Ce/Pb	Nb/U	K/Th*	Rb/Sr	Ba/Rb	La/Yb(N)**	Dy/Yb(N)**
UG-1	41.0	6354	16.4	42.9	2196	0.11	11.9	21.6	1.60
UG-2	41.7	6290	16.6	41.5	1854	0.10	10.1	24.3	1.64
UG-3	40.4	6573	22.4	48.3	2454	0.13	10.5	28.4	1.74
UG-4	40.6	6535	23.9	46.2	2422	0.12	9.83	29.1	1.83
UG-5	41.5	6469	19.1	42.4	1759	0.08	13.3	22.1	1.52
UG-6	40.6	6298	18.9	41.6	1716	0.08	13.8	22.4	1.61
UG-17	42.2	6035	18.6	47.1	1437	0.12	10.6	24.0	1.60
UG-18	42.6	6489	15.4	37.7	1693	0.11	13.2	23.5	1.52
UG-19	43.3	6318	17.6	40.1	1892	0.13	8.84	23.6	1.57
UG-20	43.4	6334	18.2	39.8	2016	0.16	7.60	24.0	1.56
UG-21	45.7	6222	16.9	39.2	1629	0.13	9.31	25.6	1.49
UG-22	46.5	4801	15.9	41.9	1702	0.08	11.9	29.7	1.65
UG-23	46.8	4915	15.7	41.5	1515	0.07	12.2	33.1	1.69
UG-24	45.6	5125	15.7	41.0	1524	0.07	12.7	31.3	1.66
UG-25	49.0	4440	14.4	40.6	1526	0.07	11.8	33.4	1.66
UG-26	44.0	6268	17.7	43.4	1474	0.09	11.7	27.7	1.63
UG-27	41.9	6471	16.5	42.4	1891	0.10	11.1	25.8	1.70
UG-28	44.6	5580	16.9	43.3	1837	0.10	10.1	23.4	1.47
Eastern Volcanoes:									
Muhavura									
UG-7	43.2	4347	12.6	31.4	1516	0.14	8.66	29.1	1.49
UG-8	43.0	5785	14.7	38.5	1945	0.12	10.9	22.7	1.50
UG-9	42.7	6458	16.1	39.2	1965	0.12	9.90	24.6	1.52
UG-10	43.5	5907	15.4	38.4	1414	0.17	6.73	28.2	1.62
UG-11	43.3	4892	12.9	36.7	1480	0.14	8.68	28.1	1.56
Sabinyo									
UG-12	43.4	6490	15.4	42.1	1767	0.11	13.1	23.2	1.51
UG-13	41.8	6190	15.2	36.9	1529	0.16	8.80	23.8	1.50
Gahinga									
UG-14	45.6	4276	13.1	34.0	1637	0.12	7.12	29.8	1.54
UG-15	42.3	6468	10.8	35.4	2180	0.14	10.6	22.2	1.55
UG-16	44.4	6633	16.3	42.9	1800	0.19	6.44	26.6	1.52

Table 2 (continued)

Toro Ankole									
Sample	Zr/Hf	Ti/Eu	Ce/Pb	Nb/U	K/Th*	Rb/Sr	Ba/Rb	La/Yb(N)**	Dy/Yb(N)**
UG-29	41.9	4556	42.6	38.6	1327	0.04	19.7	121.2	2.55
Bunyaruguru									
UG-34	41.9	6971	27.4	46.8	2546	0.09	22.3	102	2.55
UG-36	40.3	10436	31.6	48.1	2285	0.16	12.2	110	2.43
Katwe-Kikorongo									
UG-39B	37.8	9639	37.0	58.8	1546	0.05	21.7	78.3	2.64
UG-42	40.5	7427	25.8	62.2	1628	0.06	12.8	71.9	2.36
UG-43	43.3	6759	36.6	47.7	994	0.04	26.1	82.6	2.48
UG-44	34.1	10196	34.5	55.2	1372	0.04	29.4	77.4	2.69
UG-45	49.3	4975	28.0	38.5	1095	0.03	16.4	95.0	2.56
UG-46	43.9	6127	29.5	47.1	1287	0.06	12.8	87.5	2.52
UG-47	39.2	7705	25.9	82.4	1908	0.06	15.6	71.0	2.35
UG-48	40.5	7201	38.4	48.4	1023	0.04	21.2	90.3	2.60
UG-49	41.8	6937	31.2	49.2	1023	0.04	25.9	88.9	2.54
UG-52	39.5	7678	25.7	100	1782	0.08	18.9	70.9	2.34
UG-53	42.6	6238	29.4	46.2	1445	0.07	12.8	89.0	2.50
UG-55	36.1	10355	32.9	47.1	882	0.02	27.1	72.0	2.47
Fort Portal									
UG-61A	74.8	865	28.0	38.9	29.6	<0.01	176	99.4	2.71
UG-61B	75.9	862	28.9	38.4	30.0	<0.01	409	97.8	2.66
UG-63	77.5	878	27.1	38.7	16.6	<0.01	418	107	2.80

Figure 4.Primitive mantle-normalized trace element diagrams for **(A)** Toro Ankole and **(B)** Virunga lavas. The normalizing OIB values in the plots are from Sun & McDonough (1989). (A) Toro Ankole samples are divided into volcanics from Bunyaruguru and Katunga, and carbonatites from Fort Portal. Fields for Bunyaruguru and Katwe-Kikorongo volcanics (Pitcavage et al., 2021) are included for reference. (B) Virunga samples are divided by regions; Bufumbira and the eastern volcanoes of Muhavura, Gahinga, Sabinyo. Data for Bufumbira and Nyiragongo volcanics from Pitcavage et al. (2021) and Chakrabarti et al. (2009a), respectively, are shown as fields. Fields for South Kivu and Rungwe are for mafic (SiO_2 < 53 wt%) lavas compiled from GEOROC (https://georoc.mpch-mainz.gwdg.de//). Field for MER lavas are for Quaternary basaltic lavas from central and northern MER – south Afar transition (Meshesha et al., 2021; Rooney et al., 2012; Hutchison et al., 2018; Ayalew et al., 2016). Trace element diagrams for southern Ethiopia, NW Ethiopia, and central MER are additionally shown in Supplemental Figure 1.

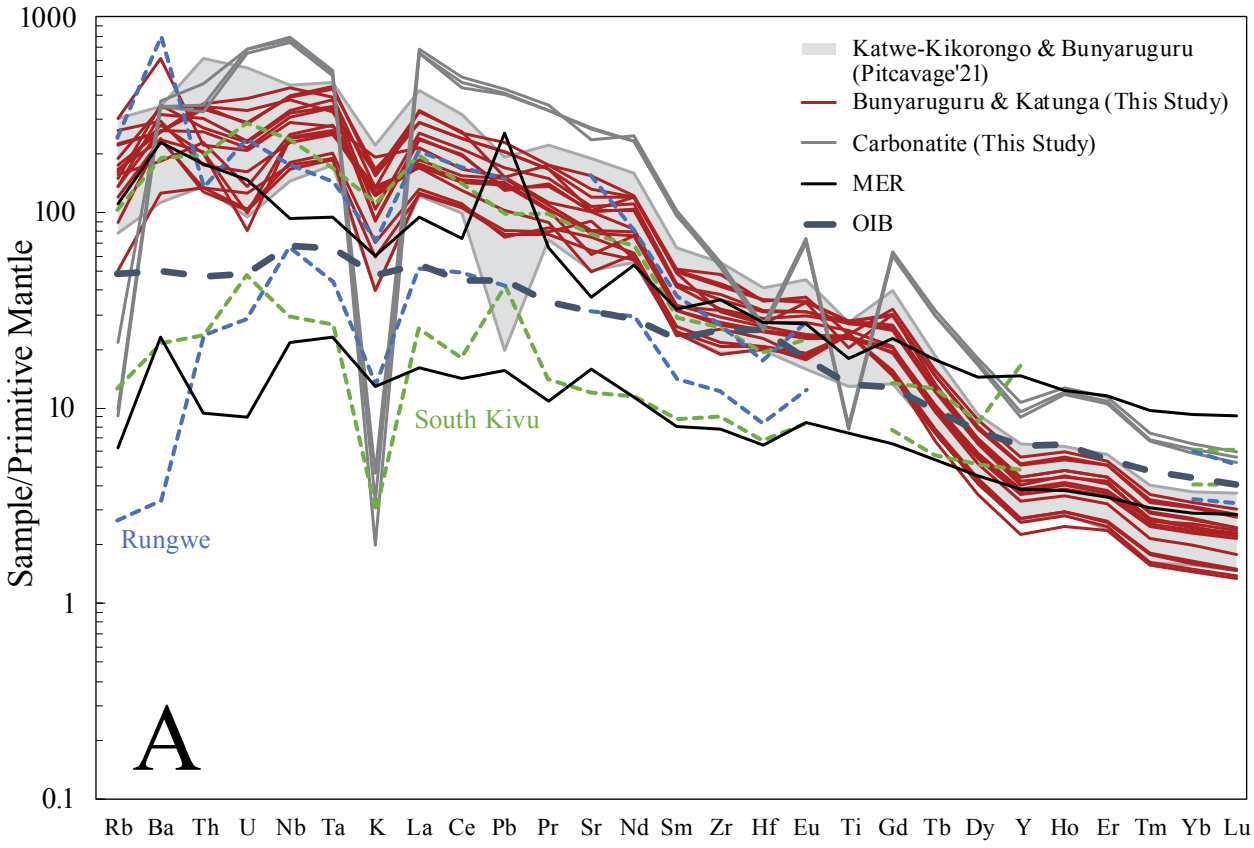
1000
100
10
1
0.1
Sample/Primitive Mantle
Katwe-Kikorongo & Bunyaruguru (Pitcavage'21)
Bunyaruguru & Katunga (This Study)
Carbonatite (This Study)
MER
OIB
South Kivu
Rungwe
A
Rb Ba Th U Nb Ta K La Ce Pb Pr Sr Nd Sm Zr Hf Eu Ti Gd Tb Dy Y Ho Er Tm Yb Lu

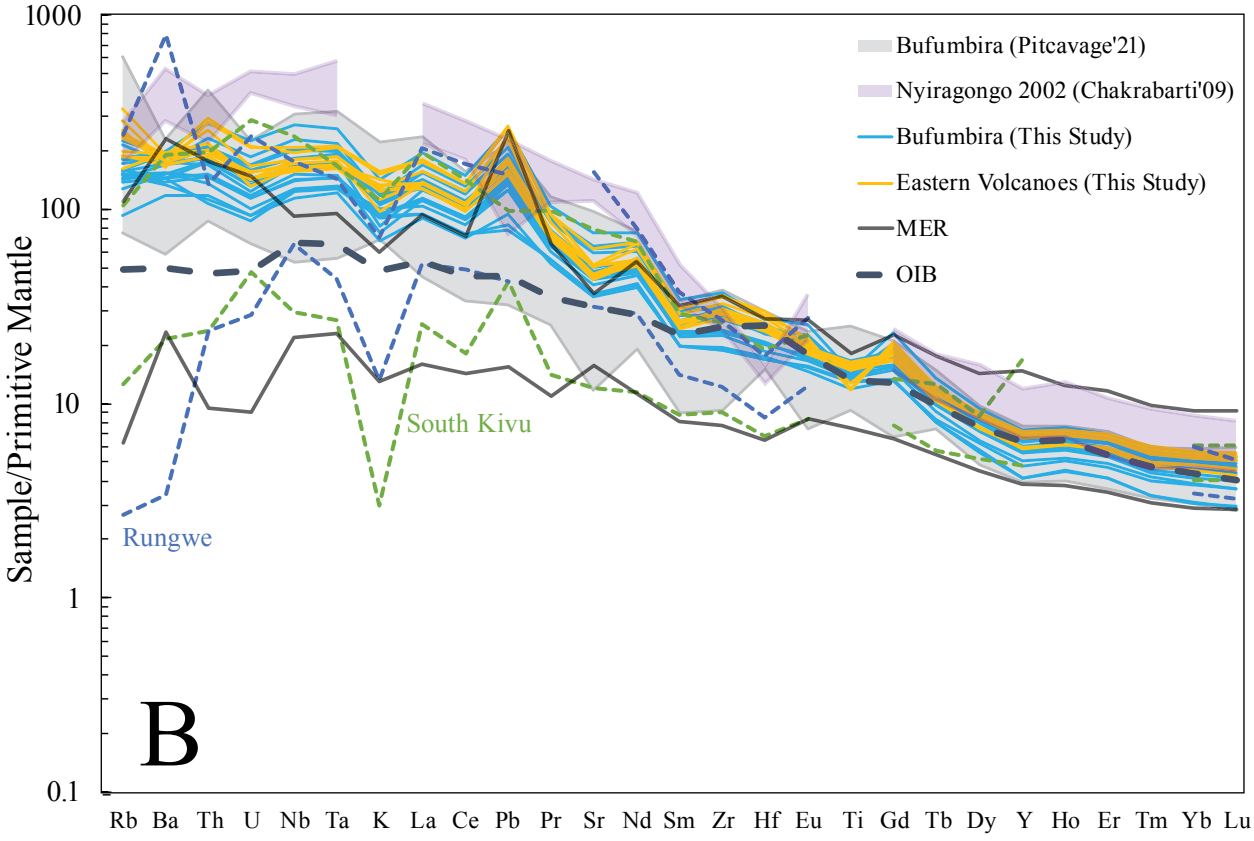
1000
100
10
1
0.1
Sample/Primitive Mantle
Bufumbira (Pitcavage'21)
Nyiragongo 2002 (Chakrabarti'09)
Bufumbira (This Study)
Eastern Volcanoes (This Study)
MER
OIB
South Kivu
Rungwe
B
Rb Ba Th U Nb Ta K La Ce Pb Pr Sr Nd Sm Zr Hf Eu Ti Gd Tb Dy Y Ho Er Tm Yb Lu

upper bounds of Rungwe and South Kivu whereas Toro Ankole mostly plot above. Toro Ankole and, to a lesser extent, Virunga samples are more fractionated in REE compared to Rungwe (average $La/Yb_N = 24$) and South Kivu (average $La/Yb_N = 20$).

Toro Ankole and Virunga lavas are more geochemically enriched than most Eastern Branch lavas, which generally show variable enrichment from southern Ethiopia, the MER, and NW Ethiopia (Figs. 4A, B; Supplementary Figs. 1A–C). The La/Yb_N of southern Ethiopia lavas ranges from 4 to 7 for pre-rift flood basalts to an average value of ~12 for syn-rift and Quaternary basalts. For the MER, there is mostly no change from early rift to Quaternary lavas (average La_N/Yb_N ~8). Finally, in the NW Ethiopian plateaus, the average La/Yb_N for pre-rift low-titanium basalts is ~3 and for high-titanium basalts it is ~8, while for Quaternary basaltic lavas it is ~7. Thus, although there are some regional and slight temporal variations in REE contents of Ethiopia lavas from the Eastern Branch, overall, they almost all have relatively less enriched incompatible trace element concentration patterns compared to Toro Ankole and Virunga lavas.

Significantly, ratios of Nb with other HFSE that are widely accepted to be least affected by weathering and alteration (e.g., Bienvenu et al., 1990) indicate some systematic differences among Toro Ankole, Virunga and Eastern Branch lavas. For example, Nb/Zr for given Nb and Zr in Toro Ankole and Virunga lavas are generally higher than Ethiopian lavas although there is some overlap between Virunga and Quaternary southern Ethiopian lavas (Fig. 5).

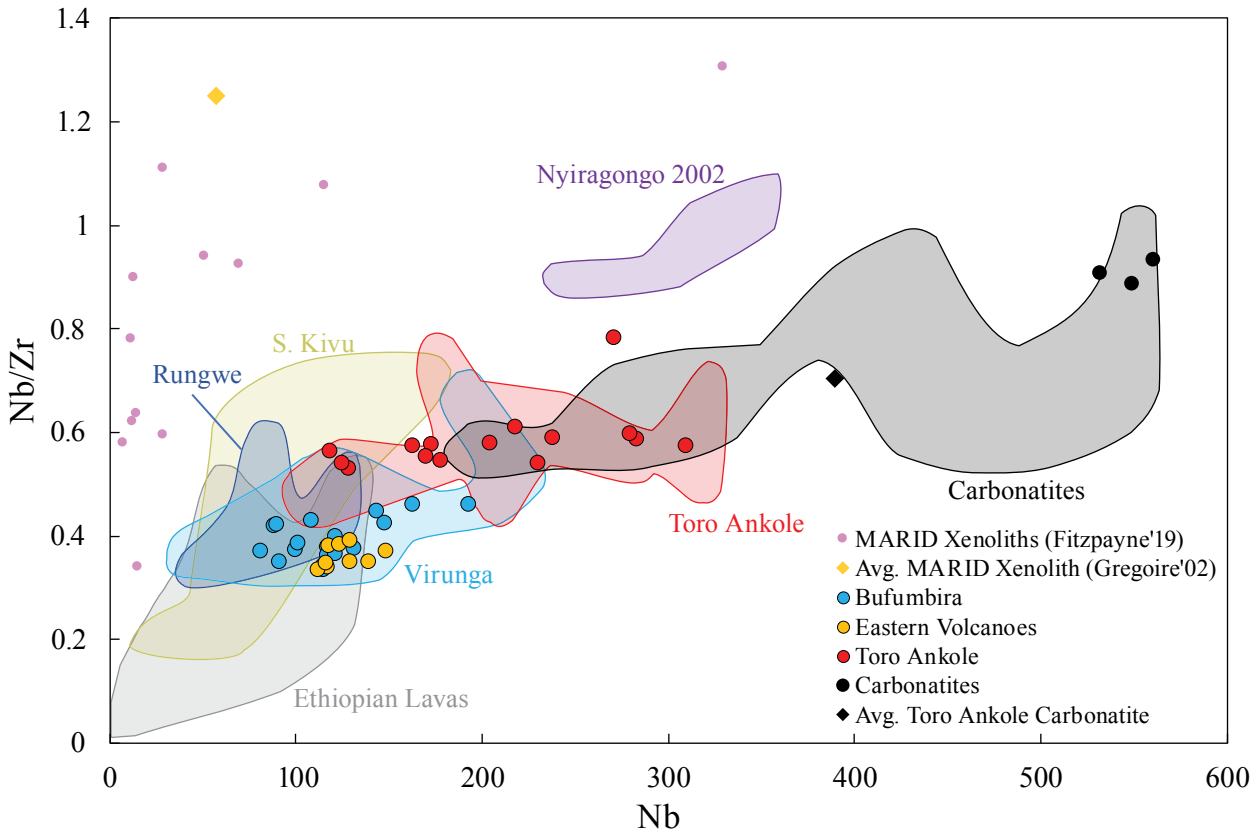

Figure 5. Nb/Zr vs Nb(ppm) plot for Toro Ankole and Virunga lavas showing extent of metasomatism experienced at source. Symbols used for Toro Ankole, Toro Ankole carbonatites, and Virunga lavas are the same as in Figure 3. Published data for Toro Ankole and Virunga (Pitcavage et al., 2021) and the 2002 Nyiragongo eruption (Chakrabarti et al., 2009a) are included as fields with corresponding colors. Fields for South Kivu, Rungwe, and Toro Ankole carbonatite data are taken from GEOROC (https://georoc.mpch-mainz.gwdg.de//). The average MARID xenolith (yellow diamond) calculated from xenoliths of Grégoire et al. (2002) and used in the REE modeling calculations discussed in the text and shown in Figures 10A and B and MARID xenoliths from Fitzpayne et al. (2019) are also shown. Eastern Branch data are represented by the Ethiopian lava field which is comprised of S. Ethiopia, NW Ethiopia, and central/northern MER lavas of Pre-Rift to Quaternary ages (George and Rogers, 2002; Stewart and Rogers, 1996; Feyissa et al., 2019; Shinjo, 2011; Rooney, 2010; Pik et al., 1999; Hutchison et al., 2018; Meshesha et al., 2021; Rooney et al., 2012; Ayalew et al., 2016).

4.4 Strontium and Pb Isotopes

Toro Ankole lavas, save for the carbonatites, have a ~moderate range of Sr ($^{87}Sr/^{86}Sr$ = 0.7050–0.7053) and Pb (e.g., $^{206}Pb/^{204}Pb$ = 18.96–19.40) isotope values (Table 3; Figs. 6A, B, and C). The former is within the range whereas the latter is slightly less radiogenic, on average, than previously published Toro Ankole data ($^{87}Sr/^{86}Sr$ = 0.7046–0.7053; $^{206}Pb/^{204}$/Pb = 19.28–19.57). In comparison, Virunga lavas have a wider range of Sr ($^{87}Sr/^{86}Sr$ = 0.7064–0.7086) and limited range of Pb (e.g., $^{206}Pb/^{204}Pb$ = 19.35–19.46) isotope values that are both completely within the range of published data ($^{87}Sr/^{86}Sr$ = 0.7055–0.7099; $^{206}Pb/^{204}Pb$ = 19.22–19.51). Notably, the large range in $^{87}Sr/^{86}Sr$ in Virunga lavas starts from ~0.7050 in the easternmost Bufumbira lavas and reaches upwards to ~0.7100 in eastern volcano lavas. The eastern volcano lavas also have more radiogenic $^{207}Pb/^{204}Pb$ and $^{208}Pb/^{204}Pb$ than Bufumbira lavas, despite their ~similar $^{206}Pb/^{204}Pb$ values. Virunga province as a whole is more radiogenic in $^{87}Sr/^{86}Sr$, $^{207}Pb^{204}Pb$, and $^{208}Pb/^{204}Pb$ than the Toro Ankole province and the Ethiopian lavas.

The carbonatites from Toro Ankole have the lowest $^{87}Sr/^{86}Sr$ (~0.7042) among Toro Ankole and Virunga samples. Their $^{87}Sr/^{86}Sr$ and $^{206}Pb/^{204}Pb$ values are respectively less radiogenic and more radiogenic than those in the carbonatites from Oldoinyo Lengai ($^{87}Sr/^{86}Sr$ = 0.7044 – 0.7050; $^{206}Pb/^{204}$/Pb = 18.51 – 19.30). Very interestingly, as have been shown previously, the eastern volcano and Bufumbira lavas define a unique, unusually vertical trend in $^{206}Pb/^{204}Pb$ versus $^{207}Pb/^{204}Pb$, $^{208}Pb/^{204}Pb$ and $^{87}Sr/^{86}Sr$ diagrams, with Toro Ankole, carbonatites, and Nyiragongo lavas defining a relatively broad base (Figs. 6B and C; see also, Vollmer and Norry, 1983a; Rogers et al., 1992.). These are in contrast to the generally positive Pb versus Pb and Sr isotope trends of other EARS lavas, particularly those of Ethiopian lavas.

Table 3. Sr, Pb isotope composition. E* = analytical error. E for $^{87}Sr/^{86}Sr$ refers to the last significant figure. **L refers to leachate whereas P refers to the residue.

Sample	$^{87}Sr/^{86}Sr$	E*	$^{206}Pb/^{204}Pb$	E	$^{207}Pb/^{204}Pb$	E	$^{208}Pb/^{204}Pb$	E
Virunga								
UG-06	0.706355	5	19.352	0.001	15.728	0.001	40.433	0.002
UG-15	0.708628	4	19.458	0.001	15.812	<0.001	40.088	0.001
UG-25	0.706730	8	19.397	0.003	15.766	0.003	40.489	0.007
Toro Ankole								
UG-34	0.705269	5	19.404	0.006	15.704	0.005	40.065	<0.001
UG-45	0.705005	3	18.958	0.003	15.671	0.002	40.424	0.006
UG-55	0.705200	3	19.168	0.010	15.668	0.009	39.786	0.022
UG-61A	0.704210	4	19.483	0.001	15.662	0.001	39.862	0.003
UG-61A P	0.704220	5	19.482	0.001	15.648	0.001	39.887	0.002
UG-61A L	0.704237	7	19.472	0.001	15.624	0.001	39.861	0.003
UG-63	0.704184	5	19.476	0.001	15.631	0.001	39.860	0.002
UG-63 P	0.704230	4	19.466	<0.001	15.624	<0.001	39.843	<0.001
UG-63 L	0.704204	6	19.535	0.001	15.709	0.001	40.053	0.002
BHVO-2 Avg.	0.703485	2	18.653	0.001	15.510	0.001	38.160	<0.001

Figure 6. **(A)** $^{87}Sr/^{86}Sr$ versus $^{206}Pb/^{204}Pb$, **(B)** $^{207}Pb/^{204}Pb$ versus $^{206}Pb/^{204}Pb$, and **(C)** $^{208}Pb/^{204}Pb$ versus $^{206}Pb/^{204}Pb$ diagrams for Toro Ankole and Virunga lavas. Symbols for Toro Ankole, Toro Ankole carbonatites, and Virunga samples are the same as in Figure 3; previously published data from the two provinces, plotted as smaller points with the respective colors, are from GEOROC (https://georoc.mpch-mainz.gwdg.de//). Toro Ankole carbonatites (GEOROC), and 2002 Nyiragongo lavas (Chakrabarti et al., 2009a), Rungwe lavas (Castillo et al., 2014), Ethiopian lavas (see Fig. 5 for details), and Oldoinyo Lengai carbonatites (GEOROC) are also plotted for reference. Fields for Paleoproterozoic to Archean crust from and near the Tanzania craton and Neoproterozoic crust reworked during the Pan-African Orogeny (Moller et al., 1998) are as also shown in (B) and (C). In (A), mantle end-member components DMM, EMI, EMII, and HIMU are from Hart et al. (1992). The FOZO field is from Stracke et al. (2005).

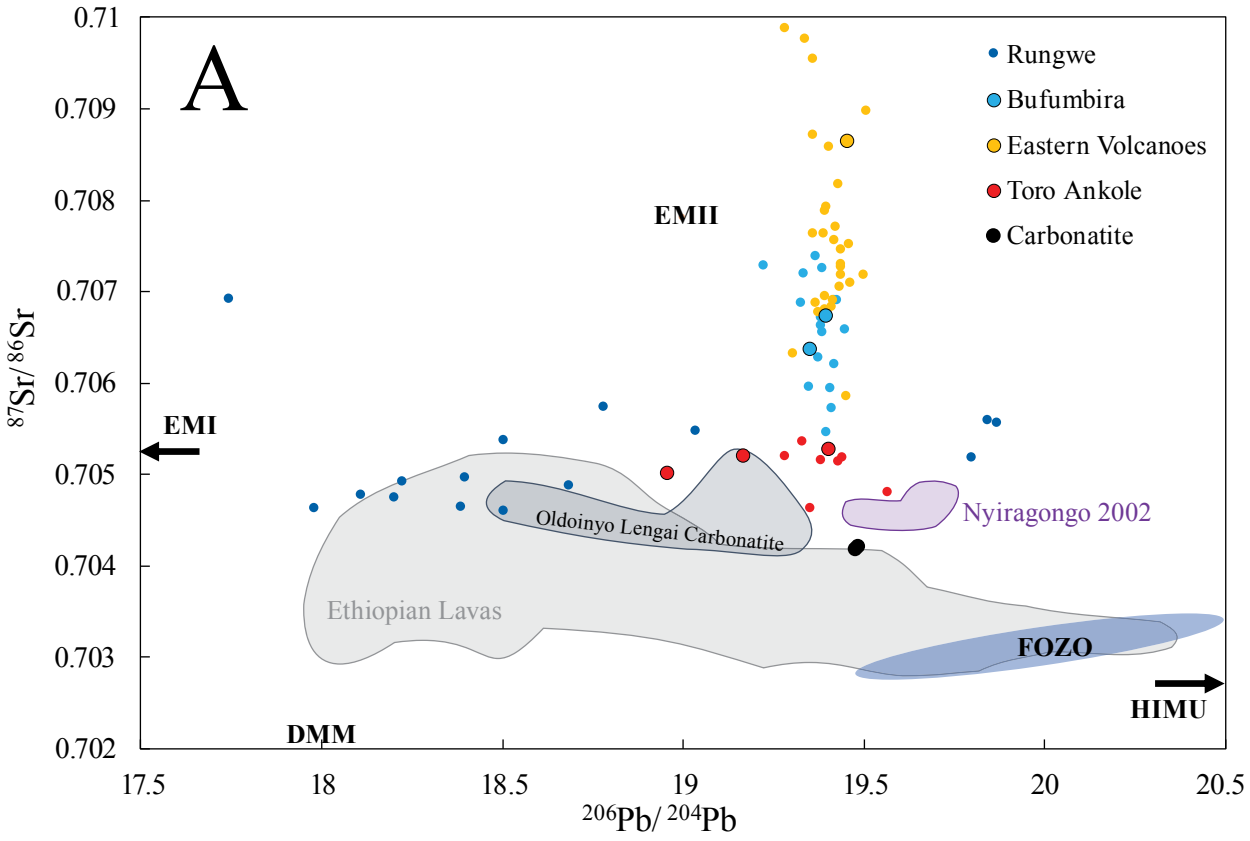
A
Rungwe
Bufumbira
Eastern Volcanoes
Toro Ankole
Carbonatite
EMII
EMI
DMM
HIMU
FOZO
Oldoinyo Lengai Carbonatite
Nyiragongo 2002
Ethiopian Lavas
0.71
0.709
0.708
0.707
0.706
0.705
0.704
0.703
0.702
87Sr/86Sr
17.5
18
18.5
19
19.5
20
20.5
206Pb/ 204Pb

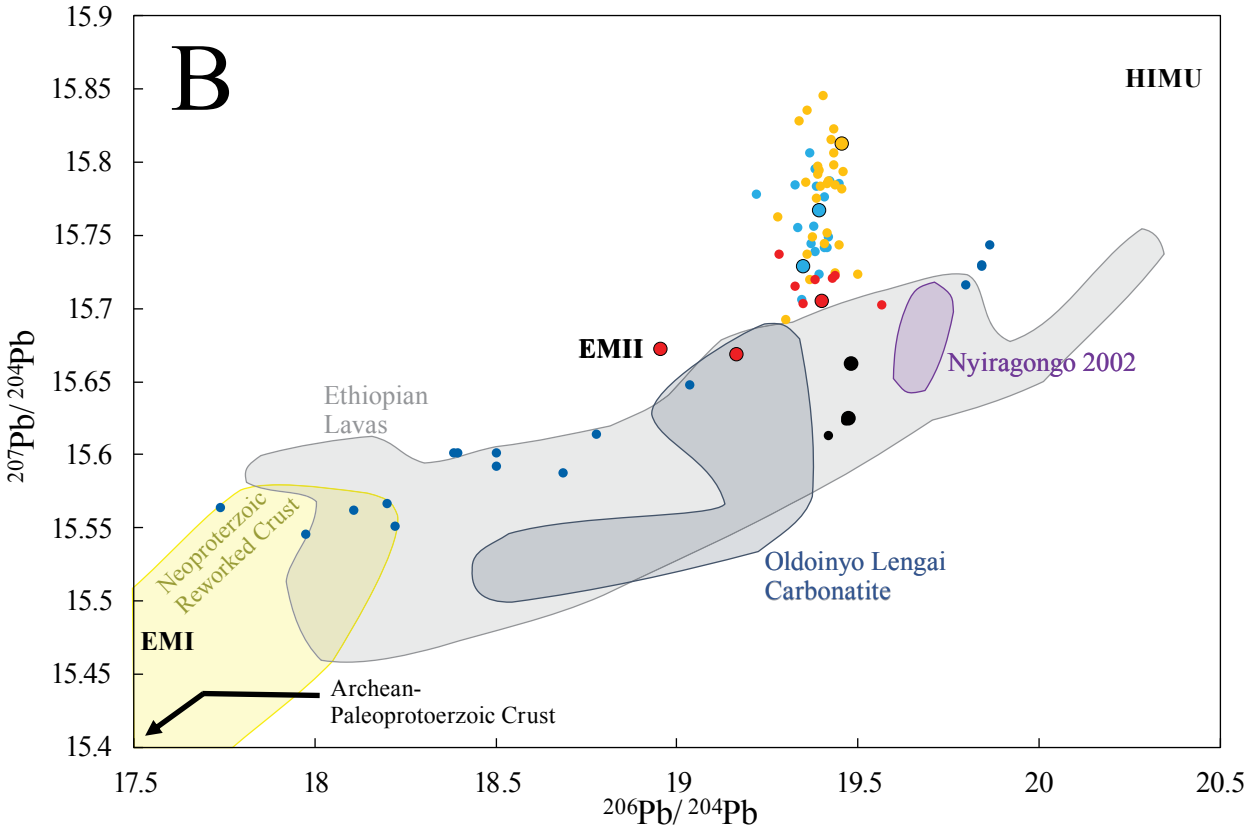
B
HIMU
EMII
EMI
Ethiopian Lavas
Nyiragongo 2002
Oldoinyo Lengai Carbonatite
Neoproterzoic Reworked Crust
Archean-Paleoprotoerzoic Crust
15.9
15.85
15.8
15.75
15.7
15.65
15.6
15.55
15.5
15.45
15.4
207Pb/ 204Pb
17.5
18
18.5
19
19.5
20
20.5
206Pb/ 204Pb

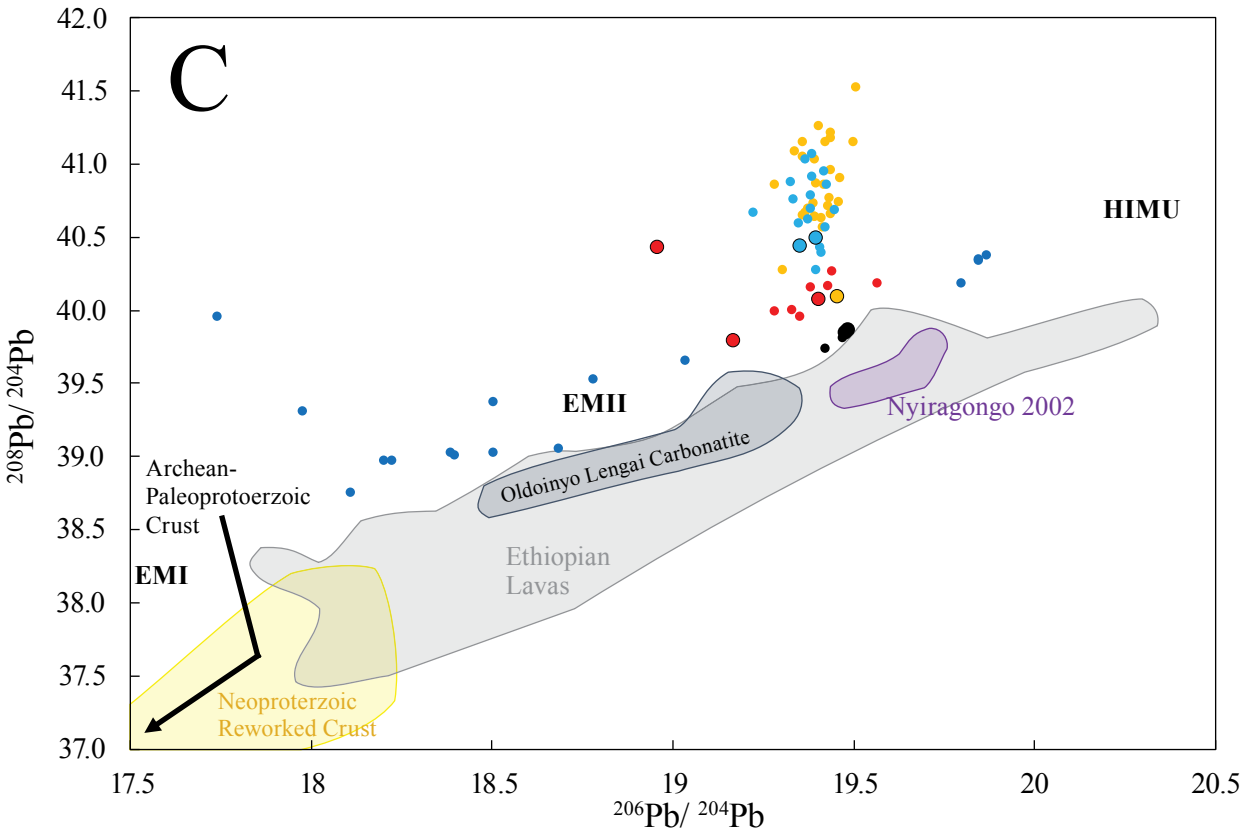
C
HIMU
EMII
EMI
Archean-
Paleoprotoerzoic
Crust
Oldoinyo Lengai Carbonatite
Nyiragongo 2002
Ethiopian
Lavas
Neoproterzoic
Reworked Crust
42.0
41.5
41.0
40.5
40.0
39.5
39.0
38.5
38.0
37.5
37.0
17.5
18
18.5
19
19.5
20
20.5
208Pb/ 204Pb
206Pb/ 204Pb

The two carbonatites analyzed for alteration studies show two slightly different results. Differences in Sr and Pb isotopes among the leachate, residue, and whole rock aliquots of sample UG-61 are unsystematic and barely outside the analytical errors (Table 3). The same is true for the Sr isotopes of sample UG-63, but the leachate is definitely more $^{207}Pb/^{204}Pb$ and $^{208}Pb/^{204}Pb$ radiogenic than the whole rock and residue. Significantly, the more radiogenic Pb isotopes of the leachate are generally consistent with the aforementioned vertical trends in Pb-Pb isotope plots shown by the analyzed and published Toro Ankole and Virunga lavas. Such vertical Pb isotope trends are also shown to variable extents by Nyiragongo 2002 erupted samples and Miocene to Quaternary lavas from the southern and NW Ethiopian regions in the Eastern Branch. These vertical isotope trends are most likely not due to surface alteration, but are most likely inherent features of their magma sources; their origin will be discussed in more detail later on. Thus, the leaching experiment indicates that the generation of secondary calcite amygdales is most likely an isochemical process, and that most of the lava samples analyzed are not greatly affected by surface weathering and alteration.

5. Discussion

5.1. Crustal Contamination

The lavas analyzed were carefully collected from fresh field outcrops as much as possible and, as described earlier, additional steps were taken to choose unweathered and unaltered rock chips to be powdered. The afore discussed leaching experiment also indicates minimal effects of surface alteration. However, the lavas were erupted through continental crust and previous results indicate that crustal contamination is greater in Western Branch than in Eastern Branch lavas (Furman, 2007 and references therein). Crustal contamination is also expected to be more pronounced in more evolved lavas. Incidentally, melting depth and lithospheric thickness is thought to be increasing northward from Virunga to Toro Ankole (90 km for Virunga and 140 km for Toro Ankole; Link et al., 2010; see also Rosenthal et al., 2009; Pitcavage et al., 2021) and, conversely, the former is more differentiated than the latter (Table 1; Fig. 2). Crustal xenoliths of varying sizes are also clearly visible in field outcrops and in many collected samples. These imply that our samples may have been contaminated by continental crust and that the degree of contamination should increase from Virunga to Toro Ankole, based on crustal thickness, or on the contrary, based on lava differentiation. Thus, it is important to first constrain the secondary effect of crustal contamination prior to discussing the detailed petrogeneses of the lavas.

A procedure commonly employed to ascertain crustal contamination is through the comparison of Ce/Pb and Nb/U ratios of lava samples in question to those of fresh, mantle-derived oceanic basalts, which have relatively constant Ce/Pb of 25 ± 5 and Nb/U of 47 ± 10 (Hofmann et al., 1986; Figs. 7A and B). Crustally contaminated samples should have Ce/Pb ≤ 20 and Nb/U ≤ 37. Interestingly, there appears to be a slight positive correlation between Ce/Pb and

Figure 7. **(A)** Ce/Pb versus MgO and **(B)** Nb/U versus MgO diagrams for Toro Ankole and Virunga lavas. In (A), data are plotted relative to primary mantle-derived melts with Ce/Pb = 25 +/- 5 (Hofmann et al., 1986). In (B), data are plotted relative to primary mantle-derived melts with Nb/U = 47 +/- 10 (Hofmann et al., 1986). Symbols for Toro Ankole, Toro Ankole carbonatite, and Virunga lavas as in Figure 3. Lavas plotting below both primary melt fields (grey lines) indicate crustal contamination. Data for Nyiragongo 2002 eruption (Chakrabarti et al., 2009a), South Kivu and Rungwe (GEOROC: https://georoc.mpch-mainz.gwdg.de//), HT/LT (High-Ti and Low-Ti, respectively) basalts and Amaro/Gamo basalts from Oligocene or Pre-Rift lavas from NW and southern Ethiopia, respectively (Pik et al., 1999; George and Rogers, 2002) are shown for reference.

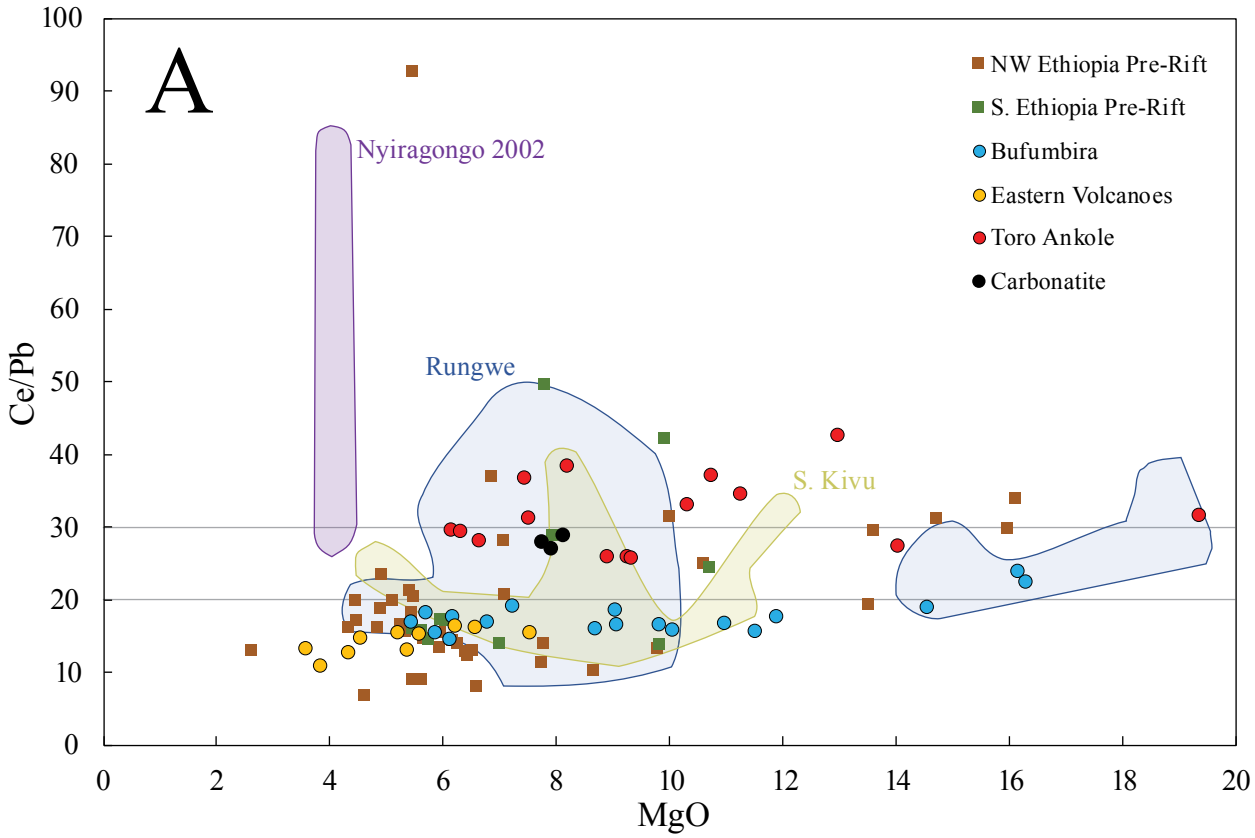
A
NW Ethiopia Pre-Rift
S. Ethiopia Pre-Rift
Bufumbira
Eastern Volcanoes
Toro Ankole
Carbonatite
Nyiragongo 2002
Rungwe
S. Kivu
Ce/Pb
MgO
0
10
20
30
40
50
60
70
80
90
100
0
2
4
6
8
10
12
14
16
18
20

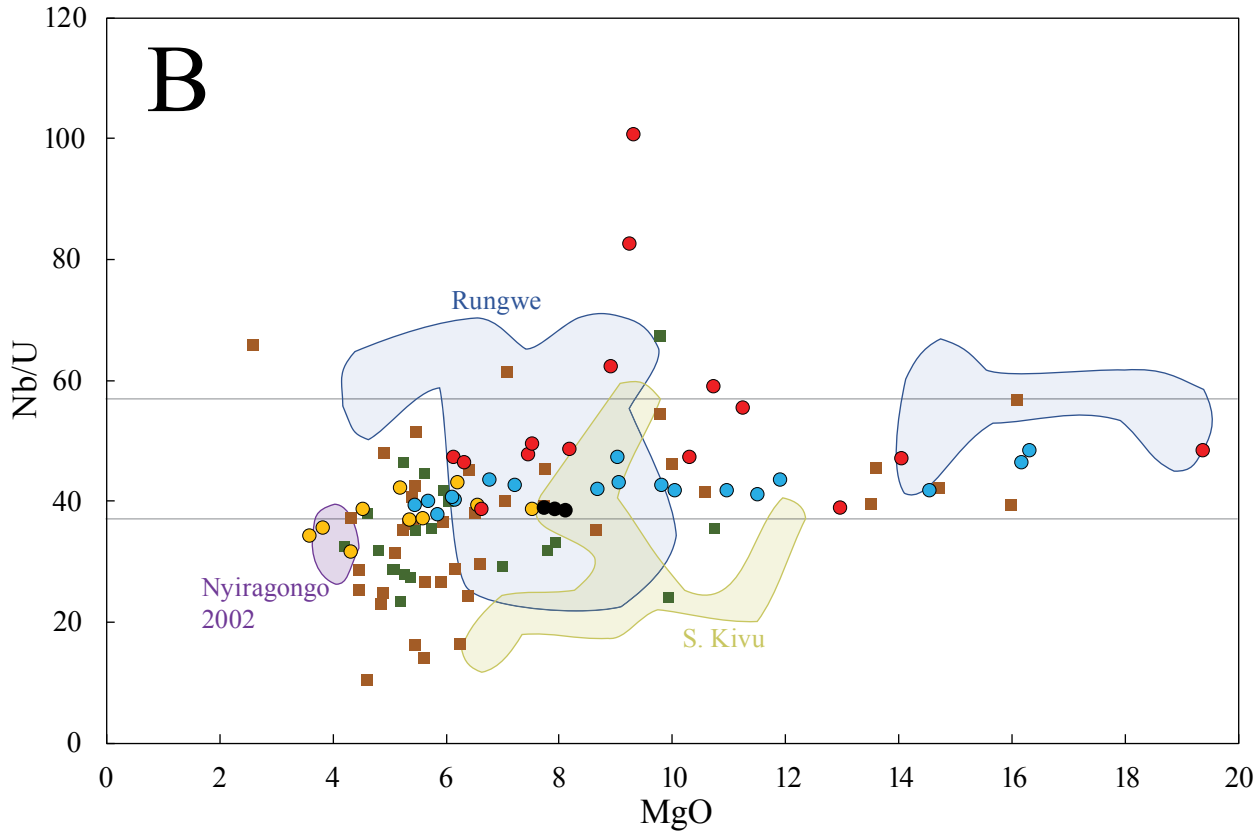
B
Rungwe
Nyiragongo
2002
S. Kivu
Nb/U
MgO
0
20
40
60
80
100
120
0
2
4
6
8
10
12
14
16
18
20

MgO in Virunga lavas, with the lowest MgO (i.e., differentiated) lavas from the eastern volcanoes having the lowest Ce/Pb (< 10; see also, e.g., De Mulder and Pasteels, 1986; Rogers et al., 1998). Moreover, almost all Virunga samples plot below the Ce/Pb values for mantle-derived basalts. All these could imply crustal contamination. However, most of our Virunga samples have Nb/U (average ~41) plotting well within the Nb/U values for mantle-derived basalts, which suggest otherwise. Additionally, despite their apparent slight positive Ce/Pb-MgO correlation, overall our Virunga samples have a limited range of Ce/Pb ratio (average ~16). Thus, it appears that even if Virunga lavas experienced crustal contamination, it must have been minimal. More likely, their ~low Ce/Pb and mantle-like Nb/U ratios are reflective of their magma source.

It is also important to note that although Toro Ankole lavas have a relatively wide range of Ce/Pb ratios (26–46), on average (~31) they plot slightly above the range of fresh oceanic basalts. Their Nb/U ratios (39–100; average ~52) are also well within the range of mantle-derived oceanic basalts. Thus, Toro Ankole lavas are most likely not contaminated by the crust. This lends additional support to the notion that Virunga lavas are minimally, if at all, contaminated, as the lithosphere in the Toro Ankole province is argued to be thicker than in the Virunga province (Rosenthal et al., 2009; Link et al., 2010; Pitcavage et al., 2021). It is also noteworthy that although volcanic eruptions in the Toro Ankole province predominantly are explosive and rapid, such that lava-crustal interactions may have been minimized (e.g., Muravyeva et al., 2014; Pitcavage et al., 2021), the Toro Ankole samples analyzed are all from lava flows, similar to the Virunga lava samples that were analyzed.

5.2. Fractional Crystallization

A fair amount of our samples is relatively primitive (≥ 8 wt % MgO), but some are more evolved that have experienced differentiation. As noted above, Virunga samples show a linear

trend from basanite to basaltic-trachyandesite through trachy-basalt, indeed suggesting some degree of differentiation (Fig. 2). Moreover, samples from the eastern volcanoes mostly plot near the end of the trend, consistent with their relatively more evolved (MgO ≤ 7.5 wt%) compositions. Fractional crystallization is most likely responsible for the differentiation of Virunga lavas as clearly illustrated by the systematic variations of their major oxides with MgO (Supplementary Figs. 2A–E). More specifically, the compositional evolution of Virunga lavas can most likely be explained by their consistent MgO versus CaO and CaO/Al_2O_3 trends; these trends are indicative of clinopyroxene fractionation (Fig. 8; Fram and Lesher, 1997; Dasgupta et al., 2010; Muravyeva et al., 2014). On the other hand, although the compositional evolution of Toro Ankole lavas does not appear to define an obvious trend, in detail their data cluster can possibly be described as the intersection of clinopyroxene fractionation and olivine fractionation trends. The relatively more complex crystal fractionation history of Toro Ankole relative to Virunga lavas could be stemming from their more primitive nature (average MgO = 10 wt%) and potentially by having different parental magmas (Tappe et al., 2003; Pitcavage et al., 2021). Thus, the former experienced some olivine fractionation first followed by additional, but minor clinopyroxene fractionation. In contrast, Virunga lavas (MgO ≤ 7.5 wt%) have generally experienced clinopyroxene fractionation only. Significantly, crystal fractionation is consistent with the increases in the bulk incompatible trace element contents in both lava suites, but not their overall concentration patterns and diagnostic trace element ratios (e.g., Figs. 4 and 5).

Figure 8. MgO versus **(A)** CaO and **(B)** CaO/Al_2O_3 diagrams for Toro Ankole and Virunga lavas. Shown in (A), are fields for olivine and clinopyroxene crystal fractionation trends from Muravyeva et al. (2014). Shown in (B) are linear trends for olivine and clinopyroxene fractionation, where the former is represented by relatively flat trends whereas the latter is represented by positively correlated trends (Fram and Lesher, 1996; Dasgupta et al., 2010). Toro Ankole and Virunga (Bufumbira and eastern volcano) lavas are plotted using the same symbols as in Figure 2. Published data from Toro Ankole and Virunga (Pitcavage et al., 2021) are also plotted as smaller symbols with the respective colors.

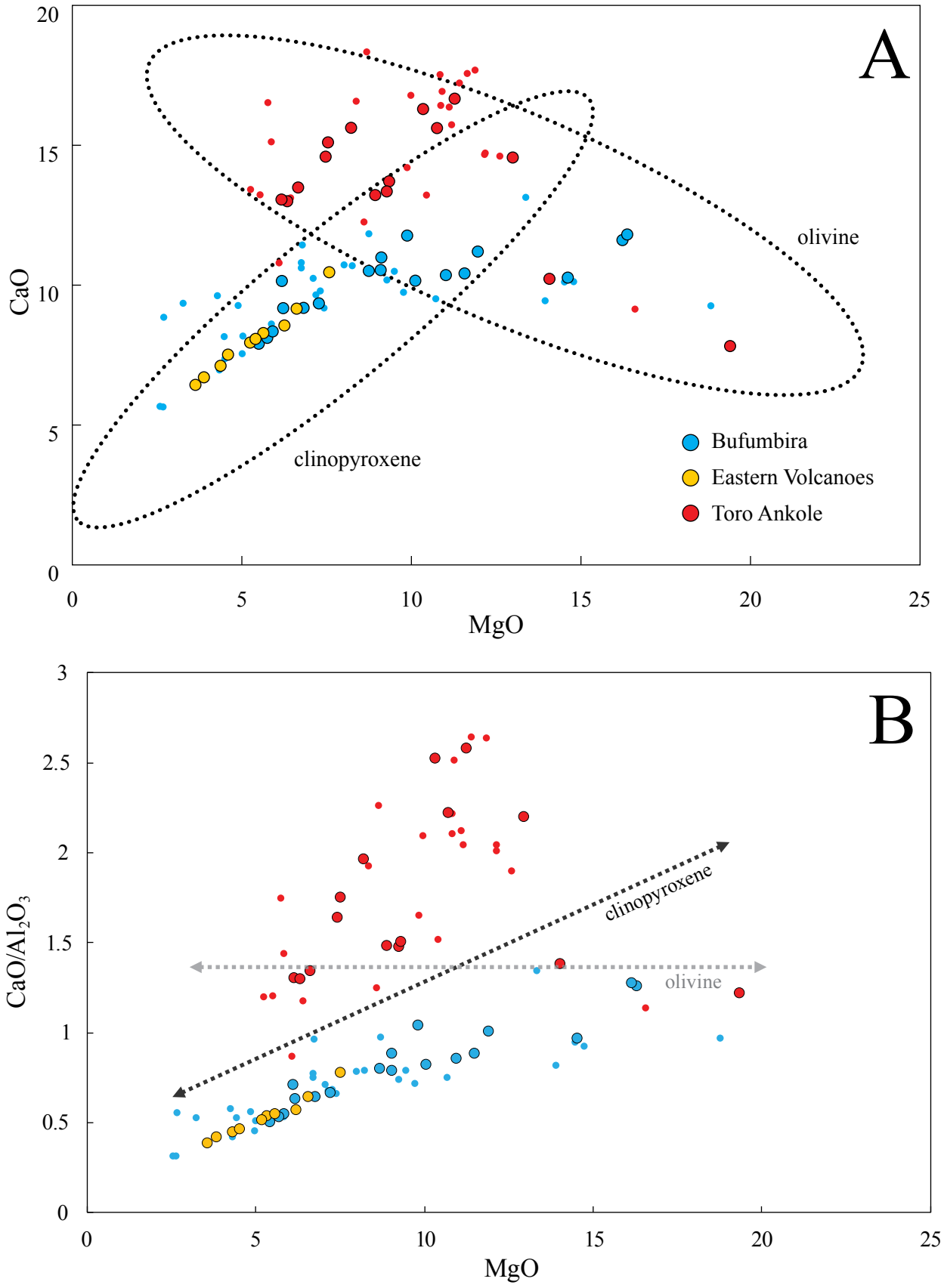
A
CaO
MgO
olivine
clinopyroxene
Bufumbira
Eastern Volcanoes
Toro Ankole
B
CaO/Al2O3
clinopyroxene
olivine

5.3. Source Mineralogy and Depth of Melting

The highly potassic and enriched lavas from Toro Ankole and Virunga (Figs. 3 and 4) are thought to have been due to low degrees of partial melting of an enriched, metasomatized CLM (e.g., Rogers et al., 1992, 1998; Furman 2007; Rosenthal et al., 2009; Muravyeva et al., 2014; Pitcavage et al., 2021). Two key phases that are widely accepted to be present in such a metasomatized source are phlogopite and amphibole. Macroscopic and microscopic observations indeed confirm the presence of phlogopite in Toro Ankole lavas, at least, with conspicuous phlogopite micro-phenocrysts to megacrysts that can range up to ≤ 5 modal %. Furthermore, the relatively low K/Th values for both Toro Ankole and Virunga lavas suggest the presence of phlogopite and/or amphibole in their source (Fig. 9; Furman, 2007). Additionally, their high Th concentrations indicate low degrees of partial melting for both regions. The slightly higher K/Th of Toro Ankole and Virunga, similar to low degree partial melts (high Th) in Chyulu Hills, is most likely due to the stronger presence of phlogopite in the source (Furman, 2007). Potassium/Rb for Virunga (134–328) and Toro Ankole (202–328; excluding carbonatites) are also within the values (< 400) of phlogopite bearing sources (Basu, 1978; Beswick, 1976; Pitcavage et al., 2021). Moreover, despite the absence of phlogopite in our Virunga lavas, their elevated Rb/Sr (> 0.1) and low Ba/Rb (< 20) values suggest otherwise (Furman and Graham, 1999; Pitcavage et al., 2021).

The lack of amphibole in the highly potassic ($K_2O/Na_2O > 1$; Fig. 4) Toro Ankole and Virunga samples suggests a greater dominance of phlogopite in their sources. Conversely, the Rb/Sr that exceeds primitive mantle values in Toro Ankole lavas implies a lower contribution from amphibole in their source. However, the low Rb/Sr (< 0.1) coupled with relatively high Ba/Rb (13–30) of Toro Ankole lavas, along with low K/Th indicate that contributions from

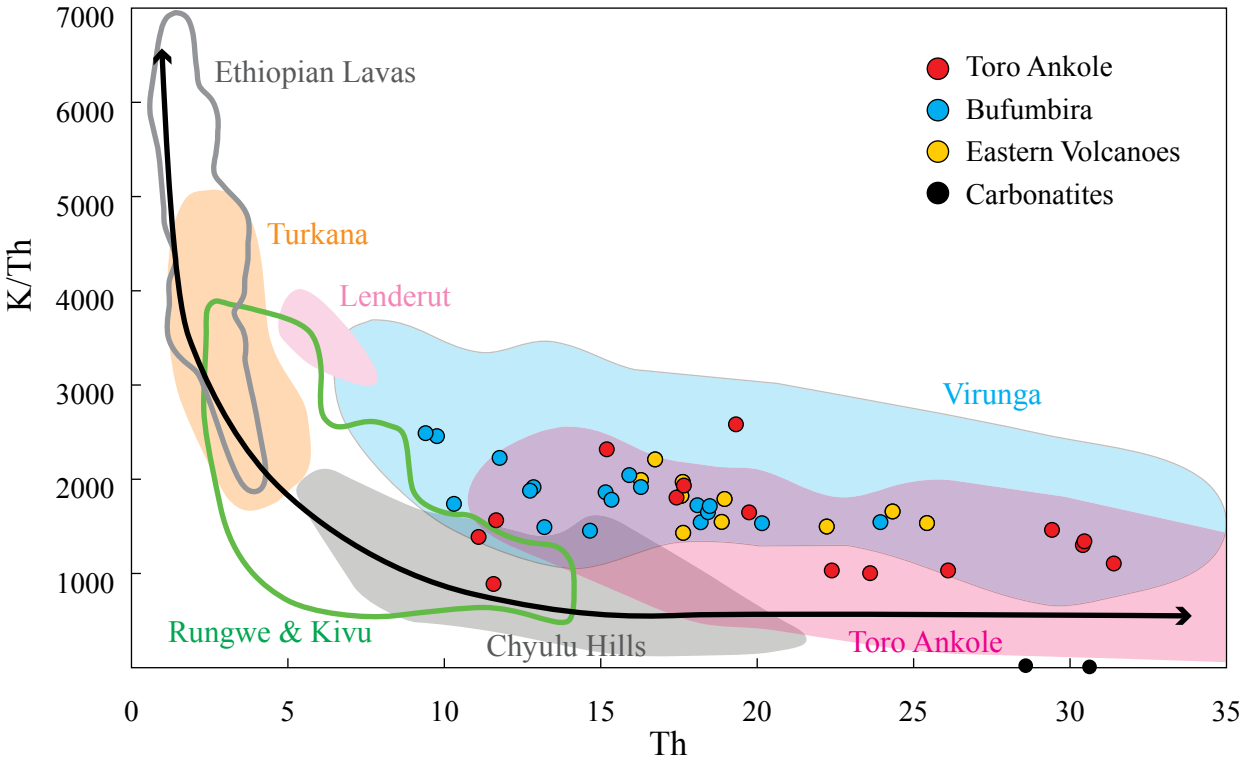

Figure 9. K/Th versus Th for Toro Ankole and Virunga lavas. In this plot, K-bearing minerals such as phlogopite and amphibole will be consumed in the source region as melting progresses (Furman, 2007). Thorium has similar bulk partition coefficient as K in spinel/garnet lherzolite, so high Th values and low K/Th would indicate low degrees of melting, whereas higher K/Th values and lower Th would indicate higher degrees of melting. Toro Ankole, Toro Ankole carbonatite, and Virunga (Bufumbira and eastern volcano) lavas are plotted using the same symbols as in Figure 3. Published data from the two volcanic provinces (Pitcavage et al., 2021) are also plotted as smaller symbols with the respective colors along with data from Nyiragongo 2002 eruption (Chakrabarti et al., 2009a). Fields for other lava suites are from Furman (2007).

amphibole cannot be completely ruled out (Furman and Graham, 1999; Pitcavage et al., 2021). Thus, despite the absence of amphibole in the lavas, amphibole's presence in the source especially for Toro Ankole lavas cannot be completely ruled out but can be assumed to be very minimal.

Garnet is another key phase that is generally accepted to be in the metasomatic CLM source. Toro Ankole and Virunga lavas show strong correlation between MgO and Al_2O_3, especially among Virunga lavas (Supplementary Fig. 2B). Both lava suites also have low abundances of HREE, with Virunga lavas having an almost flat whereas Toro Ankole having a slightly depleted HREE concentration patterns (Figs. 4A and B). These suggest that their parental lavas were produced in the presence of residual garnet (Castillo et al., 2014). This notion is supported by other geochemical tracers. The average Th/U ratios for Virunga and Toro Ankole are 5.4 and 4.9 (5.4 excluding carbonatites), respectively, well above the average value of 2.6 for a normal, peridotitic mantle (Kramers and Tolstikhin, 1997), but indicative of partial melts coming from garnet-bearing sources (Beattie, 1993; LaTourrette et al., 1993; Chakrabarti et al., 2009a). Moreover, the average Dy/Yb_N value for Virunga lavas is ~1.6 (see also Chakrabarti et al., 2009a) whereas that of Toro Ankole samples is ~2.5 (with or without carbonatites). These high Dy/Yb_N values are also suggestive of a mantle source with residual garnet (Chakrabarti et al., 2009a). The higher ratio for Toro Ankole lavas most likely implies a higher garnet content in their mantle source, but could also have been the result of differences in source composition and degrees of partial melting.

Based on the above source mineralogy, some inferences on the melting depth can be made. The likely presence of phlogopite plus garnet in the source or sources of Toro Ankole and Virunga lavas indicates a melting depth close to or possibly greater than the stability field of

phlogopite which is > 100 km or > 3 GPa (Rosenthal et al., 2009 and references therein). Using a thermobarometer based on whole rock composition from Lee et al. (2009), Pitcavage et al. (2021) estimated that Bufumbira lavas in the Virunga province equilibrated around the 2.2–5.0 GPa range, with some lavas below the peridotite *solidus*, requiring the presence of volatiles. Significantly, Pitcavage et al. (2021) used the same thermobarometer for their Katwe-Kikorongo lavas in the Toro Ankole province and resulted in pressures that exceed the optimal range for the method (> 8 GPa), suggesting a stronger need for volatiles compared to Virunga. The presence of trace diamonds in xenoliths from Toro Ankole (Nixon, 1973) further supports a melting depth possibly as far as that of some kimberlitic sources (6–8 GPa or 200–250 km; Wilson and Head, 2007). Regardless, the carbonate-influenced lavas from both Toro Ankole and Virunga imply a significant melting depth > 3 GPa based on the depth of stability for carbonates (Rogers et al., 1998; Olafsson and Eggler, 1983).

5.4. REE Partial Melting Models

To illustrate the generation of Toro Ankole and Virunga lavas from the afore discussed metasomatized source, a program called PetroGram (Gunduz and Asan, 2021) was used to model their REE contents through equilibrium batch partial melting. The model used a MARID-carbonatite melt mixture as the initial source composition, similar to that proposed by Rosenthal et al. (2009). The average composition of MARID xenoliths from South African kimberlitic lavas (Grégoire et al., 2002) was used for the MARID end-member whereas the average composition of published Toro Ankole carbonatites from GEOROC was used for the carbonatite end-member. The mixture proportion was narrowed down to ca. 97 % MARID xenoliths and 3 % Toro Ankole carbonatites and the source was set to have a mineral mode of ca. 40 %-olivine, 25 %-clinopyroxene, and 35 %-phlogopite. Adding a trace amount of garnet (0.5 %) into

the source without compromising the model results, shifts the mineral mode to ca. 60 %-olivine, 20 %-clinopyroxene, and 20 %-phlogopite. Note that inclusion of amphibole in the starting source mineral mode produced inconsistent results. Part of the reason is that the REE partition coefficients for the amphibole-carbonatitic melt system are incomplete (i.e., missing Eu, Tb, and Dy) and not uniform in the pertinent high pressure and temperature conditions. Thus, values were pulled from various publications where the temperature, pressure, and equilibrated melt type are not the same. In any case, model calculations without amphibole in the aforementioned starting mineral mode produced better fitting REE concentration patterns. As noted earlier, although amphibole appears to be present in the metasomatized source, its role is most likely very minimal, particularly for Toro Ankole and, hence, Nyiragongo lavas (see also Chakrabarti et al., 2009a).

Two sets of mineral-melt partitioning coefficients were used. One set was mostly taken from peridotite minerals that equilibrated with carbonatitic (carbonated) melts at 1.5–4.5 GPa and 1000–1500 °C and the other set was from minerals that equilibrated mostly at 6–12 GPa and 1200–1700 °C. The two sets were used to address the different depth regimes proposed for Toro Ankole and Virunga (Rosenthal et al., 2009; Chakrabarti et al., 2009a; Pitcavage et al., 2021). Some overlaps between the two sets are inevitable due to the lack of partition coefficient data in some specific pressure-temperature ranges. This is especially the case for the coefficients of phlogopite and amphibole, where values used for the high pressure set are the same as the low pressure set. Phlogopite coefficients under carbonatitic melts are unavailable, so instead data from basanite and lamproitic experiments were used as well as estimates from kamafugite lavas (LaTourrette et al., 1995; Schmidt et al., 1999; Foley et al., 1996; Melluso et al., 2008). Some values for amphibole were taken from basanite melts as well (LaTourrette et al., 1995).

Published average partition coefficient values were used when available and new averages were calculated if there are none. Details on the specific partition coefficients used for a trace element for each particular set, including their detailed references, are presented in Supplementary Table 2.

To briefly summarize, through modeling we attempt to estimate the REE contents of the lava samples generated through equilibrium batch partial melting of a metasomatized source. In general, models using partition coefficients from the deeper pressure set (mostly 6–12 GPa and 1200–1700 °C) are more successful in recreating the REE concentration patterns of Toro Ankole lavas (Fig. 10A). The use of this deeper pressure set is highly consistent with most source pressure estimates for the northern Western Branch that revolve around 30–80 kbar or 3–8 GPa) (e.g., Rosenthal et al., 2009; Pitcavage et al., 2021; Furman, 2007; Chakrabarti et al., 2009a) Also, it is noteworthy that the pressure fields for the two mixing end-members extend into very high pressure ranges. MARID assemblages in cratonic settings are found to be stable around 3–8 GPa and 900–1300 °C (Konzett et al., 1997) and the recent carbonatitic metasomatic event in Western Branch melts are proposed to be at pressures of 4–6 GPa (Rosenthal et al., 2009; Foley et al., 2009). Low degree (3–20 %) partial melting of the above mentioned MARID-carbonatite starting composition is successful in recreating our Toro Ankole REE concentration patterns (Fig. 10A). Overall, the REE patterns seem to be primarily dependent on the amount of clinopyroxene, olivine, and phlogopite in the starting composition and this is consistent with claims of a clinopyroxenitic source or a peridotite source infused with clinopyroxenitic veins (Pitcavage et al., 2021; Rosenthal et al., 2009; Foley, 1992). Thus, modeling results indeed show that Toro Ankole lavas could be originating from a source that experienced MARID-like and/or carbonatitic metasomatism (Rosenthal et al., 2009).

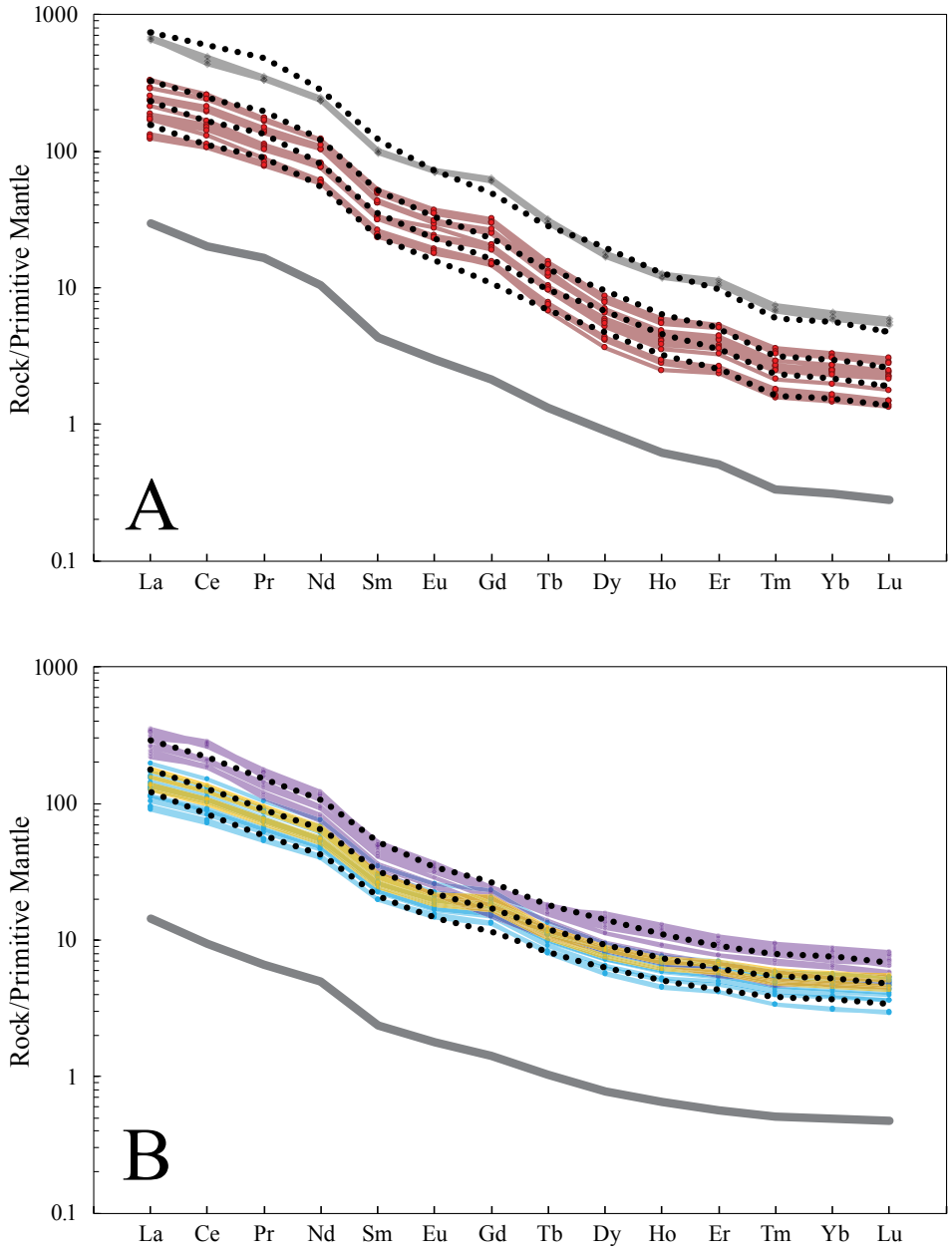

Figure 10. Forward REE melting models for **(A)** Toro Ankole and **(B)** Virunga. In (A), Toro Ankole samples are red lines while Toro Ankole carbonatites are black lines; the grey thick line is the starting composition (MARID-Carbonatite source). Dashed lines are the fractional melting lines (from top to bottom: F = 3%, 8%, 12%, and 18%) of the starting composition. In (B) 2002 Nyiragongo eruption lavas (Chakrabarti et al., 2009a) are purple lines. Bufumbira lavas are blue lines and eastern volcano lavas are orange. The thick grey line (starting composition) is the MARID-EMORB source. Dashed lines are the model fractional melting lines (from top to bottom: F = 4%, 7%, and 11%) of the starting composition. Notice how our Virunga samples are less fractionated (La_N/Yb_N) compared to Nyiragongo samples, but both are overall significantly less fractionated than Toro Ankole samples in (A). The model fractional melting lines from a MARID-EMORB starting composition provides a better fit for Virunga lavas than with the MARID-Carbonatite starting composition used for Toro Ankole lavas. This indicates a loss or change of the metasomate for Virunga lavas. Please see text for additional discussion.

Modeling the Virunga lava's REE concentration patterns proved to be more difficult. Modeled REE concentration patterns from the same source for Toro Ankole lavas are too fractionated (La/Yb_N ~104) compared to Virunga lavas (La/Yb_N ~26; excluding Nyiragongo lava; not shown). Using either the high or low pressure set of partition coefficients produce similar inaccurate results. As previously mentioned, however, most of the Virunga province is underlain by a relatively thinner crust. Moreover, Virunga's volcanic activity that preceded that of Toro Ankole occurred along a more advanced tectonic rift (Pouclet et al., 2016 and references therein). Accompanying these changes in geologic variables are a decrease in enrichment of incompatible elements (e.g., La/Yb_N) and an increase in silica saturation (Pouclet et al., 1981; Link et al., 2010; Pitcavage et al., 2021). These features could be explained by a change of metasomatic signatures of the source, from a carbonatite-metasomatized to a silicate-metasomatized CLM or vice versa (e.g., Foley, 1992; Rosenthal et al., 2009; Muravyeva et al., 2014; Pitcavage et al., 2021).

Accordingly, to model the REE contents of Virunga lavas, the Toro Ankole carbonatite end-member was replaced by an enriched- (E-)MORB from the Mid-Atlantic Ridge with a focus zone (FOZO)-like Sr-Pb-Nd isotopic compositions (Wei et al., 2020). A melt mixture of ca. 93.5 % average MARID (Grégoire et al., 2002) and 6.5 % FOZO-like E-MORB (*559-2-3* from Wei et al., 2020), using the same mineral mode % as the Toro Ankole model and with 4–11 % degrees of partial melting was able to reproduce the REE patterns of eastern volcano and Bufumbira lavas along with Nyiragongo lavas from Chakrabarti et al., 2009a (Fig. 10B). This relative success in modeling the REE contents of our Virunga samples is instructive as it shows the changing metasomatic signature from carbonatitic for Toro Ankole to silicic (albeit still highly enriched) for Virunga lavas. Such change in metasomatic signatures may imply the

depletion or exhaustion of the carbonatite and/or the shift to silicate metasomes, which coincidentally or consequentially follows the increase in extent of rifting and, hence, the degree of partial melting of the source from the Toro Ankole to Virunga province. As will be discussed in detail later, we interpret this process to be part of a dynamic model explaining the magmatism in the Western Branch and also in the Eastern Branch.

6. Regional Geologic Implications

It is clear from the prior discussion that this study favors a metasomatized CLM source for Virunga and Toro Ankole lavas, similar to the conclusions of several studies in the region (e.g., Rudnick et al., 1993; Furman, 2007; Rosenthal et al., 2009, Pitcavage et al., 2021). Results of the modeling calculations above are also consistent with an earlier proposal that the CLM beneath the region experienced both carbonatite (in Toro Ankole) and silicate (in Virunga) metasomatism (Rosenthal et al., 2009; Muravyeva et al., 2014; Pitcavage et al., 2021).

The CaO contents of Bufumbira and eastern volcano lavas are generally high with an average of 9.4 wt%, similar to the average value for OIBs (e.g., average Hawaii OIB = 7.7–9.4 wt%, average Azores OIB = 9.0–10.2 wt%; Dasgupta et al., 2010). Those of Toro Ankole (and also Nyiragongo) lavas – excluding carbonatites – are even higher, with an average of 13.7 wt% CaO. Moreover, the Zr/Hf of Virunga (43 average) and Toro Ankole (41 average) lavas are above the chondritic Zr/Hf value (36; Sun and McDonough, 1989), while Nyiragongo lavas (69–79), similar to Toro Ankole carbonatites (75–78; Table 2) have super-chondritic values. Such enrichment of Zr relative to Hf is characteristic of carbonatitic metasomatism (Chakrabarti et al., 2009a; Rudnick et al., 1993). Additional markers for a carbonatite-metasomatized source, such as Nb/Zr ratios (Castillo et al., 2014), are extreme in Toro Ankole carbonatites and Nyiragongo lavas (Fig. 5). Overall, it is clear that carbonatitic metasomatism must have played a significant role in the modification of the CLM especially beneath Toro Ankole and, to a certain extent, the Virunga province.

Silicate metasomatism has often been brought alongside carbonatitic metasomatism when assessing the CLM source of Western Branch magmatism (e.g., Furman, 1995; Rosenthal et al., 2009; Pitcavage et al., 2021). Indeed, both Toro Ankole and Virunga lavas also show signs of

silicate metasomatism. For example, Ti/Eu values (< 1500 for carbonatitic metasomatism; Rudnick et al., 1993; Klemme, 1995; Coltori et al., 1999) for Virunga and Toro Ankole lavas range from averages of 5900 and 7500 respectively, which point to silicate metasomatism rather than carbonatitic metasomatism (Table 2; Coltori et al., 1999). Accompanying these Ti/Eu values, however, are vastly different La/Yb_N values between Toro Ankole (average 87) and Virunga (average 26) lavas. Such difference in the degree of REE enrichment between Toro Ankole and Virunga, despite their similarly high Ti/Eu values, is suggestive of a relatively stronger silicate metasomatism for Virunga (Coltori et al., 1999). Significantly, the intermediate Zr/HF values of Toro Ankole and Virunga lavas relative to super-chondritic values of carbonatites may also be interpreted as signs for carbonatitic metasomatism accompanied by silicate metasomatism (Furman, 1995). Thus, silicate metasomatism must have also affected the CLM source particularly of Virunga and, to a certain extent, Toro Ankole lavas (Pitcavage et al., 2021).

6.1. The African Superplume Creates a Layered, Metasomatized CLM

A key issue then is the origin and evolution of the metasomatized Paleoproterozoic to Archean CLM beneath the Toro Ankole and Virunga provinces. In this study, the metasomatized CLM in the northern Western Branch region is simply due to mantle plume activities that have, and, still are affecting the entire EARS, from the Afar region in the north to the Rungwe province in the south (e.g., Craig et al., 1977; Rogers et al., 2000; Foley et al., 2012; Hilton et al., 2011; Castillo et al., 2014, 2020). In the Virunga province specifically, Chakrabarti et al. (2009a, 2009b) proposed that the currently erupting lavas originate from a heterogeneous, carbonate-rich mantle plume. In their proposal, Nyiragongo lavas with highly undersaturated and ultra-alkalic but OIB-like Sr-Nd-Pb isotopic compositions are generated through a deeper and lower degree of

partial melting of such a heterogeneous plume compared to Nyamuragira lavas with relatively less silica-undersaturated and less alkalic but with likewise OIB-like isotopic compositions. Indeed, the Sr-Pb isotopic values of Nyiragongo along with Toro Ankole and Eastern Branch lavas trend towards the FOZO field (Fig. 6A), suggesting a widespread injection of plume material throughout the EARS and attesting how critical such material is for EARS magmatism. Thus, studies have indicated that Toro Ankole and Virunga rift lavas, and entire EARS lavas as a whole, originate from a metasomatized CLM and/or a mantle plume.

Based on the new results and existing data, this study proposes the following tectono-magmatic model for the generation of Toro Ankole and Virunga lavas (see also Fig. 11). The entire EARS has been over the African Superplume since, perhaps, ca. 500 Ma (Vollmer and Norry, 1983a, 1983b; Muravyeva et al., 2014; Castillo et al., 2014). The Superplume is a contiguous thermo-chemical mantle anomaly that originates from the core mantle boundary – starting from the large low shear velocity province (LLSVP) underneath southern Africa and continues as upwelling anomalously hot plume material at the mantle above the transition zone (660 km depth) underneath east Africa and the Arabian peninsula (Hansen et al., 2012). The mantle anomaly most likely originates as subducted lithosphere that, although dehydrated, remains relatively volatile-rich due to the presence of high-pressure hydrous phases, marine sediments, and especially marine carbonates (Plank and Langmuir, 1998; Castillo, 2015, 2016). Carbonates can persist past shallow mantle depths in the form of carbonated serpentinites or ophio-carbonates (Kerrick and Connolly, 1998) and may well be deeply subducted or preserved as carbonated eclogite until it is released by melting in the deeper mantle (Dasgupta et al., 2004).

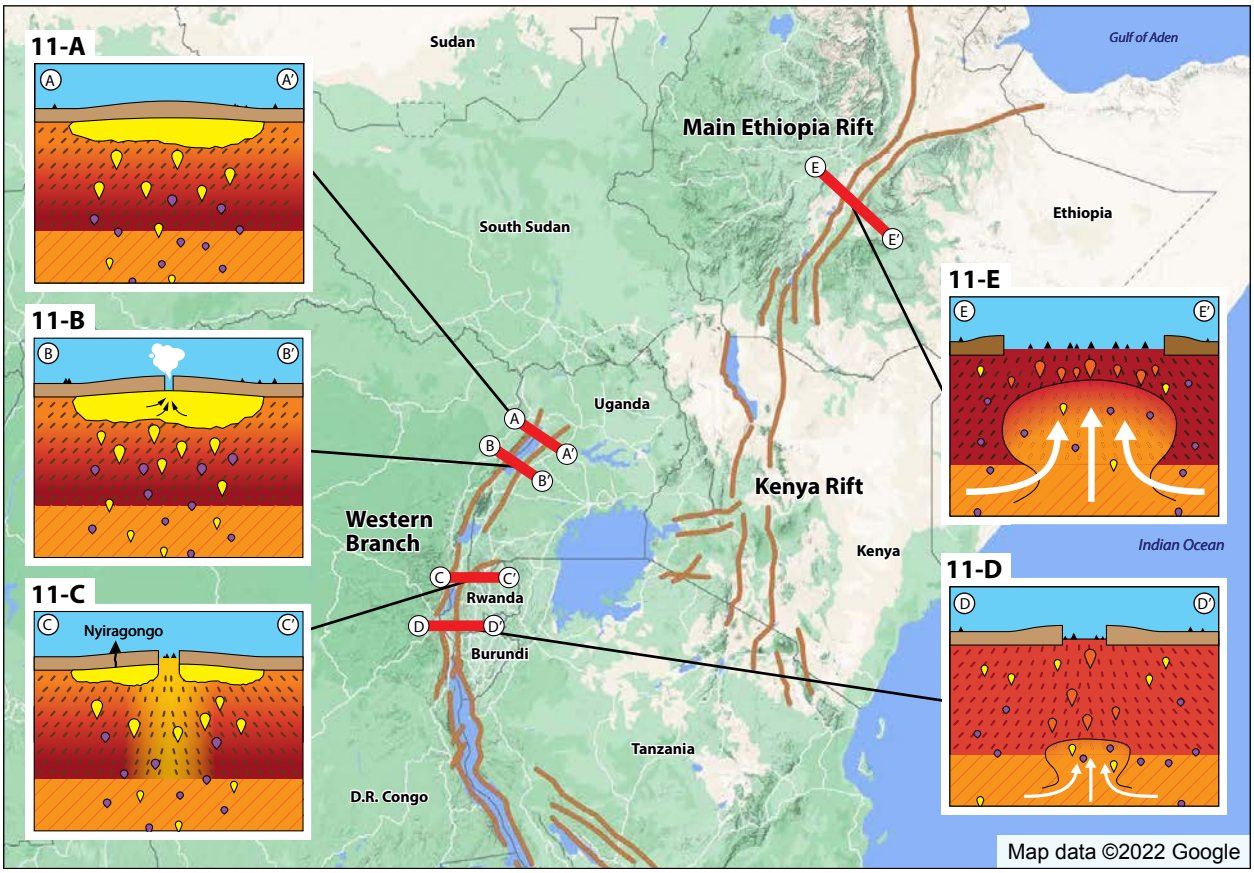

Figure 11. A proposed tectono-magmatic model for the development and evolution of the EARS. Panels 11A–E show the cross sections corresponding to the marked locations on the physical map. (A) Volatiles (yellow) exsolving from low-degree partial melts (purple) upwelling from the African Superplume ponded below and pressurized the pre-rift crust. With rift initiation (B), the ponded and pressurized volatiles and melts erupt rapidly in Toro Ankole. As rifting progresses (C) in Virunga, the volatiles are gradually exhausted and replaced with melts from successive upper layers of the plume silicate-metasomatized CLM layers, starting with the uppermost layer that was in equilibrium with the volatiles. However, there are exceptions like underneath the Nyiragongo volcano, where the silicate-metasomatized uppermost layer still retains some volatiles. Eventually, with more advanced rifting, adiabatic upwelling of the asthenosphere drawn from outside the region is additionally involved, as in South Kivu (D) and even more so in the MER (D). See text for further discussion.

The carbonate material is critical as it serves as a fluxing agent, providing CO_2 that promotes partial melting within the thermo-chemical anomaly (e.g., Dasgupta et al., 2004; Castillo, 2015, 2016) and also as a source of radiogenic Pb due to their inherently high U/Pb ratio (or μ) that is responsible for the highly Pb radiogenic HIMU and/or less Pb radiogenic FOZO mantle plume signatures (Vidal et al., 1992; Thirlwall, 1997; Castillo, 2015, 2016). Thus, the thermo-chemical anomaly or the African Superplume continuously provides along the entire length of EARS volatile-rich, small degree partial melts that upwell and/or stream through the overlying asthenosphere and CLM or upper mantle *sensu lato* (Fig. 11; Castillo et al., 2014).

Although quite compositionally heterogeneous initially as they leave the thermo-chemical anomaly, the volatile-rich melts converge to a common, less heterogenous composition through mixing. Specifically, as the melts stream upward, they continuously interact with the upper mantle and, hence, change their compositions through a process similar to the chromatographic effect on melts percolating upward through the mantle (Navon and Stolper, 1987). Additionally, pressure is released as the melts travel up such that the volatiles (particularly CO_2) exsolve as a distinct phase that, at first, is in equilibrium with the melts. Hence, a liquid-vapor fractionation takes place wherein highly incompatible trace elements including the alkalis partition into the vapor phase and/or these elements are fluxed by the volatiles (Winter, 2013). As the exsolved volatiles travel faster than the melts, prior to crustal rifting these extremely geochemically enriched volatiles accumulate and are trapped or ponded under intense pressure beneath the still unbroken and cold east African continental crust (Fig. 11A). The exsolved and, then, trapped volatiles continuously interact with the upper layers or horizons of the CLM just below the crust but some of them permeate the crust and escape in fumaroles, hot springs, and mazuku gas vents as well as mix with the groundwater. This volatile-

crust interaction is evident in the high CO_2 and mantle-like $^3He/^4He$ (~6 R_A – value relative to air) values measured throughout the EARS, despite the low $^3He/^4He$ (~0.05 R_A – Marty et al., 1996) of the underlying crust (Barry et al., 2013; Castillo et al., 2014, 2020; Halldórsson et al., 2014, 2022). Consequently, the crust is also compositionally altered, as clearly reflected by the extremely radiogenic Pb isotopic composition of the crust in the Western Branch (Vollmer and Norry, 1983a, 1983b; Chakrabarti et al., 2009a). Additional evidence for the effects of the trapped volatiles and upwelling partial melts on crustal composition will be presented later during the discussion of MARID xenoliths at the end of the section.

Significantly, the upper mantle beneath the EARS where the exsolved volatiles and remaining partial melts streamed or permeated through also changes its bulk silicate composition, or is metasomatized, in a manner similar to the inverse chromatographic effect in the mantle after the passage of melts (Navon and Stolper, 1987). Thus, the upper mantle beneath the entire EARS has, and is still experiencing silicate metasomatism and its bulk composition has become relatively less heterogeneous (Castillo et al., 2014).

In the herein proposed model, the intense pressure exerted by the trapped volatiles (primarily CO_2) plays a supporting role in rifting the east African crust, which is already regionally domed and stressed, most likely due to the thermal and buoyancy effects of the upwelling partial melts and volatiles. At the initiation of tectonic rifting along the Western Branch, as in the Toro Ankole province, the trapped, pressurized volatiles plus melts generated through low-degree, volatile-fluxed partial melting of the uppermost layers or horizons of the metasomatized, Paleoproterozoic to Archean CLM are suddenly released (Fig. 11B). Thus, the initial volcanism is highly explosive. As mentioned before, Toro Ankole volcanism is indeed mostly characterized by pyroclastic eruptions in maars and low-lying craters that are all

indicative of very explosive, rapid eruptions. Isotopic disequilibrium and chemical zoning in clinopyroxenes and the host rock indeed argue for rapidly ascending melts from the local source (Muravyeva et al., 2014). Moreover, the resultant lavas are extremely Si-undersaturated and highly enriched in volatiles, alkalis, and incompatible elements (Table 1 and 2). Carbonatite volcanism also occasionally occurs, drawn from accumulated small-volume carbonatitic melts (Dasgupta, 2006) in discreet pockets in the volatile-soaked upper CLM layers. Hence, all Toro Ankole volcanic products (e.g., foidites, kamafugites, carbonatites) clearly bear the imprint of carbonatite metasomatism.

As tectonic rifting progresses, as in the Virunga province, the number of trapped volatiles decreases whereas the proportion of melts through volatile-flux melting of the uppermost layers of the Paleoproterozoic to Archean CLM that has been in equilibrium for quite some time with the trapped volatiles increases (Fig. 11C). Hence, volcanic eruptions are less explosive and the resultant lavas are slightly less Si-undersaturated and less enriched in volatiles, alkalis, and incompatible elements compared to Toro Ankole lavas. As rifting continues, the pressure is significantly decreased, eventually leading to adiabatic decompression melting of the upper, but subsequentially deeper layers of the metasomatized CLM. Thus, the source of erupting Virunga lavas changes from the carbonatite-metasomatized to silicate-metasomatized CLM.

It is noteworthy, however, that at this early rifting stage, rift magmatism is also not yet fully developed. Hence, the above-described transition of magmatism from a carbonatite- to silicate-metasomatized CLM source is highly idealized. For example, the currently erupting Nyiragongo lavas in the westernmost part of Virunga are compositionally akin to Toro Ankole lavas (Fig. 2) as most probably, their lavas are also from predominantly volatile-rich melts still trapped beneath the western lip of the rifted crust (Fig. 11C). In comparison, the simultaneously

erupting Nyamuragira lavas just north of Nyiragongo are most probably drawn from the less volatile-bearing upper CLM layers near the center of the young, narrow rift. Hence, Nyiragongo lavas contain more signals of carbonatite metasomatism than Nyamuragira lavas (cf. Chakrabarti et al., 2009a). It should also be noted that despite Nyiragongo lavas having highly enriched incompatible trace element patterns (Fig. 4B; average La/Yb_N ~41), these are not to the same degree as the highly fractionated Toro Ankole lavas (Fig. 4A; average La/Yb_N ~87). Moreover, our partial melt modeling was able to replicate the REE patterns of Nyiragongo lavas using an E-MORB end-member similar to the rest of Virunga lavas as opposed to a carbonatite end-member for Toro Ankole lavas (Figs. 10A and B). Thus, it can be inferred that the source for the anomalous Nyiragongo lavas is transitional between carbonatite- and silicate-metasomatized Paleoproterozoic to Archean CLM.

6.2. Pb and Sr Isotopic Signature of the Lavas

It is explicit in the above dynamic model that the general decrease in the degree of Si-undersaturation and in volatile, alkali, and incompatible trace element enrichments from Toro Ankole to Virunga lavas is causally connected to the progress of tectonic rifting in the Western Branch. However, the unusual vertical trends in Pb and Sr isotopic plots (Fig. 6) deserve some explanations. These isotopic trends have been previously explained through mixing between metasomatic mantle fluids and the CLM and/or continental crust (Vollmer and Norry, 1983a) or possibly between the CLM and enriched mantle 2 (EM2) source (e.g., Chakrabarti et al., 2009a). However, the latter proposal is clearly inconsistent with the relatively unradiogenic Pb isotopes of Paleoproterozoic to Archean stable/cratonic crust (Figs. 6B and 6C; Moller et al., 1998) and the radiogenic Pb isotopes of EM2 (Figs. 6B and 6C; Hart, 1988). In this study, we propose that such vertical isotopic trends are simply a consequence of the afore posited compositional

layering of the metasomatized upper CLM beneath the EARS, especially beneath the Western Branch.

The unusual isotopic features of Toro Ankole and Virunga lavas stem from their limited range of $^{206}Pb/^{204}Pb$ but large variations in $^{207}Pb/^{204}Pb$, $^{208}Pb/^{204}Pb$, and $^{87}Sr/^{86}Sr$ values, both within individual lava suites and among the suites (Fig. 6). This feature can be explained simply by the length of time (possibly up to 500 m.y.) and relative mobilities of the radioactive parent elements (i.e., U-Th and Rb) relative to radiogenic daughter elements (i.e., Pb and Sr, respectively) during metasomatism. Specifically, Toro Ankole and Virunga lavas are extremely enriched in highly incompatible trace elements, except that the former has no anomalous positive Pb concentration anomaly unlike the latter (Pitcavage et al., 2021). This is highly consistent with the systematically higher Ce/Pb of Toro Ankole (~low Pb) relative to Virunga (~high Pb) lavas (Fig. 7A). Moreover, although the carbonatite and Toro Ankole lavas are the most enriched in almost all incompatible trace elements, they are unusually depleted in Rb (Fig. 4A). All these indicate that the source, particularly its exsolved and trapped volatile component, of Toro Ankole (plus Nyiragongo) lavas contains extremely high U/Pb (or μ), Th/Pb (or ω), and relatively low Rb/Sr ratios.

To explain such trace element ratios in the exsolved volatiles, first it is important to emphasize that metasomatism is a *subsolidus* geochemical process in the presence of plenty of fluids (Vollmer and Norry, 1983b; Roden and Murthy, 1985). Second, this study adopts the new perspective on the relative mobilities of elements in hydrothermal, Cl-bearing fluids in *subsolidus* to *above solidus* geochemical reactions described in detail by Castillo (2022, 2021). Critically, intraplate or OIB magmas coming from mantle plumes indeed contain high, though variable amounts of Cl (Stroncik and Haase, 2004; Kendrick et al., 2015; Hanyu et al., 2019).

Briefly, the relative mobilities of elements in hydrothermal fluids in *above solidus* condition can be roughly estimated by their ionic potential (i.p.) values, which in turn are roughly similar to *solidus* and *subsolidus* silicate partition coefficient (K_d) values, but with subtle but critical differences. Trace elements like the large-ion lithophiles (LIL) and light REEs with low (≤ 2.9) i.p. values are highly fluid mobile, middle to heavy REEs such as Lu and Yb plus Y with intermediate ($2.9 \sim 4.0$) i.p. values are immobile and HFSE and U with intermediate to high (≥ 4.0) are variably mobile (Castillo, 2022, 2021). Hence, for example, Nb can be partially mobilized more than Zr during metasomatism (i.e., Nb/Zr ratios increase with metasomatism – Fig. 5), contrary to the widely accepted notion that Nb and Zr are both immobile in *subsolidus* to *above solidus* conditions (cf. Floyd and Winchester, 1978).

More relevant to the Pb isotopes is that Th and U are both incompatible lithophile elements that can be fluxed or sequestered easily by the exsolved volatiles. On the other hand, although Pb is also highly fluid-mobile, it is a chalcophile as well as a siderophile element that should partition as a Pb-Cl complex retained in the silicate CLM (Castillo, 2022, 2021). In other words, the trapped volatiles, which exsolve from partial melts from the African Superplume, are extremely enriched in U and Th but poor in Pb. Moreover, the trapped volatiles are fairly well-mixed as diffusion is faster in fluids than in silicates, and additional volatiles are continuously coming from the superplume below. Hence, the Toro Ankole (including carbonatites) and Nyiragongo lavas mainly sourced from the trapped volatiles have a narrow range of Pb isotopic compositions (Figs. 6 and 11). Moreover, such a well-mixed, limited range in Pb contents and Pb isotopic values in Toro Ankole and Nyiragongo lavas and carbonatites that form the base of the anomalous vertical isotopic trends collectively represent the proposed common “V” composition of EARS lavas (Castillo et al., 2014).

However, as posited earlier in our model, individual Virunga lava suites sequentially originate from different metasomatized Paleoproterozoic to Archean CLM layers as tectonic rifting progresses. The uppermost CLM layers are in equilibrium with the trapped volatiles that have extremely high μ and it also has high μ; hence Pb with highly radiogenic $^{207}Pb/^{204}Pb$ is continuously being generated and continuously transfers to individual upper CLM layers as Pb-Cl complex. Hence, Bufumbira and eastern volcano lavas derived from the uppermost CLM layers have variable and extremely high $^{207}Pb/^{204}Pb$ for given (common) $^{206}Pb/^{204}Pb$ values (Fig. 6B). A simple way to illustrate the unique radiogenic Pb signature of each CLM layer is by using the logic how Paterson (1956) defined the Geochron, which is the locus of $^{207}Pb/^{204}Pb$ for given $^{206}Pb/^{204}Pb$ values of Earth materials since 4.56 Ga. That is, the Geochron represents positively correlated radiogenic $^{207}Pb/^{204}Pb$ and $^{206}Pb/^{204}Pb$ values that have accumulated from Earth material with different μ values since 4.56 Ga. Note that in young Earth (≤ 4.56 Ga), however, these same radiogenic values would have been trending ca. vertical, as the same material with different μ values did not have enough time to generate ^{206}Pb, but has grown ^{207}Pb already. This is the same case when the upper layers of the Paleoproterozoic to Archean CLM are suddenly (i.e., in k.y. timescale) sampled by volcanism when rifting initiates and then progresses: Virunga volcanoes erupt lavas from successive CLM layers with high $^{207}Pb/^{204}Pb$ for given $^{206}Pb/^{204}Pb$ values. Each layer is akin to a "young Earth system" except that it has more variable and more radiogenic $^{207}Pb/^{204}Pb$ generated by the trapped volatiles and co-existing upper CLM layers with extremely high μ. As a whole, mixing of lavas from the carbonatite-metasomatized and silicate-metasomatized upper CLM layers (altogether constituting a vertical series of young Earth systems) generates the vertical $^{207}Pb/^{204}Pb$ versus $^{206}Pb/^{204}Pb$ trend. A similar scenario is proposed for the unusually high $^{208}Pb/^{204}Pb$ for given $^{206}Pb/^{204}Pb$ values of the lavas (Fig. 6C).

Despite the relatively longer radiogenic half-life of ^{232}Th compared to ^{238}U, the trapped volatiles and upper CLM layers have extremely high Th/Pb (or ω) values due to the difference in fluid mobility (Castillo, 2022). Thus, the radiogenic Pb transferred from the volatiles to the successive CLM upper layers that feed into Virunga lavas also have high and variable $^{208}Pb/^{204}Pb$ but a relatively limited range of $^{206}Pb/^{204}Pb$.

A similar explanation is also applicable to the vertical $^{87}Sr/^{86}Sr$ versus $^{206}Pb/^{204}Pb$ trend of the lavas (Fig. 6A). Although Rb is more fluid-mobile than Sr in *subsolidus* to *above solidus* geochemical reactions (Castillo, 2022), Rb is depleted in the exsolved fluid (Fig. 4A) most likely due to its incompatibility with carbonatitic melts (Dasgupta et al., 2009); instead, it should preferentially move into potassium silicate minerals (e.g., phlogopite; Foley et al., 1996; Krmicek et al., 2014) in the upper CLM layers. Hence, lavas from the volatile-rich source (e.g., carbonatites) of Toro Ankole and Nyiragongo lavas have relatively low Rb and, accordingly, a well-mixed and uniform $^{87}Sr/^{86}Sr$. In contrast, partial melts of the upper CLM layers, likely abundant with phlogopite and K-feldspar, generate Virunga lavas with highly variable, radiogenic $^{87}Sr/^{86}Sr$ (Fig. 6A). Again, these CLM layers are sequentially sampled by Virunga volcanism as rifting progresses. The vertical $^{87}Sr/^{86}Sr$ array is again most likely due to mixing of melts from different carbonatite-metasomatized and silicate-metasomatized upper CLM layers.

The lithology and major-trace element and isotopic compositions of South Kivu and Rungwe lavas are more variable than Toro Ankole (and Nyiragongo) lavas and overlap more with Virunga lavas (Figs. 2, 4, and 6). This is primarily because the Rungwe and particularly South Kivu provinces are located along Western Branch segments that are at slightly more advanced stages of rift development (Fig. 11D). As there is a dearth of combined Sr and Pb isotopic data for South Kivu lavas, the Nb/Zr and $^{87}Sr/^{86}Sr$ values of the lavas from the different

provinces are used instead to provide a useful overview of the compositional evolution of Western Branch lavas as rifting progresses (Fig. 12). Carbonatite, Toro Ankole, and Nyiragongo lavas have the highest Nb/Zr and intermediate $^{87}Sr/^{86}Sr$ values as they represent the initial, carbonatite-rich signature of the trapped volatiles that are released during rift initiation. As rifting progresses, Virunga volcanism initially samples the carbonatite-metasomatized uppermost layers of the Paleoproterozoic to Archean CLM (decreasing Nb/Zr and ~increasing $^{87}Sr/^{86}Sr$ values), and then, the deeper, silicate-metasomatized CLM layers (~low Nb/Zr and high $^{87}Sr/^{86}Sr$ values). Significantly, South Kivu and Rungwe lavas erupted from presumably more advanced stages of rifting plot at the intersection of Toro Ankole and Virunga lavas (~middle range of Nb/Zr and $^{87}Sr/^{86}Sr$ values), and close to the proposed common source "V" (Castillo et al., 2014). Moreover, Rungwe and South Kivu lavas in particular extend towards the DMM end-component through MER and other Ethiopian lavas (lowest Nb/Zr and $^{87}Sr/^{86}Sr$ values). The same trends can be seen in Nb/Zr versus $^{143}Nd/^{144}Nd$ (Castillo et al., 2014; see inset in Fig. 12). For South Kivu, the trend indicates an increasing contribution from an asthenospheric or possibly DMM source (Fig. 11D). This is because wider crustal rifts translate to more mantle upwelling from below, which draws the less viscous asthenospheric layer from the surrounding upper mantle.

A similar case can be made for Rungwe lavas, but a possible complication is that a mantle plume directly stemming from the African Superplume may be present here because of the occurrence of $^{3}He/^{4}He$ ratios that are significantly above the nominal 6 Ra values observed along the EARS (Hilton et al., 2011; Halldórsson et al., 2014, 2022). The Rungwe plume appears to have the common "V" composition (~middle range of Nb/Zr and $^{87}Sr/^{86}Sr$ values; Castillo et al., 2014). Moreover, as will be discussed next, the Rungwe province is uniquely situated in the

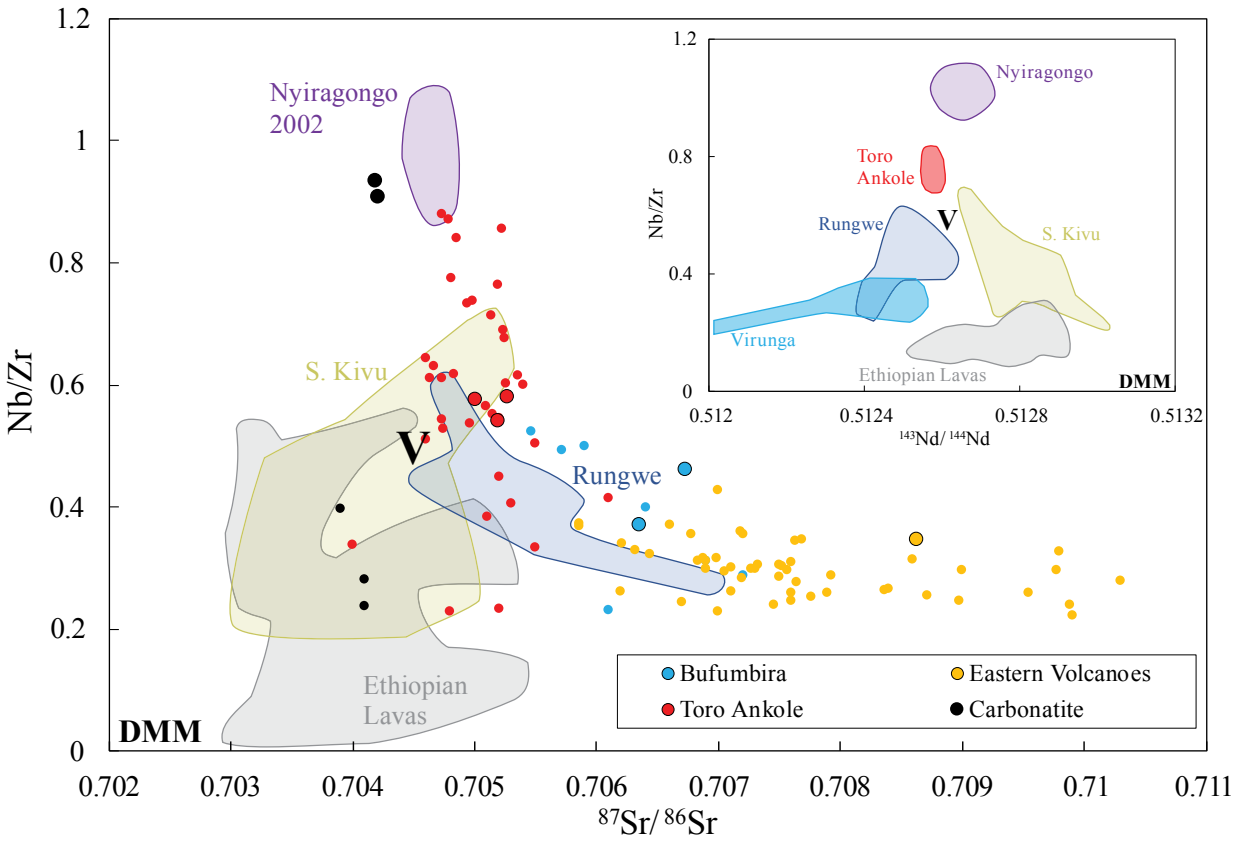

Figure 12. Nb/Zr versus $^{87}Sr/^{86}Sr$ diagram for Toro Ankole and Virunga lavas. Symbols for Toro Ankole, Toro Ankole carbonatites, and Virunga samples are the same as in Figure 3; previously published data from the two provinces are plotted as smaller points with their respective colors (GEOROC; https://georoc.mpch-mainz.gwdg.de//). The overlap between Ethiopian lavas and DMM suggests a high asthenospheric influence in the source. The common "V" composition (modified after Castillo et al., 2014) is at the ~intersection of South Kivu, Ethiopian and Western Branch data. Fields shown are for lavas from Nyiragongo (Chakrabarti et al., 2009a), South Kivu (GEOROC; https://georoc.mpch-mainz.gwdg.de//), Rungwe (Castillo et al., 2014), and Ethiopia (as in Fig. 5). Inset shows the Nb/Zr versus $^{143}Nd/^{144}Nd$ plot from Castillo et al. (2014).

boundary between the Mozambique Mobile Belt and the Archean Tanzania craton (Castillo et al., 2014). Thus, the available limited data best suggest that the South Kivu province represents the end stages of the juvenile rifting along the Western Branch, transitioning to the more advanced rifting along the MER. Thus, the geochemical signature of its associated volcanism is also transitioning from the extremely alkalic and enriched Western Branch lavas to that of the more voluminous, relatively less alkalic and less enriched Ethiopian lavas. Altogether, the proposed dynamic model is consistent with the notion of an increasing shift from a metasomatized CLM dominant source towards an asthenospheric source as rifting progresses in the EARS, similar to other continental rift settings (Mana et al., 2012; Perry et al., 1988; Rocholl et al., 1995; Thomson and Gibson, 1994; Chin, 2018). However, it is also emphasized herein that the whole process is complex as although the metasomatism is caused by the African Superplume, it is also occasionally disturbed locally by individual plume (stem) activities.

6.3. Why are Western Branch Lavas Compositionally Different from Eastern Branch Lavas?

First, the geologic setting of the Eastern Branch is significantly different compared to the Western Branch. As discussed earlier, most of the lithosphere traversed by the Eastern Branch particularly in Ethiopia belongs to the Mozambique Mobile Belt, which consists of reworked lithosphere attributed to the Neoproterozoic East African Orogeny (Stern, 1994). In contrast, the lithosphere underlying the Western Branch is a more stable Paleoproterozoic to Archean lithosphere (i.e., the Tanzania craton; Foley et al., 2012; Link et al., 2010). Second, rifting began early in the Eastern Branch at ca. 35 Ma near the Gulf of Aden (d'Acremont et al., 2005) and at ca. 15-18 Ma along the MER (Wolfenden et al., 2005). As such, the bulk of Eastern Branch rifts spanning Ethiopia are more tectonically mature than the juvenile Western Branch rifts, and, hence, their associated rift magmatism are most likely in different stages of evolution (Figs. 11A

to E). Despite such differences, however, we argue that a common mantle plume source component coming from the African Superplume is present beneath both the Western Branch and Eastern Branch (see also Castillo et al., 2014).

As also mentioned before, South Kivu and Rungwe lavas collectively trend from the Toro-Ankole – Virunga compositional join (or "V") towards the DMM end-component through MER or Ethiopian lavas (Fig. 12). Conversely, MER and the rest of Ethiopian lavas trend from near DMM towards "V", suggesting contributions from these two end-sources (Figs. 5; 12). It must be recalled, however, that for the northern Western Branch lavas, Nb/Zr decreases and $^{87}Sr/^{86}Sr$ increases as rifting progresses, consistent with our proposed model for a shift from a volatile or carbonatite-metasomatized to a silicate-metasomatized source. As rifting progresses in the South Kivu and to a lesser extent Rungwe province, Western Branch data seem to diverge at the "V" composition. Such intermediate Nb/Zr and $^{87}Sr/^{86}Sr$ compositional domain, which can also be seen in the plot of $^{87}Sr/^{86}Sr$ vs $^{206}Pb/^{204}Pb$ (Fig. 13; see also, Castillo et al., 2014) suggests "V" is not an end-source component, but instead a common source composition for many lavas from both branches. The common component is most likely produced through the convergence of two binary mixing arrays: the younger Neoproterozoic Mozambique Mobile Belt or the older Paleoproterozoic to Archean cratonic lithosphere and the FOZO OIB source component (Hart et al., 1992; Stracke et al., 2005; Castillo, 2016). Nyiragongo and Toro Ankole lavas analyzed in this study plot along mixing lines between FOZO and Paleoproterozoic to Archean lithosphere (Archean Tanzania craton), whereas MER and other Eastern Branch lavas plot along mixing lines between FOZO and Neoproterozoic Pan-African continental lithosphere.

Notably, the range of Sr and Pb isotopic ratios in MARID xenoliths (Fitzpayne et al., 2019) is used herein as a major argument for the above proposed Paleoproterozoic to Archean

stable craton – FOZO mixing (Fig. 13). This is because we concur that such isotopic range from "depleted MARID" to "enriched MARID" as defined by Giuliani et al. (2015) is a product of mixing between an enriched end-member (recycled crustal components) and metasomatized lithospheric melts (e.g., kimberlitic melts; Fitzpayne et al., 2019). However, we propose that the depleted to enriched MARID array is simply a segment of the Paleoproterozoic to Archean craton – FOZO mixing array. Moreover, the metasomatized lithospheric melts are relatively homogeneous in composition (or "V") simply because the CLM is warm as it is in a metamorphic environment and, thus, fully interacts with the trapped melts (plus volatiles) from the African Superplume before rifting for a long time (perhaps up to 500 m.y.). In contrast, the Paleoproterozoic to Archean crust is colder, stronger and less susceptible to wholesale metasomatism. Thus, a simple binary mixing between melts with a "V" composition and/or melts coming from FOZO directly, and Paleoproterozoic to Archean craton can produce the range of MARID xenoliths. In sum, the MARID xenoliths along with Toro Ankole and Nyiragongo lavas and carbonatites are a range of mixing products between the local Paleoproterozoic to Archean continental lithosphere and the African Superplume (FOZO). This scenario is consistent with Rosenthal et al. (2009)'s proposal for a MARID-carbonatitic plume mixing source for Toro Ankole. It is also highly consistent with our REE partial melt model (Fig. 10) for generating Toro Ankole and Virunga lavas.

On the other hand, Ethiopian lavas plot along binary mixing lines between Neoproterozoic Pan-African continental lithosphere and FOZO (Fig. 13). Such mixing trends are consistent with our proposed model – that Eastern Rift lavas are compositionally different from Western Rift lavas partly because of their different geologic settings (see also Castillo et al., 2014). Moreover, the difference between the old, stable craton in the Western Branch and the

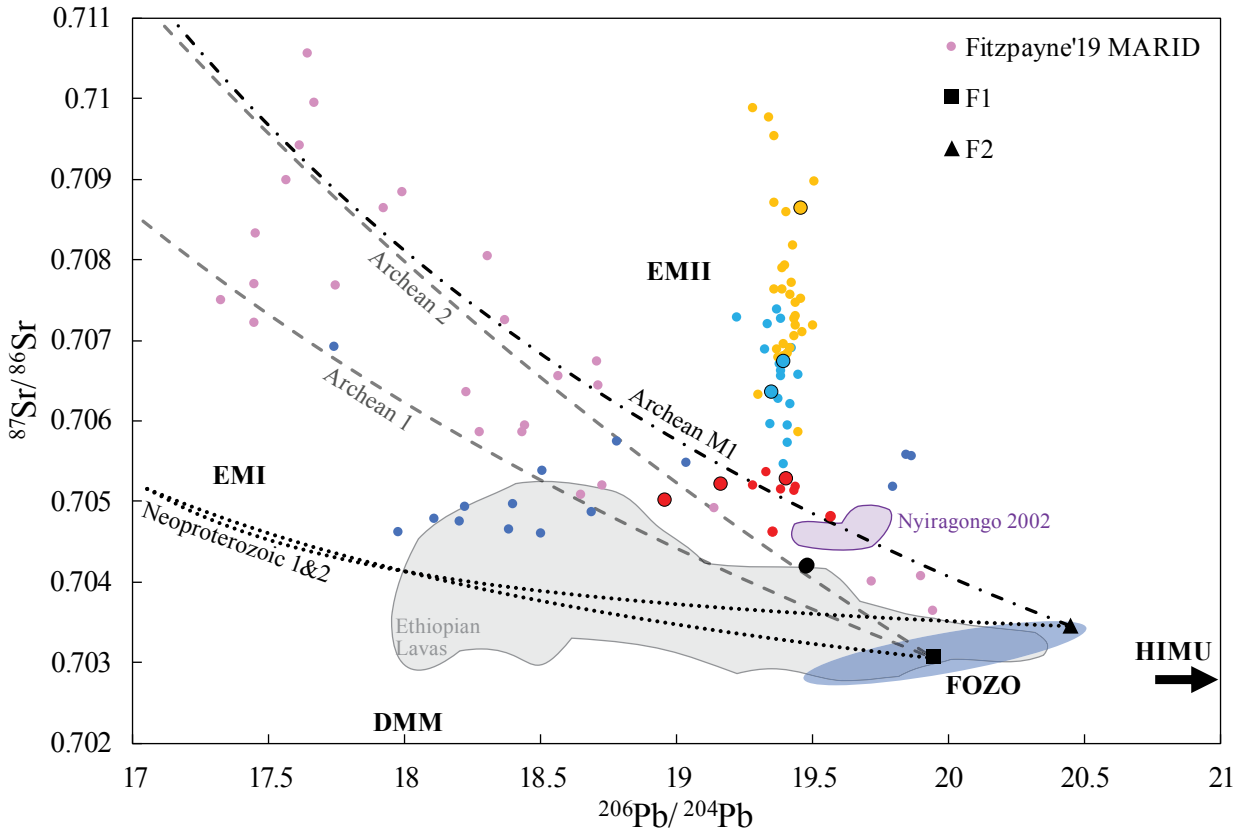

Figure 13. Simple two-component $^{87}Sr/^{86}Sr$ versus $^{206}Pb/^{204}Pb$ mixing models for Toro Ankole, Virunga, and Ethiopian lavas involving Archean or Neoproterozoic crustal rocks and FOZO mantle component. Field for FOZO is from Stracke et al. (2005). The upper (*F2*) and middle (*F1*) points in the FOZO field are OIB samples "74-393" (Sr = 1200 ppm; $^{87}Sr/^{86}Sr$ = 0.703454; Pb = 3.54 ppm; $^{206}Pb/^{204}Pb$ = 20.45) from Chauvel et al. (1997) and "199[7]" (Sr = 473 ppm; $^{87}Sr/^{86}Sr$ = 0.703060; Pb = 2.79 ppm; $^{206}Pb/^{204}Pb$ = 19.946) from Palacz et al. (1986), respectively. The Neoproterozoic 1 mixing line is between Proterozoic granulite reworked during the Pan-African orogeny ("T144-2"; $^{87}Sr/^{86}Sr$ = 0.705157, $^{206}Pb/^{204}Pb$ = 17.051; from Moller et al., 1998) and FOZO *F1* and the Neoproterozoic 2 mixing line is between the same granulite and FOZO *F2*. Archean 1 is a mixing line between FOZO *F1* and a granodiorite from the Archean Tanzania craton ("A164-1"; $^{87}Sr/^{86}Sr$ = 0.714823; $^{206}Pb/^{204}Pb$ = 15.294; Moller et al., 1998). Archean 2 is a mixing line between FOZO *F1* and a tonalitic gneiss from the Archean Tanzania craton ("A159-1"; $^{87}Sr/^{86}Sr$ = 0.727279, $^{206}Pb/^{204}Pb$ = 14.084; Moller et al., 1998). Archean M1 is a mixing line between FOZO *F2* and a metamorphized Archean granulite from the Lowlands of the Mozambique Belt ("PG-3"; $^{87}Sr/^{86}Sr$ = 0.731776, $^{206}Pb/^{204}Pb$ = 14.806; Moller et al., 1998). Due to a wide range in Sr and Pb concentrations for both Proterozoic and Archean crustal rocks, average lower continental crust values for Sr and Pb were used (Rudnick and Gao, 2003). Also shown are MARID xenoliths from Fitzpayne et al. (2019). Symbols used as in Figure 6A.

younger, mobile belt in Ethiopia could possibly explain why rifting started earlier in the Eastern Branch than in the Western Branch. Notably, the pre-rift lavas in southern Ethiopia and some of the NW plateau lavas are also mildly alkaline, but are very different from the highly-alkalic and Si-undersaturated Toro Ankole lavas. In our proposed model, the dearth of volatile- and alkali-rich and highly Si-undersaturated lavas in Ethiopia is because the relatively younger, reworked continental crust is relatively unstable compared to that in the Archean craton and, thus, cannot effectively trap or pond exsolved volatiles and low degree partial melts from the African Superplume. Clearly, however, in the southern section of the Eastern Branch that is also underlain by older, Paleoproterozoic to Archean basement, highly alkalic (e.g., Chyulu Hills) and carbonatitic (Oldoinyo Lengai) lavas occur. Also notable, Rungwe lavas plot across both mixing lines (Paleoproterozoic to Archean crust and Neoproterozoic crust), most likely because of Rungwe's location near the boundary between the Archean craton and Pan-African terranes (Castillo et al., 2014). Finally, as tectonic rifting is more advanced in Ethiopia, more Eastern Branch lavas trend toward the asthenospheric source (i.e., DMM; Figs. 12 and 13).

In summary, the geochemically distinct lavas from the various EARS segments could be attributed to the interactions between the common, limitedly geochemically variable and most-voluminous plume component (i.e., FOZO: Hart et al., 1992; Stracke et al., 2005; Castillo, 2015, 2016) coming from the African Superplume and local CLM. Equally important, the degree of such interactions is causally linked to the degree of rift development. Although not discussed in detail, this general tectono-magmatic model is locally interrupted by the presence of distinct plume stems or individual upwellings from the superplume, such as in the Afar region (e.g., Craig et al., 1977) and in the Rungwe province (Hilton et al., 2011; Castillo et al., 2014, 2020). Moreover, although also not discussed in detail, a fourth end-member source of EARS lavas is

DMM. This source is sequestered from the surrounding low viscous asthenosphere as rifts become fully developed. Its contribution and role in EARS magmatism are not present in Toro Ankole and Virunga lavas, then show up initially in South Kivu lavas and more so in MER lavas (Fig. 11; see also Furman et al., 2006b; Rooney et al., 2012; Castillo et al., 2014, 2020), and is especially true as MORBs further to the north in the fully rifted Red Sea and Gulf of Aden (e.g., Schilling et al., 1992).

7. Summary and Conclusions

The Western Branch of the EARS hosts diverse suites of lavas, including atypical ones, that seem to be unique to individual volcanic provinces despite their spatial proximity to one other. Clearly the heterogeneity in the source accounts for some of the observed differences, but detailed evaluation of new and available data indicates that Western Branch volcanism represents the juvenile part of a common dynamic process linking magmatism and tectonism in the entire EARS. In our proposed model, the long-term metasomatism by the African Superplume creates a compositionally layered, highly-pressurized Paleoproterozoic to Archean CLM beneath the Western Branch. The compositional layering is due to the continuous arrival of small degree partial melts coming from the thermo-chemical mantle anomaly, inherent heterogeneity of the partial melts and lithospheric mantle, and faster upward velocity of exsolved volatiles relative to small degree partial melts in the CLM. As crustal rifting initiates and evolves, there is a shift in lava composition due to a shift from a volatile or carbonatite-metasomatized source in Toro Ankole to a silicate-metasomatized source in Virunga, then, to the addition of an asthenospheric source in South Kivu, and ultimately to MER-like magmatism. Furthermore, we propose that part of the difference in Western Branch and the Eastern Branch magmatism can be explained by the interactions between the local continental lithosphere and the African Superplume. Very young Toro Ankole and Nyiragongo rift lavas are produced by some of the lowest degree of partial melting of a mixed Paleoproterozoic to Archean lithosphere – FOZO source at great pressure, whereas more mature MER and other Ethiopian lavas are mostly produced by larger degrees of partial melting of a mixed Neoproterozoic mobile lithosphere – FOZO source at lower pressure.

In conclusion, rifting and volcanism in Toro Ankole, Virunga, and the MER represent temporally and tectonically progressive stages of a common tectono-magmatic process. Evolution in rifting consequentially causes an evolution in magmatism, as it also dictates the evolution of the source of lavas for each volcanic province. Such an evolutionary process and the diverse magmatism throughout the EARS ultimately stem from the continuous interaction of the local lithosphere and the underlying superplume.

8. Acknowledgements

This thesis, in full, contains material currently being prepared for publication. Abe, Hugo; Castillo, Paterno R.; Day, James M.D.; Halldórsson, Sæmundur A.; Scarsi, Paolo; Natukunda, James F.; Bahati Godfrey. “The geochemistry and Sr-Pb isotopes of Toro Ankole and Virunga lavas provide constraints for a unified tectono-magmatic evolution of the East African Rift System”. The thesis author was the primary investigator and author of this paper.

REFERENCES

Adam, J., & Green, T. (2001). Experimentally determined partition coefficients for minor and trace elements in peridotite minerals and carbonatitic melt, and their relevance to natural carbonatites. *European Journal of Mineralogy*, *13*(5), 815–827.

Ayalew, D., Jung, S., Romer, R. L., Kersten, F., Pfänder, J. A., & Garbe-Schönberg, D. (2016). Petrogenesis and origin of modern Ethiopian rift basalts: Constraints from isotope and trace element geochemistry. *Lithos*, *258*, 1–14.

Barette, F., Poppe, S., Smets, B., Benbakkar, M., & Kervyn, M. (2017). Spatial variation of volcanic rock geochemistry in the Virunga Volcanic Province: Statistical analysis of an integrated database. *Journal of African Earth Sciences*, *134*, 888–903.

Barker, D. S., & Nixon, P. H. (1989). High-Ca, low-alkali carbonatite volcanism at Fort Portal, Uganda. *Contributions to Mineralogy and Petrology*, *103*(2), 166–177.

Barry, P. H., Hilton, D. R., Fischer, T. P., de Moor, J. M., Mangasini, F., & Ramirez, C. (2013). Helium and carbon isotope systematics of cold "mazuku" CO2 vents and hydrothermal gases and fluids from Rungwe Volcanic Province, southern Tanzania. *Chemical Geology*, *339*, 141–156.

Basu, A. R. (1978). Trace elements and Sr-isotopes in some mantle-derived hydrous minerals and their significance. *Geochimica et Cosmochimica Acta*, *42*(6), 659–668. https://doi.org/https://doi.org/10.1016/0016-7037(78)90084-4

Beattie, P. (1993). Uranium–thorium disequilibria and partitioning on melting of garnet peridotite. *Nature*, *363*(6424), 63–65.

Bell, K., & Powell, J. L. (1969). Strontium isotopic studies of alkalic rocks: the potassium-rich lavas of the Birunga and Toro—Ankole Regions, East and Central Equatorial Africa. *Journal of Petrology*, *10*(3), 536–572.

Bellon, H., & Pouclet, A. (1980). Datations K-Ar de quelques laves du Rift-ouest de l'Afrique Centrale; implications sur l'évolution magmatique et structurale. *Geologische Rundschau*, *69*(1), 49–62.

Beswick, A. E. (1976). K and Rb relations in basalts and other mantle derived materials. Is phlogopite the key? *Geochimica et Cosmochimica Acta*, *40*(10), 1167–1183.

Bienvenu, P., Bougault, H., Joron, J. L., Treuil, M., & Dmitriev, L. (1990). MORB alteration: rare-earth element/non-rare-earth hygromagmaphile element fractionation. *Chemical Geology*, *82*, 1–14.

Blundy, J., & Dalton, J. (2000). Experimental comparison of trace element partitioning between clinopyroxene and melt in carbonate and silicate systems, and implications for mantle metasomatism. *Contributions to Mineralogy and Petrology*, *139*(3), 356–371.

Boven, A., Pasteels, P., Punzalan, L. E., Yamba, T. K., & Musisi, J. H. (1998). Quaternary perpotassic magmatism in Uganda (Toro-Ankole Volcanic Province): age assessment and significance for magmatic evolution along the East African Rift. *Journal of African Earth Sciences*, *26*(3), 463–476.

Brenan, J. M., & Watson, E. B. (1991). Partitioning of trace elements between carbonate melt and clinopyroxene and olivine at mantle PT conditions. *Geochimica et Cosmochimica Acta*, *55*(8), 2203–2214.

Castillo, P. R. (2015). The recycling of marine carbonates and sources of HIMU and FOZO ocean island basalts. *Lithos*, *216–217*, 254–263. https://doi.org/https://doi.org/10.1016/j.lithos.2014.12.005

Castillo, P. R. (2016). A proposed new approach and unified solution to old Pb paradoxes. *Lithos*, *252–253*, 32–40. https://doi.org/https://doi.org/10.1016/j.lithos.2016.02.015

Castillo, P. R. (2021). Chlorine from seawater is key to the generation of calc-alkaline lavas. *Journal of Asian Earth Sciences*, *213*, 104753. https://doi.org/https://doi.org/10.1016/j.jseaes.2021.104753

Castillo, P. R. (2022). Arc magmatism and porphyry-type ore deposition are primarily controlled by chlorine from seawater. *Chemical Geology*, *589*, 120683. https://doi.org/https://doi.org/10.1016/j.chemgeo.2021.120683

Castillo, P. R., Hilton, D. R., & Halldórsson, S. A. (2014). Trace element and Sr-Nd-Pb isotope geochemistry of Rungwe Volcanic Province, Tanzania: implications for a Superplume source for East Africa Rift magmatism. *Frontiers in Earth Science*, *2*. https://www.frontiersin.org/article/10.3389/feart.2014.00021

Castillo, P. R., Liu, X., & Scarsi, P. (2020). The geochemistry and Sr-Nd-Pb isotopic ratios of high 3He/4He Afar and MER basalts indicate a significant role of the African Superplume in EARS magmatism. *Lithos*, *376*, 105791.

Chakrabarti, R., Basu, A. R., Santo, A. P., Tedesco, D., & Vaselli, O. (2009a). Isotopic and geochemical evidence for a heterogeneous mantle plume origin of the Virunga volcanics, Western rift, East African Rift system. *Chemical Geology*, *259*(3–4), 273–289.

Chakrabarti, R., Sims, K. W. W., Basu, A. R., Reagan, M., & Durieux, J. (2009b). Timescales of magmatic processes and eruption ages of the Nyiragongo volcanics from 238U-230Th-226Ra-210Pb disequilibria. *Earth and Planetary Science Letters*, *288*(1–2), 149–157.

Chauvel, C., McDonough, W., Guille, G., Maury, R., & Duncan, R. (1997). Contrasting old and young volcanism in Rurutu Island, Austral chain. *Chemical Geology*, *139*(1), 125–143. https://doi.org/https://doi.org/10.1016/S0009-2541(97)00029-6

Chin, E. J. (2018). Deep crustal cumulates reflect patterns of continental rift volcanism beneath Tanzania. *Contributions to Mineralogy and Petrology*, *173*(10), 1–22.

Class, C., Altherr, R., Volker, F., Eberz, G., & McCulloch, M. T. (1994). Geochemistry of Pliocene to Quaternary alkali basalts from the Huri Hills, northern Kenya. *Chemical Geology*, *113*(1–2), 1–22.

Coltorti, M., Bonadiman, C., Hinton, R. W., Siena, F., & Upton, B. G. J. (1999). Carbonatite metasomatism of the oceanic upper mantle: evidence from clinopyroxenes and glasses in ultramafic xenoliths of Grande Comore, Indian Ocean. *Journal of Petrology*, *40*(1), 133–165.

Craig, H., Lupton, J. E., & Horowiff, R. M. (1977). Isotope geochemistry and hydrology of geothermal waters in the Ethiopian Rift Valley. *Scripps Inst. of Oceanography. Ept*, 14–77.

d'Acremont, E., Leroy, S., Beslier, M.-O., Bellahsen, N., Fournier, M., Robin, C., Maia, M., & Gente, P. (2005). Structure and evolution of the eastern Gulf of Aden conjugate margins from seismic reflection data. *Geophysical Journal International*, *160*(3), 869–890.

Dasgupta, R., Hirschmann, M. M., & Withers, A. C. (2004). Deep global cycling of carbon constrained by the solidus of anhydrous, carbonated eclogite under upper mantle conditions. *Earth and Planetary Science Letters*, *227*(1–2), 73–85.

Dasgupta, R., & Hirschmann, M. M. (2006). Melting in the Earth's deep upper mantle caused by carbon dioxide. *Nature*, *440*(7084), 659–662.

Dasgupta, R., Hirschmann, M. M., McDonough, W. F., Spiegelman, M., & Withers, A. C. (2009). Trace element partitioning between garnet lherzolite and carbonatite at 6.6 and 8.6 GPa with applications to the geochemistry of the mantle and of mantle-derived melts. *Chemical Geology*, *262*(1–2), 57–77.

Dasgupta, R., Jackson, M. G., & Lee, C.-T. A. (2010). Major element chemistry of ocean island basalts—Conditions of mantle melting and heterogeneity of mantle source. *Earth and Planetary Science Letters*, *289*(3–4), 377–392.

Day, J. M. D., Peters, B. J., & Janney, P. E. (2014). Oxygen isotope systematics of South African olivine melilitites and implications for HIMU mantle reservoirs. *Lithos*, *202*, 76–84.

de Mulder, M., & Pasteels, P. (1986). K-Ar geochronology of the Karisimbi volcano (Virunga, Rwanda-Zaire). *Journal of African Earth Sciences (1983)*, *5*(6), 575–579.

Durkin, K., Castillo, P. R., Straub, S. M., Abe, N., Tamura, Y., & Yan, Q. (2020). An origin of the along-arc compositional variation in the Izu-Bonin arc system. *Geoscience Frontiers*, *11*(5), 1621–1634. https://doi.org/https://doi.org/10.1016/j.gsf.2019.12.004

Ebinger, C. J. (1989a). Tectonic development of the western branch of the East African rift system. *Geological Society of America Bulletin*, *101*(7), 885–903.

Ebinger, C. J. (1989b). Geometric and kinematic development of border faults and accommodation zones, Kivu-Rusizi rift, Africa. *Tectonics*, *8*(1), 117–133.

Ebinger, C., Bechtel, T., Forsyth, D., & Bowin, C. (1989a). Effective Elastic Plate Thickness Beneath the East African and Afar Plateaus and Dynamic Compensation of the Uplifts. *Journal of Geophysical Research*, *94*, 2883–2901. https://doi.org/10.1029/JB094iB03p02883

Ebinger, C. J., Deino, A. L., Drake, R. E., & Tesha, A. L. (1989b). Chronology of volcanism and rift basin propagation: Rungwe volcanic province, East Africa. *Journal of Geophysical Research: Solid Earth*, *94*(B11), 15785–15803.

Ebinger, C. J., & Sleep, N. H. (1998). Cenozoic magmatism throughout east Africa resulting from impact of a single plume. *Nature*, *395*(6704), 788–791.

Ebinger, C. J., Yemane, T., Harding, D. J., Tesfaye, S., Kelley, S., & Rex, D. C. (2000). Rift deflection, migration, and propagation: Linkage of the Ethiopian and Eastern rifts, Africa. *Geological Society of America Bulletin*, *112*(2), 163–176.

Feyissa, D. H., Kitagawa, H., Bizuneh, T. D., Tanaka, R., Kabeto, K., & Nakamura, E. (2019). Transition from Plume-driven to Plate-driven Magmatism in the Evolution of the Main Ethiopian Rift. *Journal of Petrology*, *60*(8), 1681–1715.

Fitzpayne, A., Giuliani, A., Maas, R., Hergt, J., Janney, P., & Phillips, D. (2019). Progressive metasomatism of the mantle by kimberlite melts: Sr–Nd–Hf–Pb isotope compositions of MARID and PIC minerals. *Earth and Planetary Science Letters*, *509*, 15–26.

Floyd, P. A., & Winchester, J. A. (1978). Identification and discrimination of altered and metamorphosed volcanic rocks using immobile elements. *Chemical Geology*, *21*(3–4), 291–306.

Foley, S. (1992). Vein-plus-wall-rock melting mechanisms in the lithosphere and the origin of potassic alkaline magmas. *Lithos*, *28*(3–6), 435–453.

Foley, S. F., Jackson, S. E., Fryer, B. J., Greenouch, J. D., & Jenner, G. A. (1996). Trace element partition coefficients for clinopyroxene and phlogopite in an alkaline lamprophyre from Newfoundland by LAM-ICP-MS. *Geochimica et Cosmochimica Acta*, *60*(4), 629–638.

Foley, S. F., Yaxley, G. M., Rosenthal, A., Buhre, S., Kiseeva, E. S., Rapp, R. P., & Jacob, D. E. (2009). The composition of near-solidus melts of peridotite in the presence of CO2 and H2O between 40 and 60 kbar. *Lithos*, *112*, 274–283. https://doi.org/https://doi.org/10.1016/j.lithos.2009.03.020

Foley, S. F., Link, K., Tiberindwa, J. v, & Barifaijo, E. (2012). Patterns and origin of igneous activity around the Tanzanian craton. *Journal of African Earth Sciences*, *62*(1), 1–18.

Fram, M. S., & Lesher, C. E. (1997). Generation and polybaric differentiation of East Greenland Early Tertiary flood basalts. *Journal of Petrology*, *38*(2), 231–275.

Furman, T. (1995). Melting of metasomatized subcontinental lithosphere: undersaturated mafic lavas from Rungwe, Tanzania. *Contributions to Mineralogy and Petrology*, *122*(1), 97–115.

Furman, T. (2007). Geochemistry of East African Rift basalts: An overview. *Journal of African Earth Sciences*, *48*(2), 147–160. https://doi.org/https://doi.org/10.1016/j.jafrearsci.2006.06.009

Furman, T., & Graham, D. (1999). Erosion of lithospheric mantle beneath the East African Rift system: geochemical evidence from the Kivu volcanic province. In *Developments in Geotectonics* (Vol. 24, pp. 237–262). Elsevier.

Furman, T., Kaleta, K. M., Bryce, J. G., & Hanan, B. B. (2006a). Tertiary mafic lavas of Turkana, Kenya: constraints on East African plume structure and the occurrence of high-μ volcanism in Africa. *Journal of Petrology*, *47*(6), 1221–1244.

Furman, T., Bryce, J., Rooney, T., Hanan, B., Yirgu, G., & Ayalew, D. (2006b). Heads and tails: 30 million years of the Afar plume. *Geological Society, London, Special Publications*, *259*(1), 95–119.

Furman, T., Nelson, W. R., & Elkins-Tanton, L. T. (2016). Evolution of the East African rift: Drip magmatism, lithospheric thinning and mafic volcanism. *Geochimica et Cosmochimica Acta*, *185*, 418–434.

George, R., & Rogers, N. (2002). Plume dynamics beneath the African plate inferred from the geochemistry of the Tertiary basalts of southern Ethiopia. *Contributions to Mineralogy and Petrology*, *144*(3), 286–304.

Girnis, A. v, Bulatov, V. K., Lahaye, Y., & Brey, G. P. (2006). Partitioning of trace elements between carbonate-silicate melts and mantle minerals: experiment and petrological consequences. *Petrology*, *14*(5), 492–514

Girnis, A. v, Bulatov, V. K., Brey, G. P., Gerdes, A., & Höfer, H. E. (2013). Trace element partitioning between mantle minerals and silico-carbonate melts at 6–12 GPa and applications to mantle metasomatism and kimberlite genesis. *Lithos*, *160*, 183–200.

Giuliani, A., Phillips, D., Woodhead, J. D., Kamenetsky, V. S., Fiorentini, M. L., Maas, R., Soltys, A., & Armstrong, R. A. (2015). Did diamond-bearing orangeites originate from MARID-veined peridotites in the lithospheric mantle? *Nature Communications*, *6*(1), 6837. https://doi.org/10.1038/ncomms7837

Green, T. H., Adam, J., & Siel, S. H. (1992). Trace element partitioning between silicate minerals and carbonatite at 25 kbar and application to mantle metasomatism. *Mineralogy and Petrology*, *46*(3), 179–184.

Grégoire, M., Bell, D., & le Roex, A. (2002). Trace element geochemistry of phlogopite-rich mafic mantle xenoliths: their classification and their relationship to phlogopite-bearing peridotites and kimberlites revisited. *Contributions to Mineralogy and Petrology*, *142*(5), 603–625.

Guibert, P., Delaloye, M., & Hunziker, J. (1975). Contribution à l'étude géologique du volcan Mikeno, cha\^\ine des Virunga (République du Za\"\ire). *CR Scé. Soc. Phys. Hist. Nat., Genève, Ns*, *10*(1), 57–66.

Gündüz, M., & Asan, K. (2021). PetroGram: An excel-based petrology program for modeling of magmatic processes. *Geoscience Frontiers*, *12*(1), 81–92.

Halldórsson, S. A., Hilton, D. R., Scarsi, P., Abebe, T., & Hopp, J. (2014). A common mantle plume source beneath the entire East African Rift System revealed by coupled helium-neon systematics. *Geophysical Research Letters*, *41*(7), 2304–2311.

Halldórsson, S. A., Hilton, D. R., Marshall, E. W., Ranta, E., Ingvason, A., Chakraborty, S., Robin, J. G., Rasmussen, M. B., Gibson, S. A., Ono, S., & others. (2022). Evidence from gas-rich ultramafic xenoliths for Superplume-derived recycled volatiles in the East African sub-continental mantle. *Chemical Geology*, *589*, 120682.

Hansen, S. E., Nyblade, A. A., & Benoit, M. H. (2012). Mantle structure beneath Africa and Arabia from adaptively parameterized P-wave tomography: Implications for the origin of Cenozoic Afro-Arabian tectonism. *Earth and Planetary Science Letters*, *319*, 23–34.

Hanyu, T., Shimizu, K., Ushikubo, T., Kimura, J.-I., Chang, Q., Hamada, M., Ito, M., Iwamori, H., & Ishikawa, T. (2019). Tiny droplets of ocean island basalts unveil Earth's deep chlorine cycle. *Nature Communications*, *10*(1), 60. https://doi.org/10.1038/s41467-018-07955-8

Harðarson, B. S. (2015). *The Western Branch of the East African Rift : A Review of Tectonics , Volcanology and Geothermal Activity*.

Hart, S. R. (1988). Heterogeneous mantle domains: signatures, genesis and mixing chronologies. *Earth and Planetary Science Letters*, *90*(3), 273–296.

Hart, S. R., Hauri, E. H., Oschmann, L. A., & Whitehead, J. A. (1992). Mantle plumes and entrainment: isotopic evidence. *Science*, *256*(5056), 517–520.

Hilton, D. R., Halldórsson, S. A., Barry, P. H., Fischer, T. P., de Moor, J. M., Ramirez, C. J., Mangasini, F., & Scarsi, P. (2011). Helium isotopes at Rungwe Volcanic Province, Tanzania, and the origin of East African plateaux. *Geophysical Research Letters*, *38*(21).

Hofmann, A. W., Jochum, K. P., Seufert, M., & White, W. M. (1986). Nb and Pb in oceanic basalts: new constraints on mantle evolution. *Earth and Planetary Science Letters*, *79*(1–2), 33–45.

Holmes, A., & Harwood, H. F. (1932). Petrology of the volcanic fields east and south-east of Ruwenzori, Uganda. *Quarterly Journal of the Geological Society*, *88*(1–4), 370–442.

Hutchison, W., Mather, T. A., Pyle, D. M., Boyce, A. J., Gleeson, M. L. M., Yirgu, G., Blundy, J. D., Ferguson, D. J., Vye-Brown, C., Millar, I. L., & others. (2018). The evolution of magma during continental rifting: New constraints from the isotopic and trace element signatures of silicic magmas from Ethiopian volcanoes. *Earth and Planetary Science Letters*, *489*, 203–218.

Jochum, K.P., Weis, U., Schwager, B., Stoll, B., Wilson, S.A., Haug, G.H., Andreae, M.O. and Enzweiler, J. (2016). Reference values following ISO guidelines for frequently requested rock reference materials. *Geostandards and Geoanalytical Research*, *40*(3), 333–350.

Kampunzu, A. B., Bonhomme, M. G., & Kanika, M. (1998). Geochronology of volcanic rocks and evolution of the Cenozoic Western Branch of the East African Rift System. *Journal of African Earth Sciences*, *26*(3), 441–461.

Kendrick, M. A., Jackson, M. G., Hauri, E. H., & Phillips, D. (2015). The halogen (F, Cl, Br, I) and H2O systematics of Samoan lavas: Assimilated-seawater, EM2 and high-3He/4He components. *Earth and Planetary Science Letters*, *410*, 197–209. https://doi.org/https://doi.org/10.1016/j.epsl.2014.11.026

Kerrick, D. M., & Connolly, J. A. D. (1998). Subduction of ophicarbonates and recycling of CO2 and H2O. *Geology*, *26*(4), 375–378.

Klemme, S. vd, der Laan, S. R., Foley, S. F., & Günther, D. (1995). Experimentally determined trace and minor element partitioning between clinopyroxene and carbonatite melt under upper mantle conditions. *Earth and Planetary Science Letters*, *133*(3–4), 439–448.

Konzett, J., Sweeney, R. J., Thompson, A. B., & Ulmer, P. (1997). Potassium Amphibole Stability in the Upper Mantle: an Experimental Study in a Peralkaline KNCMASH System to 8.5 GPa. *Journal of Petrology*, *38*(5), 537–568. https://doi.org/10.1093/petroj/38.5.537

Kramers, J. D., & Tolstikhin, I. N. (1997). Two terrestrial lead isotope paradoxes, forward transport modelling, core formation and the history of the continental crust. *Chemical Geology*, *139*(1–4), 75–110.

Krmicek, L., Halavinova, M., Romer, R. L., Galiova, M. V., & Vaculovic, T. (2014). Phlogopite/matrix, clinopyroxene/matrix and clinopyroxene/phlogopite trace-element partitioning in a calc-alkaline lamprophyre: new constrains from the Krizanovice minette dyke (Bohemian Massif). *Journal of Geosciences*, *59*(1), 87–96.

LATIN, D., NORRY, M. J., & TARZEY, R. J. E. (1993). Magmatism in the Gregory Rift, East Africa: Evidence for Melt Generation by a Plume. *Journal of Petrology*, *34*(5), 1007–1027. https://doi.org/10.1093/petrology/34.5.1007

LaTourrette, T. Z., Kennedy, A. K., & Wasserburg, G. J. (1993). Thorium-uranium fractionation by garnet: evidence for a deep source and rapid rise of oceanic basalts. *Science*, *261*(5122), 739–742.

LaTourrette, T., Hervig, R. L., & Holloway, J. R. (1995). Trace element partitioning between amphibole, phlogopite, and basanite melt. *Earth and Planetary Science Letters*, *135*(1–4), 13–30.

le Maitre, R. W., Streckeisen, A., Zanettin, B., le Bas, M. J., Bonin, B., & Bateman, P. (2005). *Igneous rocks: a classification and glossary of terms: recommendations of the International Union of Geological Sciences Subcommission on the Systematics of Igneous Rocks*. Cambridge University Press.

Lee, C.-T. A., Luffi, P., Plank, T., Dalton, H., & Leeman, W. P. (2009). Constraints on the depths and temperatures of basaltic magma generation on Earth and other terrestrial planets using new thermobarometers for mafic magmas. *Earth and Planetary Science Letters*, *279*(1–2), 20–33.

Link, K., Koehn, D., Barth, M. G., Tiberindwa, J. v, Barifaijo, E., Aanyu, K., & Foley, S. F. (2010). Continuous cratonic crust between the Congo and Tanzania blocks in western Uganda. *International Journal of Earth Sciences*, *99*(7), 1559–1573. https://doi.org/10.1007/s00531-010-0548-8

Liu, L., Ma, Y., Yan, W., & Liu, X. (2019). Trace element partitioning between MgAl2O4-spinel and carbonatitic silicate melt from 3 to 6 GPa, with emphasis on the role of cation order-disorder. *Solid Earth Sciences*, *4*(2), 43–65.

Mana, S., Furman, T., Carr, M. J., Mollel, G. F., Mortlock, R. A., Feigenson, M. D., Turrin, B. D., & Swisher Iii, C. C. (2012). Geochronology and geochemistry of the Essimingor volcano: melting of metasomatized lithospheric mantle beneath the North Tanzanian Divergence zone (East African Rift). *Lithos*, *155*, 310–325.

Marty, B., Pik, R., & Gezahegn, Y. (1996). Helium isotopic variations in Ethiopian plume lavas: nature of magmatic sources and limit on lower mantle contribution. *Earth and Planetary Science Letters*, *144*(1), 223–237. https://doi.org/https://doi.org/10.1016/0012-821X(96)00158-6

McDougall, I. A. N., & Brown, F. H. (2009). Timing of volcanism and evolution of the northern Kenya Rift. *Geological Magazine*, *146*(1), 34–47.

Melluso, L., Lustrino, M., Ruberti, E., Brotzu, P., de Barros Gomes, C., Morbidelli, L., Morra, V., Svisero, D. P., & d'Amelio, F. (2008). Major-and trace-element composition of olivine, perovskite, clinopyroxene, Cr–Fe–Ti oxides, phlogopite and host kamafugites and kimberlites, Alto Paranaiba, Brazil. *The Canadian Mineralogist*, *46*(1), 19–40.

Meshesha, D., Chekol, T., & Negussia, S. (2021). Major and trace element compositions of basaltic lavas from western margin of central main Ethiopian rift: enriched asthenosphere vs. mantle plume contribution. *Heliyon*, e08634.

Möller, A., Mezger, K., & Schenk, V. (1998). Crustal age domains and the evolution of the continental crust in the Mozambique Belt of Tanzania: combined Sm–Nd, Rb–Sr, and Pb–Pb isotopic evidence. *Journal of Petrology*, *39*(4), 749–783.

Morley, C. K., Wescott, W. A., Stone, D. M., Harper, R. M., Wigger, S. T., & Karanja, F. M. (1992). Tectonic evolution of the northern Kenyan Rift. *Journal of the Geological Society*, *149*(3), 333–348.

Muravyeva, N. S., Belyatsky, B. v, Senin, V. G., & Ivanov, A. v. (2014). Sr–Nd–Pb isotope systematics and clinopyroxene-host disequilibrium in ultra-potassic magmas from Toro-Ankole and Virunga, East-African Rift: Implications for magma mixing and source heterogeneity. *Lithos*, *210*, 260–277.

Navon, O., & Stolper, E. (1987). Geochemical consequences of melt percolation: the upper mantle as a chromatographic column. *The Journal of Geology*, *95*(3), 285–307.

Nixon, P. H. (1973). *Kimberlitic volcanoes in East Africa*. HM Stationery Office.

Norrish, K., & Hutton, J. T. (1969). An accurate X-ray spectrographic method for the analysis of a wide range of geological samples. *Geochimica et Cosmochimica Acta*, *33*(4), 431–453.

Olafsson, M., & Eggler, D. H. (1983). Phase relations of amphibole, amphibole-carbonate, and phlogopite-carbonate peridotite: petrologic constraints on the asthenosphere. *Earth and Planetary Science Letters*, *64*(2), 305–315.

Palacz, Z. A., & Saunder, A. D. (1986). Coupled trace element and isotope enrichment in the Cook-Austral-Samoa Islands, Southwest Pacific. *Earth and Planetary Science Letters*, *79*(3), 270–280. https://doi.org/https://doi.org/10.1016/0012-821X(86)90185-8

Patterson, C. (1956). Age of meteorites and the earth. *Geochimica et Cosmochimica Acta*, *10*(4), 230–237.

Perry, F. v, Baldridge, W. S., & DePaolo, D. J. (1988). Chemical and isotopic evidence for lithospheric thinning beneath the Rio Grande rift. *Nature*, *332*(6163), 432–434.

Pik, R., Deniel, C., Coulon, C., Yirgu, G., & Marty, B. (1999). Isotopic and trace element signatures of Ethiopian flood basalts: evidence for plume–lithosphere interactions. *Geochimica et Cosmochimica Acta*, *63*(15), 2263–2279.

Pin, C., & Bassin, C. (1992). Evaluation of a strontium-specific extraction chromatographic method for isotopic analysis in geological materials. *Analytica Chimica Acta*, *269*(2), 249–255.

Pitcavage, E., Furman, T., Nelson, W. R., Kalegga, P. K., & Barifaijo, E. (2021). Petrogenesis of primitive lavas from the Toro Ankole and Virunga Volcanic Provinces: Metasomatic mineralogy beneath East Africa's Western Rift. *Lithos*, *396*, 106192.

Plank, T., & Langmuir, C. H. (1998). The chemical composition of subducting sediment and its consequences for the crust and mantle. *Chemical Geology*, *145*(3–4), 325–394.

Pouclet, A., Menot, R. P., & Piboule, M. (1981). DISCRIMINANT FACTOR-ANALYSIS APPLIED TO CENTRAL-AFRICA RIFT LAVAS (ZAIRE, RWANDA, UGANDA). *Comptes Rendus De L Academie Des Sciences Serie II*, *292*(8), 679–+.

Pouclet, A., Bellon, H., & Bram, K. (2016). The Cenozoic volcanism in the Kivu rift: Assessment of the tectonic setting, geochemistry, and geochronology of the volcanic activity in the South-Kivu and Virunga regions. *Journal of African Earth Sciences*, *121*, 219–246.

Roberts, E. M., Stevens, N. J., O'Connor, P. M., Dirks, P., Gottfried, M. D., Clyde, W. C., Armstrong, R. A., Kemp, A. I. S., & Hemming, S. (2012). Initiation of the western branch of the East African Rift coeval with the eastern branch. *Nature Geoscience*, *5*(4), 289–294.

Rocholl, A., Stein, M., Molzahn, M., Hart, S. R., & Wörner, G. (1995). Geochemical evolution of rift magmas by progressive tapping of a stratified mantle source beneath the Ross Sea Rift, Northern Victoria Land, Antarctica. *Earth and Planetary Science Letters*, *131*(3–4), 207–224.

Roden, M. F., & Murthy, V. R. (1985). Mantle metasomatism. *Annual Review of Earth and Planetary Sciences*, *13*(1), 269–296.

Rogers, N. W. (2006). Basaltic magmatism and the geodynamics of the East African Rift System. *Geological Society, London, Special Publications*, *259*(1), 77. https://doi.org/10.1144/GSL.SP.2006.259.01.08

Rogers, N. W., de Mulder, M., & Hawkesworth, C. J. (1992). An enriched mantle source for potassic basanites: evidence from Karisimbi volcano, Virunga volcanic province, Rwanda. *Contributions to Mineralogy and Petrology*, *111*(4), 543–556.

Rogers, N. W., James, D., Kelley, S. P., & de Mulder, M. (1998). The generation of potassic lavas from the eastern Virunga province, Rwanda. *Journal of Petrology*, *39*(6), 1223–1247.

Rogers, N., Macdonald, R., Fitton, J. G., George, R., Smith, M., & Barreiro, B. (2000). Two mantle plumes beneath the East African rift system: Sr, Nd and Pb isotope evidence from Kenya Rift basalts. *Earth and Planetary Science Letters*, *176*(3), 387–400. https://doi.org/https://doi.org/10.1016/S0012-821X(00)00012-1

Rooney, T. O. (2010). Geochemical evidence of lithospheric thinning in the southern Main Ethiopian Rift. *Lithos*, *117*(1–4), 33–48.

Rooney, T. O., Hanan, B. B., Graham, D. W., Furman, T., Blichert-Toft, J., & Schilling, J.-G. (2012). Upper Mantle Pollution during Afar Plume–Continental Rift Interaction. *Journal of Petrology*, *53*(2), 365–389. https://doi.org/10.1093/petrology/egr065

Rosenthal, A., Foley, S., Pearson, G., Nowell, G., & Tappe, S. (2009). Petrogenesis of strongly alkaline primitive volcanic rocks at the propagating tip of the western branch of the East African Rift. *Earth and Planetary Science Letters*, *284*, 236–248. https://doi.org/10.1016/j.epsl.2009.04.036

Rudnick, R. L., McDonough, W. F., & Chappell, B. W. (1993). Carbonatite metasomatism in the northern Tanzanian mantle: petrographic and geochemical characteristics. *Earth and Planetary Science Letters*, *114*(4), 463–475.

Rudnick, R. L., Gao, S., Holland, H. D., Turekian, K. K., & others. (2003). Composition of the continental crust. *The Crust*, *3*, 1–64.

Sahama, T. G., & TG, S. (1978). *The Nyiragongo main cone*.

Scarsi, P., & Craig, H. (1996). Helium isotope ratios in Ethiopian Rift basalts. *Earth and Planetary Science Letters*, *144*(3), 505–516. https://doi.org/https://doi.org/10.1016/S0012-821X(96)00185-9

Schilling, J.-G., Kingsley, R. H., Hanan, B. B., & McCully, B. L. (1992). Nd-Sr-Pb isotopic variations along the Gulf of Aden: Evidence for Afar mantle plume-continental lithosphere interaction. *Journal of Geophysical Research: Solid Earth*, *97*(B7), 10927–10966.

Schmidt, K. H., Bottazzi, P., Vannucci, R., & Mengel, K. (1999). Trace element partitioning between phlogopite, clinopyroxene and leucite lamproite melt. *Earth and Planetary Science Letters*, *168*(3–4), 287–299.

Shinjo, R., Chekol, T., Meshesha, D., Itaya, T., & Tatsumi, Y. (2011). Geochemistry and geochronology of the mafic lavas from the southeastern Ethiopian rift (the East African Rift System): assessment of models on magma sources, plume–lithosphere interaction and plume evolution. *Contributions to Mineralogy and Petrology*, *162*(1), 209–230.

Smith, M., & Mosley, P. (1993). Crustal heterogeneity and basement influence on the development of the Kenya Rift, East Africa. *Tectonics*, *12*(2), 591. https://doi.org/10.1029/92TC01710

Späth, A., le Roex, A. P., & Opiyo-Akech, N. (2000). The petrology of the Chyulu Hills Volcanic Province, southern Kenya. *Journal of African Earth Sciences*, *31*(2), 337–358. https://doi.org/https://doi.org/10.1016/S0899-5362(00)00092-0

Stern, R. J. (1994). ARC ASSEMBLY AND CONTINENTAL COLLISION IN THE NEOPROTEROZOIC EAST AFRICAN OROGEN: Implications for the Consolidation of Gondwanaland. *Annual Review of Earth and Planetary Sciences*, *22*(1), 319–351. https://doi.org/10.1146/annurev.ea.22.050194.001535

Stewart, K., & Rogers, N. (1996). Mantle plume and lithosphere contributions to basalts from southern Ethiopia. *Earth and Planetary Science Letters*, *139*(1–2), 195–211.

Stoppa, F., Woolley, A. R., Lloyd, F. E., & Eby, N. (2000). Carbonatite lapilli-bearing tuff and a dolomite carbonatite bomb from Murumuli crater, Katwe volcanic field, Uganda. *Mineralogical Magazine*, *64*(4), 641–650.

Stracke, A., Hofmann, A. W., & Hart, S. R. (2005). FOZO, HIMU, and the rest of the mantle zoo. *Geochemistry, Geophysics, Geosystems*, *6*(5).

Stroncik, N. A., & Haase, K. M. (2004). Chlorine in oceanic intraplate basalts: Constraints on mantle sources and recycling processes. *Geology*, *32*(11), 945–948.

Sun, S.-S., & McDonough, W. F. (1989). Chemical and isotopic systematics of oceanic basalts: implications for mantle composition and processes. *Geological Society, London, Special Publications*, *42*(1), 313–345.

Sweeney, R. J., Green, D. H., & Sie, S. H. (1992). Trace and minor element partitioning between garnet and amphibole and carbonatitic melt. *Earth and Planetary Science Letters*, *113*(1–2), 1–14.

Tappe, S., Foley, S. F., & Pearson, D. G. (2003). The kamafugites of Uganda: a mineralogical and geochemical comparison with their Italian and Brazilian analogues. *Periodico Di Mineralogia*, *72*(SPEC. ISSUE 1), 51–77.

Thirlwall, M. F. (1997). Pb isotopic and elemental evidence for OIB derivation from young HIMU mantle. *Chemical Geology*, *139*(1–4), 51–74.

Thompson, R. N., & Gibson, S. A. (1994). Magmatic expression of lithospheric thinning across continental rifts. *Tectonophysics*, *233*(1–2), 41–68.

Vidal, P. (1992). Mantle: More HIMU in the future? *Geochimica et Cosmochimica Acta*, *56*(12), 4295–4299.

Vollmer, R., & Norry, M. J. (1983a). Possible origin of K-rich volcanic rocks from Virunga, East Africa, by metasomatism of continental crustal material: Pb, Nd and Sr isotopic evidence. *Earth and Planetary Science Letters*, *64*(3), 374–386.

Vollmer, R., & Norry, M. J. (1983b). Unusual isotopic variations in Nyiragongo nephelinites. *Nature*, *301*(5896), 141–143.

Wei, X., Zhang, G.-L., Castillo, P. R., Shi, X.-F., Yan, Q.-S., & Guan, Y.-L. (2020). New geochemical and Sr-Nd-Pb isotope evidence for FOZO and Azores plume components in the sources of DSDP Holes 559 and 561 MORBs. *Chemical Geology*, *557*, 119858. https://doi.org/https://doi.org/10.1016/j.chemgeo.2020.119858

Wilson, L., & Head Iii, J. W. (2007). An integrated model of kimberlite ascent and eruption. *Nature*, *447*(7140), 53–57.

Winter, J. D. (2013). *Principles of igneous and metamorphic petrology*. Pearson education.

Wolfenden, E., Ebinger, C., Yirgu, G., Renne, P. R., & Kelley, S. P. (2005). Evolution of a volcanic rifted margin: Southern Red Sea, Ethiopia. *Geological Society of America Bulletin*, *117*(7–8), 846–864.